

---

Electronic Thesis and Dissertation Repository

---

6-17-2013 12:00 AM


## Butyl Rubber-Aliphatic Polyester Graft Copolymers for Biomedical Applications: Synthesis and Analysis of Chemical, Physical and Biological Properties

Bethany A. Turowec  
*The University of Western Ontario*

Supervisor  
Dr. Elizabeth Gillies  
*The University of Western Ontario*

Graduate Program in Biomedical Engineering  
A thesis submitted in partial fulfillment of the requirements for the degree in Master of Engineering Science  
© Bethany A. Turowec 2013

Follow this and additional works at: <https://ir.lib.uwo.ca/etd>

 Part of the [Biomaterials Commons](#), [Polymer Chemistry Commons](#), and the [Polymer Science Commons](#)

---

### Recommended Citation

Turowec, Bethany A., "Butyl Rubber-Aliphatic Polyester Graft Copolymers for Biomedical Applications: Synthesis and Analysis of Chemical, Physical and Biological Properties" (2013). *Electronic Thesis and Dissertation Repository*. 1313.  
<https://ir.lib.uwo.ca/etd/1313>

This Dissertation/Thesis is brought to you for free and open access by Scholarship@Western. It has been accepted for inclusion in Electronic Thesis and Dissertation Repository by an authorized administrator of Scholarship@Western. For more information, please contact [wlsadmin@uwo.ca](mailto:wlsadmin@uwo.ca).

BUTYL RUBBER-ALIPHATIC POLYESTER GRAFT COPOLYMERS FOR  
BIOMEDICAL APPLICATIONS: SYNTHESIS AND ANALYSIS OF CHEMICAL,  
PHYSICAL AND BIOLOGICAL PROPERTIES

(Thesis format: Monograph)

by

Bethany Turowec

Graduate Program in Biomedical Engineering

A thesis submitted in partial fulfillment  
of the requirements for the degree of  
Master of Engineering Science

The School of Graduate and Postdoctoral Studies  
The University of Western Ontario  
London, Ontario, Canada

© Bethany Turowec, 2013

## Abstract

Biomaterials can be used in a wide variety of medical applications owing to their breadth of characteristics that can be imparted by varying their chemical structures. Butyl rubber (IIR), which is a copolymer of isobutylene (IB) and small percentages of isoprene (IP), is particularly attractive as a biomaterial because of its elastomeric mechanical properties, biocompatibility, impermeability and high damping characteristics. IIR is typically vulcanized through chemical-based crosslinking mechanisms. However, these methods are not acceptable for biological applications. This thesis focuses on the synthesis of IIR-polyester graft copolymers by grafting biodegradable and biocompatible polyesters including poly(caprolactone) (PCL) and poly(D,L-lactide) (PDLLA) to the IIR backbone, and on the study of their properties. These graft copolymers were synthesized by the grafting of amine-terminated polyesters on a modified IIR backbone having activated carbonate moieties. The resulting copolymers with varying polyester content were characterized by a wide range of chemical techniques including nuclear magnetic resonance and infrared spectroscopic methods as well as size exclusion chromatography. IIR-polyester copolymers displayed an increase in Young's modulus (E) and ultimate tensile strength (UTS) relative to IIR, while maintaining cell-biomaterial interactions and non-toxicity. Despite significant polyester content, the copolymers did not exhibit any significant degradation, even in 5 M NaOH at 37°C. Overall, this study reveals how the properties of IIR can be readily tuned through the preparation of graft copolymers and provides a comprehensive evaluation of these properties for their further study in biomedical applications.

## Keywords

butyl rubber, biodegradable polymers, poly(caprolactone), poly(lactide), graft copolymer, thermoplastic elastomer, ultimate tensile strength

## Acknowledgments

I would like to thank Dr. Elizabeth Gillies for her input, guidance and motivation throughout my graduate studies. It was her patience, as well as continual optimism that drove me through to completion of this project. Furthermore, the breadth of skills and knowledge that I attained in the Gillies lab has increased my analytical thinking and problem-solving abilities that will be applicable in future endeavours. I would also like to thank LANXESS Inc. for their financial and research contributions. Although many LANXESS Inc. employees were involved in this project, each individual's input was greatly appreciated and provided a positive input toward goal completion. Particular acknowledgment is given to Lorenzo Ferrari for his continued support throughout the duration of the Gillies lab involvement with LANXESS Inc.

Next, some of the greatest help and support received stemmed from fellow colleagues, both past and present, of the Gillies lab. It was because of their knowledge and helpful attitudes that not only provided the avenues necessary to complete this degree, but also made the duration fun, positive and exciting. I would like to specifically thank Solmaz Karamdoust for her constant help concerning any aspect of the butyl rubber project, as well as her and Rasoul Soleimani for obtaining DSC data, Ryan Amos for cell culture training, Ryan McBride for help analyzing and generating SEC traces for the degradation study and Aneta Borecki, the lab technician, for collecting SEC data.

Thank you to the examiners, Dr. Amin Rizkalla, Dr. Joe Gilroy and Dr. JunYang that have taken time to read and consider this thesis. I would also like to thank support staff at UWO: Dr. Mat Willans (NMR), Dr. Heng-Yong Nie (AFM training), Dr. Paul Ragona and group (training and equipment usage), Nicole Bechard and Karen Nygard (Biotron microscopy), chemstores staff and the Biomedical Engineering department.

Finally, I would like to thank my family and friends, but especially my parents, Sonia and Tony Turowec. I am forever grateful for your resounding love, support and advice and cannot imagine life without your blessings.

# Table of Contents

Abstract.....	ii
Acknowledgments.....	iii
Table of Contents.....	iv
List of Tables.....	vii
List of Figures.....	viii
List of Schemes.....	xiv
List of Equations.....	xvi
List of Abbreviations.....	xvii
List of Appendices.....	xxi
1 Introduction.....	1
1.1 Polymers and their Importance as Biomaterials.....	1
2 Background and Literature Review.....	3
2.1 Polymers as Biomaterials.....	3
2.2 Natural Polymers.....	3
2.2.1 Collagen.....	4
2.2.2 Chitosan.....	5
2.2.3 Hyaluronic Acid.....	5
2.2.4 Applications.....	6
2.3 Synthetic Polymers.....	9
2.3.1 Biodegradable.....	9
2.3.2 PIB and IIR Copolymers.....	17
2.4 Applications of IIR Materials.....	28
2.5 Evaluation of Biomaterials.....	31
2.5.1 Chemical Characterization.....	31

2.5.2	Physical Characterization.....	32
2.5.3	Biological Characterization .....	45
2.6	Thesis Objectives .....	51
3	Results and Discussion.....	53
3.1	Synthesis and Chemical Characterization of IIR-PCL Copolymers.....	53
3.1.1	ROP of $\epsilon$ -caprolactone from the IIR Backbone .....	53
3.1.2	Grafting of PCL onto the IIR Backbone .....	57
3.2	Grafting of PDLLA onto the IIR Backbone .....	65
3.2.1	PDLLA Functionalization.....	65
3.2.2	IIR and PDLLA Grafting .....	68
3.3	Preparation of IIR-PCL/PDLLA Blends.....	71
3.4	Physical Characterization of Graft Copolymers .....	72
3.4.1	Atomic Force Microscopy .....	72
3.4.2	Water Contact Angle Measurements .....	78
3.4.3	Tensile Testing.....	80
3.5	Degradation Study of IIR-PCL/PLA Graft Copolymers .....	88
3.5.1	Mass Evolution and Scanning Electron Microscopy .....	88
3.5.2	Size Exclusion Chromatography.....	95
3.6	Bioassays and Compatibility.....	99
3.6.1	Cell Growth on Polymer Films .....	99
3.6.2	MTT Toxicity Assay.....	103
4	Materials and Methods.....	105
4.1	General Procedures and Materials .....	105
4.2	Graft Copolymer Synthesis and Chemical Characterization .....	106
4.2.1	Synthesis of Polymer 3.8a.....	106
4.2.2	Synthesis of Polymer 3.9a.....	107

4.2.3	Synthesis of Polymer 3.12 .....	108
4.2.4	Synthesis of Graft Copolymer 3.14 .....	108
4.3	Physical Characterization.....	110
4.3.1	Atomic Force Microscopy .....	110
4.3.2	Water Contact Angle.....	110
4.3.3	Scanning Electron Microscopy .....	110
4.3.4	Mechanical Testing of Graft Copolymers.....	110
4.3.5	Degradation Study .....	111
4.4	Biological Characterization .....	112
4.4.1	Cell Growth on Polymer Films .....	112
4.4.2	MTT Toxicity Assay.....	113
5	Conclusions and Future Work.....	115
	References.....	117
	Appendices.....	128
	Curriculum Vitae .....	136

## List of Tables

Table 2.1 – Air loss after automobile driving tests (Reproduced with permission from John Wiley & Sons). <sup>109</sup> .....	21
Table 3.1 – Varying conditions to afford IIR and PCL graft copolymers by ROP of $\epsilon$ -caprolactone from –OH moiety on IIR backbone.....	54
Table 3.2 – PCL thermal properties (provided by Polymer Source <sup>TM</sup> ). .....	58
Table 3.3 – IIR-PCL graft copolymers. ....	63
Table 3.4 – PDLLA homopolymer and IIR-PDLLA graft copolymer: PDLLA content and thermal properties. ....	69
Table 3.5 – Contact angle of PCL and PDLLA homopolymers and copolymers.....	78
Table 3.6 – Tensile data of graft copolymers and IIR. ....	81
Table 3.7 – Tensile data of polymer blends.....	86
Table 4.1 – Modified protocol adapted from ISO 10993 Technical Committee. (2007). International Organization for Standardization (ISO) .....	114



## List of Figures

Figure 2.1 – Common tripeptide sequence of collagen composed of glycine (Gly), proline (Pro) and hydroxyproline (Hyp) leading to helical structure. (Reprinted from Progress in Polymer Science, 35/4, Puppi <i>et. al.</i> , Polymeric materials for bone and cartilage repair (403-440). Copyright (2010), with permission from Elsevier.....	4
Figure 2.2 – Structure of chitosan.....	5
Figure 2.3 – Chemical structure of hyaluronic acid.....	6
Figure 2.4 – Structural representations of diisocyanates. ....	10
Figure 2.5 – Chemical structures of various POEs. ....	11
Figure 2.6 – Chemical structures of PDLA (S-enantiomer), PLLA (R-enantiomer), PDLLA (racemic mixture) and PCL.....	14
Figure 2.7 – Molecular weight changes for a porous PCL structure (triangle) and a linear PCL structure (square). Reproduced with permission from Taylor & Francis, 2007.....	16
Figure 2.8 – Commercialized IIR production: general IIR slurry polymerization (Reproduced with permission from John Wiley & Sons, 1990). <sup>109</sup> .....	19
Figure 2.9 – Isoprene unit enters chain predominantly in trans-1,4 configuration.....	19
Figure 2.10 – Monomer-concentration dependence on number of active sites and styrene conversion (left); monomer-concentration dependence on MW of grafted PS and MW of PS homopolymer (Biomaterials, 29, 2008, 448-460 © 2007 Elsevier Ltd. with kind permission from Springer Science and Business Media). ....	27
Figure 2.11 – Fluorescence confocal microscopy images following adsorption of a rhodamine-fibrinogen conjugate. PEO content: a) 2%, b) 4%, c) 6%, d) 12%, e) 24% and f) 34% (Reprinted with permission from <i>Macromolecules</i> 2011, 44, 6405. Copyright (2011) American Chemical Society). ....	29

Figure 2.12 – Cartoon representation of PIB-b-PS showing elastomeric entanglements (PIB) and hard segments (PS) (Reprinted from Biomaterials, 29/4, Pinchuk <i>et. al.</i> , Medical applications of poly(styrene- <i>block</i> -isobutylene- <i>block</i> -styrene) (“SIBS”) (448-460). Copyright (2008), with permission from Elsevier).....	30
Figure 2.13 – Contact angle measurement ( $\theta_c$ ) and interphase-energy between 3 phases (values in Young’s equation found below).....	33
Figure 2.14 – Temperature dependence of stiffness of typical thermoplastic elastomers (Reprinted from Handbook of Thermoplastic Elastomers, 1 <sup>st</sup> Edition, Drobny, Jiri George, Introduction (1-7). Copyright (2007), with permission from Elsevier). <sup>58</sup> .....	37
Figure 2.15 – Instron (3300 series) tensile testing instrument.....	39
Figure 2.16 – Definitions of uniaxial stress, strain and elastic deformation. (Reprinted from Nanomaterials, Nanotechnologies and Design: An Introduction for Engineers and Architects, 1st Edition, Ashby, Michael F., Chapter 4 – Material Classes, Structure and properties. Copyright (2009), with permission from Elsevier). <sup>189</sup> .....	41
Figure 2.17 – Stress strain curve for a polymer. Definitions of uniaxial stress, strain and elastic deformation. (Reprinted from Nanomaterials, Nanotechnologies and Design: An Introduction for Engineers and Architects, 1st Edition, Ashby, Michael F., Chapter 4 – Material Classes, Structure and properties. Copyright (2009), with permission from Elsevier). <sup>189</sup> .....	42
Figure 2.18 – Material property charts showing: a) Young’s modulus and its relation to material density; b) Young’s modulus and material strength to defined the yield strain ( $\sigma_y/E$ ), where a material no longer behaves elastically. (Reprinted from Nanomaterials, Nanotechnologies and Design: An Introduction for Engineers and Architects, 1st Edition, Ashby, Michael F., Chapter 4 – Material Classes, Structure and properties. Copyright (2009), with permission from Elsevier). <sup>189</sup> .....	44
Figure 2.19 – PCL and PCL-Col (collagen) materials: confocal scanning laser microscopies showing differences in cell proliferation on different surfaces (Reprinted from Biomaterials,	

25/11, Cheng and Teoh, Surface modification of ultra thin poly ( $\epsilon$ -caprolactone) films using acrylic acid and collagen (1991-2001). Copyright (2003), with permission from Elsevier).. 46

Figure 2.20 – Morphologies of hMSCs cultured on various substrates: B) glass control; C) PLCL; D) AAc-PLCL and E) gelatin-AAc-PLCL. Scale bar = 200  $\mu\text{m}$  (Reprinted with permission from Shin, Y. M.; Kim, K.-S.; Lim, Y. M.; Nho, Y. C.; Shin, H.

*Biomacromolecules* 2008, 9, 1772. Copyright 2008 American Chemical Society). ..... 47

Figure 2.21 – (a-f) Myoblasts stained for vinculin (light speckles), F-actin (outer periphery) and nuclei, scale bar = 50  $\mu\text{m}$ . (a) 4 h after seeding on glass coverslip control, (b) 4 h after seeding on C500 surface, (c) 4 h after seeding on C6000 surface, (d) 12 h after seeding on glass coverslip control, (e) 12 h after seeding on C500 surface, and (f) 12 h after seeding on C6000 surface (Reprinted with permission from Dugan, J. M.; Gough, J. E.; Eichhorn, S. J. *Biomacromolecules* 2010, 11, 2498, Copyright 2010 American Chemical Society). ..... 48

Figure 2.22 – Confocal microscopy images of C2C12 cells adhered to control and copolymer surfaces: a) glass (control); b) IIR (control); c) 18wt% PEO ; d) 32wt% PEO; e) 65 wt% PEO; f) 83 wt% PEO. Nuclei (dark inner portion) and F-actin fibres (lighter periphery) with image area = 0.22 x 0.22 mm (Reprinted with permission from John Wiley & Sons, 2013). 49

Figure 3.1 – NMR spectra showing: a) hydroxylated IIR; b) 50 wt% IIR-PCL graft copolymer following methanol precipitation (label k denotes terminal methylene PCL); c) second precipitation in acetone of the same polymer from b), confirming a decrease in PCL content to 16 wt% (label k denotes terminal PCL methylene). ..... 55

Figure 3.2 – SEC trace for 50 wt% PCL shows free homopolymer. 50 wt% PCL (post-purification) trace reveals homopolymer removal achieved with secondary precipitation. Detection was based on differential refractive index..... 56

Figure 3.3 – PCL (900 g/mol) functionalization (with k referring to the terminal methylene): a) 3.7a; b) 3.8a; c) 3.9a. .... 59

Figure 3.4 – SEC traces of PCL derivatives throughout the functionalization process: a) 3.7a – 3.9a (900 g/mol); b) 3.7b – 3.9b (3500 g/mol). ..... 59

Figure 3.5 – <sup>1</sup> H NMR spectra (CDCl <sub>3</sub> , 600MHz) of a) activated IIR; b) copolymer 3.15; and c) copolymer 3.16 showing how PCL content can be determined based on the relative intensities of PCL to PIB, as well as reaction conversion determination based on peaks from 4.8-5.3 ppm. ....	62
Figure 3.6 – SEC traces for: ungrafted IIR (3.1) and each IIR-PCL graft copolymer (3.14-3.16). ....	63
Figure 3.7 – Schematic depicting PDLLA functionalization: a) 3.10 (2800 g/mol), starting material; b) 3.11, <i>t</i> -BOC protected β-alanine derivative; c) 3.12, amine-liberated derivative. In 3.10-3.12, f represents the terminal methylene. ....	66
Figure 3.8 – SEC traces elucidating functionalization of PDLLA 3.10-3.12. ....	67
Figure 3.9 – PDLLA content in copolymer 3.17: determined via integration corresponding to PDLLA multiplet from 5.13-5.23 ppm and PIB singlet at 1.41 ppm. ....	69
Figure 3.10 – SEC traces of ungrafted IIR (polymer 3.1) and IIR-PDLLA graft copolymer (3.17). ....	70
Figure 3.11 – Topography of copolymers: a) 3.14; b) 3.15; c) 3.16; d) 3.17. ....	73
Figure 3.12 – Phase contrast of copolymers: a) 3.14; b) 3.15; c) 3.16; d) 3.17. ....	74
Figure 3.13 – AFM analysis of copolymer 3.16. Before annealing: a) topography; b) phase contrast. After annealing: c) topography; d) phase contrast. ....	75
Figure 3.14 – Topography images of IIR-polyester blends: a) 15 wt% PCL; b) 32 wt% PCL; c) 44 wt% PCL; d) 30 wt% PDLLA. ....	76
Figure 3.15 – Phase contrast of polymer blends: a) 15 wt% PCL; b) 32 wt% PCL; c) 44 wt% PCL; d) 30 wt% PDLLA. ....	77
Figure 3.16 – Stress-strain curve for: a) IIR; b) copolymer 3.14; c) copolymer 3.15; d) copolymer 3.16; e) copolymer 3.17. ....	81

Figure 3.17 – Stress vs Strain of a variety of materials (with permission to reprint from MIT OpenCourseWare, <a href="http://flic.kr/p/66XeQc">http://flic.kr/p/66XeQc</a> ).....	82
Figure 3.18 – Thermoplastic PURs with varying soft segment contents. (Reprinted from Polymer, 49/19, Xu <i>et. al.</i> , Morphology and properties of thermoplastic polyurethanes with dangling chains in ricinoleate-based soft segments (4248-4258). Copyright (2008), with permission from Elsevier). <sup>244</sup> .....	83
Figure 3.19 – Toughness-Modulus plot for current implant materials and the mechanical regions for orthopedic hard tissue, orthopedic soft tissue, and cardiovascular tissue. (Reprinted with permission from Taylor & Francis, 2013). <sup>246</sup> .....	85
Figure 3.20 – Stress-strain curve for: a) 15 wt% PCL blend; b) 32 wt% PCL blend; c) 44 wt% PCL blend; d) 30 wt% PDLLA blend. ....	85
Figure 3.21 – Mass loss of copolymers 3.14-3.16, PCL and IIR controls.....	89
Figure 3.22 – Mass loss of copolymer 3.17 as well as PDLLA and IIR controls.....	90
Figure 3.23 – SEM imaging taken at 100X magnification under variable pressure mode at $T_0$ and 4 months of: a) and b) IIR; c) and d) copolymer 3.14; e) and f) copolymer 3.15; g) and h) copolymer 3.16. ....	91
Figure 3.24 – SEM imaging taken at 100X magnification under variable pressure mode at $T_0$ and 2 months of: a) and b) copolymer 3.17. Macroscopic images of $T_0$ -2 months of: c) copolymer 3.17. ....	92
Figure 3.25 – Successive macroscopic images representing $T_0$ , 1 month, 2 months, 3 months and 4 months of: a) IIR control; b) copolymer 3.14; c) copolymer 3.15; d) copolymer 3.16. ....	93
Figure 3.26 – MW data for IIR control as well as copolymer 3.14, 3.15, 3.16 and 3.17: a) change in $M_n$ ; b) change in $M_w$ .....	95
Figure 3.27 – MW profiles elucidating each time point over the 4 month study period for: a) IIR control; b) copolymer 3.14; c) copolymer 3.15; d) copolymer 3.16. ....	96

Figure 3.28 – MW profile elucidating each time point over the 2 month study period for copolymer 3.17. ....	97
Figure 3.29 – Growth of murine myoblast cells on: a) glass; b) IIR; c) PCL; d) PDLLA Cell imaging of copolymers: e) 3.14; f) 3.15; g) 3.16; h) 3.17.....	100
Figure 3.30 – Cell adhesivity quantified by determining average cell concentrations for each substrate. ....	102
Figure 3.31 – MTT cytotoxicity assay performed on: a) graft copolymers 3.14-3.16; b) graft copolymer 3.17. ....	104

## List of Schemes

Scheme 2.1 – Hydrolysis of PCL to 6-hydroxylcaproic acid and acetyl coenzyme A intermediates followed by elimination from the body through the citric acid cycle. ....	12
Scheme 2.2 – Mechanism of stannous octoate polymerization of PCL: 1/2 – formation of stannous alkoxide initiator; 3 – deactivation of catalyst; 4 – coordination/insertion of monomer; 5 – chain transfer of active polymerizing centre to alcohol. ....	13
Scheme 2.3 – Cationic polymerization of IB governed by initiation, propagation and termination. ....	20
Scheme 2.4 – Vulcanization of IIR: a) sulfur-based crosslinking; b) dioxime curing; c) general structure of resin capable of vulcanization.....	23
Scheme 2.5 – IIR bromination followed by isomerization and HX elimination. ....	24
Scheme 2.6 – Reaction schematic elucidating SIBS production via bifunctional HDCE initiator.....	25
Scheme 2.7 – Synthesis of IIR-PEO graft copolymers.....	26
Scheme 3.1 – Epoxidation followed by hydroxylation of IIR with 2.2mol% IP and subsequent ROP of $\epsilon$ -caprolactone from IIR backbone.....	53
Scheme 3.2 – Synthesis of <i>t</i> -BOC-protected $\beta$ -alanine anhydride. ....	57
Scheme 3.3 – Functionalization of PCL (3.7a/b) by first reacting with BOC-protected $\beta$ -alanine (3.6) to produce the protected derivative (3.8a/b), followed by deprotection with TFA ( $n = 8$ for 900 g/mol PCL, 3.7a, initiated with ethylene glycol derivative and $n = 31$ for 3500 g/mol PCL, 3.7b initiated with ethanol).....	58
Scheme 3.4 – <i>p</i> -nitrophenyl chloroformate (PNPC) activated rubber synthesis. ....	61
Scheme 3.5 – Synthesis of PCL graft copolymers: 3.14 – 15 wt% PCL ( $n=8$ ); 3.15 – 32 wt% PCL ( $n=31$ ); 3.16 – 44 wt% PCL ( $n=31$ ).....	61

Scheme 3.6 – Functionalization of 3.10 by first reacting with BOC-protected $\beta$ -alanine (3.6) to afford 3.11, followed by deprotection with TFA (3.12). .....	65
Scheme 3.7 – Synthesis of PDLLA Graft copolymer: 3.17 – 30 wt% PDLLA. ....	68



## List of Equations

Equation 1 – Definition of polydispersity index where $M_n$ is the total weight of the sample divided by the number of molecules (arithmetic mean) and $M_w$ fairly accounts for the contributions of different sized chains.....	32
Equation 2 – where $\Theta$ = measured contact angle and $\gamma$ is the surface tension of the solid-gas (SG), solid-liquid (SL) and liquid-gas (LG) interface.....	33
Equation 3 – Young’s modulus determination for a material at a given strain and stress.....	39
Equation 4 – Linear relationship relating the shear strain, $\gamma$ to the shear stress, $\tau$ .....	40
Equation 5 – Linear relationship showing proportionality between the dilatation, $\Delta$ and pressure, $p$ . .....	40
Equation 6 – Definition of Poisson’s ratio where $\epsilon_t$ is the transverse strain and $\epsilon$ is the axial strain.....	40
Equation 7 – Relation between Young’s modulus (E), shear modulus (G) and bulk modulus (K). .....	41
Equation 8 – Definition of plastic strain. ....	42
Equation 9 – Where <b><i>mia</i></b> = average mass of initial 3 discs for a given time point and <b><i>mfa</i></b> = average mass of final 3 discs for a given time point.....	111

## List of Abbreviations

( <sup>1</sup> H) NMR	hydrogen nuclear magnetic resonance spectroscopy
AFM	atomic force microscopy
BDR	butadiene rubber
BIIR	bromo-butyl rubber
BOC	di- <i>tert</i> -butyl dicarbonate
br. s	broad singlet
CA	cyanoacrylate
CIIR	chloro-butyl rubber
DAPI	4'-6-diamidino-2-phenylindole dihydrochloride
DCM	dichloromethane
DES	drug eluting stent
DMEM	Dulbecco's Modified Eagle Medium
DPNR	deproteinized natural rubber
DSC	differential scanning calorimetry
E	Young's modulus
ECM	extracellular matrix
FTIR	fourier transform infrared spectroscopy
G	shear modulus
GPC	gel permeation chromatography
HA	hyaluronic acid
HSD	honestly significant difference
IB	isobutylene
IIR	butyl rubber
IP	isoprene

J	coupling constant
K	bulk modulus
<i>m</i> -CPBA	meta-chloroperoxybenzoic acid
$M_n$	number-average molecular weight
MSA	methanesulfonic acid
MTT	3-(4,5-Dimethylthiazol-2-yl)-2,5-Diphenyltetrazolium Bromide
$M_w$	weight-average molecular weight
MW	molecular weight
$M_z$	z-average molecular weight
$M_v$	viscosity molecular weight
NBR	acrylonitrile butadiene rubber
NR	natural rubber
p	pressure
PBD	poly(butadiene)
PBS	phosphate buffered saline
PCL	poly(caprolactone)
PDI	polydispersity index
PDLA	poly(D-lactide)
PDLLA	poly(D,L-lactide)
PEG	poly(ethylene glycol)
PEO	poly(ethylene oxide)
PIB	poly(isobutylene)
PLLA	poly(L-lactide)
PMMA	poly(methyl methacrylate)
PNPC	4 ( <i>para</i> )-nitrophenyl chloroformate

POE	poly(ortho esters)
PS	poly(styrene)
PUR	poly(urethane)
PVC	poly(vinyl chloride)
RB-402	butyl rubber (LANXESS Inc. derivative)
ROP	ring-opening polymerization
RT	room temperature
SBR	styrene butadiene rubber
SDS	sodium lauryl sulfate
SEC	size exclusion chromatography
SEM	scanning electron microscopy
SIBS	styrene-isobutylene-styrene
SMP	shape memory polymer
TE	tissue engineering
TFA	trifluoroacetic acid
T <sub>g</sub>	glass transition temperature
THF	tetrahydrofuran
T <sub>m</sub>	melt transition temperature
TPE	thermoplastic elastomer
UTS	ultimate tensile strength
WCA	water contact angle
wt%	weight percentage
$\gamma$	shear strain
$\Delta$	dilatation
$\epsilon$	strain

$\epsilon_b$	elongation at break
$\epsilon_t$	lateral strain
$\nu$	Poisson's ratio
$\sigma$	stress
$\sigma_{el}$	elastic limit
$\sigma_y$	yield strength
$\tau$	shear stress

## List of Appendices

Appendix A – <sup>1</sup> H NMR depicting functionalization of 3.7b: a) initial homopolymer; b) reacted with <i>t</i> -BOC-protected β-alanine (3.8b); c) and deprotected with TFA (3.9b). .....	128
Appendix B – <sup>1</sup> H NMR showing PCL content of: a) copolymer 3.16 (44 wt% PCL) and b) copolymer 3.15 (32wt% PCL). .....	129
Appendix C – FTIR of: a) 3.8a and 3.9a; b) 3.11 and 3.12. ....	130
Appendix D – FTIR of: a) copolymer 3.14; b) copolymer 3.15. ....	131
Appendix E – FTIR of: a) copolymer 3.16; b) copolymer 3.17. ....	132
Appendix F – DSC traces of: IIR-PCL copolymer after 1 <sup>st</sup> precipitation; IIR-PCL copolymer after a 2 <sup>nd</sup> precipitation into acetone, ridding of free homopolymer as evidenced by disappearance of the second T <sub>m</sub> at 53°C. ....	133
Appendix G – DSC trace depicting the two T <sub>g</sub> s of copolymer 3.17. ....	133
Appendix H – DSC traces depicting T <sub>g</sub> and T <sub>m</sub> of IIR-PCL graft copolymers: a) copolymer 3.14; b) copolymer 3.15; c) copolymer 3.16. ....	134
Appendix I – DSC traces depicting T <sub>g</sub> and T <sub>m</sub> of IIR-PCL/PLA blends. ....	134
Appendix J – Raw data coinciding with Figure 3.21 for the degradation study of IIR-PCL copolymers and IIR control. ....	135
Appendix K – Raw data coinciding with Figure 3.22 for the degradation study of IIR-PDLLA copolymer and IIR control. ....	135

# Chapter 1

---

## 1 Introduction

### 1.1 Polymers and their Importance as Biomaterials

Biomaterials possess the ability to perform with an appropriate host response in specific applications.<sup>1</sup> They are used extensively in a wide variety of applications, ranging from cardiovascular, dental and neural implants to orthopaedic prosthetics and drug delivery systems. Biomaterials have always been important as vehicles for the treatment of disease, thereby constantly improving health care. Early examples dating back thousands of years ago are metals and wood for teeth replacement and glass for eyeball prosthetics. However, the discovery of synthetic polymers such as poly(methacrylates) and poly(urethanes) led to a much broader range of application possibilities. Moreover, naturally occurring materials such as collagen are also being developed for better applicability in biological systems.

Although biomaterials perhaps play a role in the lives of many individuals, there are several difficulties involved with their use. The main issues stem from deficiencies in understanding physical, chemical and biological responses that a given biomaterial may elicit in biological systems, as well as the lack of proper performance in a specific application.<sup>2</sup> Since many biomaterials were not originally designed to be used in a clinical setting, taking off-the-shelf products has proved to be problematic.<sup>3</sup> Examples of such consist of dialysis tubing derived from cellulose acetate, Dacron for synthesis of vascular grafts and poly(urethane) for the fabrication of artificial hearts. The aforementioned applications were unsuccessful as cellulose acetate caused platelet activation, Dacron grafts were limited to large-diameter vessel applications and poly(urethane) did not supply sufficient blood-material interactions, respectively.<sup>4</sup>

In order to reduce issues related to using materials in applications for which they were not specifically designed, research has been directed toward modifying chemical structures to improve their mechanical properties, degradability and biocompatibility.<sup>5</sup> Modern biomaterial production involves thorough understanding of cell-polymer

interactions in order to prevent or minimize undesirable cellular responses.<sup>6</sup> Applications such as polymer-coated stents for drug, protein and hormone delivery, tissue engineering (TE) and other polymer/cell combinations such as artificial corneas, cartilage and bone, makes it very important to understand biological response.<sup>5</sup> Biomaterials have made great impacts on medicine and current technology and will therefore impact biomedical application advancements. As the aging population of developed countries continues to grow, the demand for biomedical products to enhance life quality and longevity will proportionally increase.

The focus of this thesis will be on preparing new potential biomaterials based on butyl rubber (IIR)-polyester copolymers. The incorporation of an elastomeric component in the biomaterial is especially important when considering its ability to mimic soft tissues. Because humans predominantly consist of soft tissues, biomaterials that possess similar mechanical and viscoelastic properties have potential for application in a multitude of areas ranging from vascular prostheses (blood-interfacing implants) to breast implants (non-blood-interfacing). Although elastomers are attractive due to their compliance with soft or cardiovascular tissues, mechanical property enhancements may be required for various applications. Therefore, in order to provide strength and rigidity, the incorporation of polyesters (hard phase) with IIR (soft phase) will provide physical crosslinks. The properties presented by these copolymers may be analogous to thermoplastic elastomers (TPE). TPEs are typically composed of a phase which is hard at ambient temperature, while the other is elastomeric. Phases are most commonly bonded chemically through block/graft copolymerization.<sup>7</sup> Without the hard phase, the elastomer phase would flow freely, rendering it unsuitable for biomedical applications requiring rigidity. For example, elastin and collagen are important components of various arteries. Although functions of such soft tissues vary, it is the combination of the elastomeric elastin with harder collagen that provides appropriate mechanical properties. With this understanding, it will be interesting to investigate how the properties of IIR can be varied chemically, physically and biologically to afford potential biomaterials.



## Chapter 2

---

### 2 Background and Literature Review

#### 2.1 Polymers as Biomaterials

Polymers are particularly interesting for use as biomaterials; their chemical, physical and biological properties vary across a wide variety of structures, rendering them useful in many different applications. In addition, through modification of the polymer backbone, these properties can be specifically tuned. However, it is important to understand how each polymer or polymeric system will impact its performance. Since applications can range from soft tissue/organ replacement, drug delivery, wound dressings, to even reconstruction of bone deficiencies, investigating a range of varying polymers to facilitate new materials for biomedical applications has become increasingly apparent.

#### 2.2 Natural Polymers

Biomedical applications involving the use of natural polymers such as collagen, chitosan and alginate date back thousands of years. Natural polymers possess the obvious advantages associated with biocompatibility; they do not elicit inflammatory responses or other unsuitable side-effects that may result through the use of synthetic systems.

Although synthetic polymers are desirable as their properties can be tuned and controlled with ease, the inherent issues stemming from biocompatibility still present natural polymers as viable candidates for use as biomaterials.<sup>8</sup> There are a wide variety of natural polymers, leading to different avenues and applications. Proteins, such as collagen and silk fibroin; polysaccharides, such as chitosan, hyaluronic acid, alginates, dextrans and starch-based materials; and microbial polyesters, such as polyhydroxyalkanoates are all viable natural materials that are under current investigation for biomedical usage.

However, focus will be directed toward some notable materials including collagen, chitosan and hyaluronic acid.

## 2.2.1 Collagen

Collagen is the most abundant protein in the body, which is owed to its high composition in both skin and other musculoskeletal tissues.<sup>9</sup> Type-I collagen (skin, tendon and bone) is the most prevalent in mammals, providing the structural integrity and architecture.<sup>8</sup> Type-I is composed of three polypeptide subunits consisting of similar amino acid compositions: 33% glycine (Gly), 25% proline (Pro) and 25% hydroxyproline (Hyp). These subunit chains allow collagen to undergo transcription, translation and post-translational modification processes in fibroblasts and osteoblasts. Since these amino acid subunits form polypeptides in typical sequences, it causes collagen to have a helical structure, thereby providing it with its mechanical strength and resiliency (Figure 2.1).<sup>10</sup> Moreover, its flexibility can be tuned by increasing the glycine content if it is required for a specific application. It is because of this mechanical strength that utilizing collagen for biomedical applications such as scaffolds,<sup>11,12</sup> drug-delivery systems,<sup>13,14</sup> shields for contact lenses,<sup>15</sup> sponges,<sup>16</sup> hydrogels,<sup>17,18</sup> nanoparticles<sup>19,20</sup> and skin replacements,<sup>21,22</sup> is advantageous. In addition, its low antigenicity and good cell-binding properties make it attractive for TE applications.<sup>23,24</sup> Collagen sponges have been fabricated for cell and tissue attachment,<sup>25,26</sup> and to also enhance bone formation due to osteoblast differentiation.<sup>27,28</sup> However, because it requires crosslinking agents for certain applications, this may render it unsuitable due to toxic byproducts.

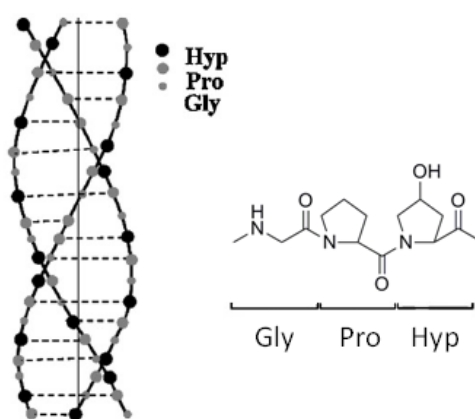


**Figure 2.1 – Common tripeptide sequence of collagen composed of glycine (Gly), proline (Pro) and hydroxyproline (Hyp) leading to helical structure. (Reprinted from Progress in Polymer Science, 35/4, Puppi *et. al.*, Polymeric materials for bone and cartilage repair (403-440). Copyright (2010), with permission from Elsevier.**

## 2.2.2 Chitosan

Chitosan is a linear polyelectrolyte copolymer, which is composed of randomly distributed 2-acetamido-2-deoxy- $\beta$ -D-glucopyranose and N-acetyl-D-glucosamine (chitin) units. Most units in the copolymer consist of the deacetylated version (2-amino-2-deoxy- $\beta$ -D-glucopyranose) making it hydrophilic thereby promoting cell adhesion, proliferation and differentiation (Figure 2.2). Chitosan, like most natural polymers, is biocompatible, and possesses other desirable properties including high charge density, non-toxicity and mucoadhesion, rendering it appropriate for pharmaceutical and cosmetic applications.<sup>8</sup> The chain of chitosan is somewhat stiff, stabilizing a liquid crystalline phase in acetic acid.<sup>29</sup> The predominantly explored applications of chitosan involve non-viral gene delivery due to its cationic nature allowing complex formation with DNA molecules.<sup>30-32</sup> Moreover, chitosan-based products are also appropriate for the delivery of chemotherapeutics such as antibiotics, antiparasitics, anaesthetics and painkillers, via routes involving injectable chitosan hydrogels. Chitosan's novel properties make it an appropriate natural polymer for property modification to result in a viable biomaterial for cell therapy, TE and gene therapy. These TE applications include skin, bone, cartilage, liver, nerve and blood vessel.<sup>33,34</sup> However, its chemical modification cannot correct deficiencies concerning mechanical weakness and instability, incapacity to maintain a predefined shape, as well as impurities affecting material properties.<sup>35</sup>

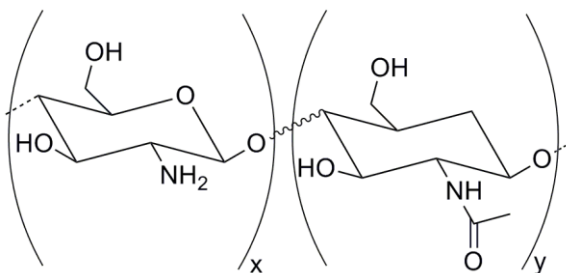


**Figure 2.2 – Structure of chitosan.**

## 2.2.3 Hyaluronic Acid

Hyaluronic acid (HA) is an example of a polysaccharide, which consists of a high molecular weight (MW) and linear backbone. Typically referred to as hyaluronan, this polymer exists as a polyanion with alternating disaccharide units of  $\beta$ -1,3-N-acetyl-D-

glucosamine and glucuronic acid (Figure 2.3). HA is the main component of the extracellular matrix (ECM). Not only does it serve as structural support, but it also interacts with proteins, proteoglycans and other bioactive molecules, thereby contributing to regulating processes such as cell behaviour, inflammation, angiogenesis and healing.<sup>36</sup> Again, good biocompatibility as well as viscoelastic properties render HA attractive for delivery systems, cell encapsulation; but most notably for TE due to its availability and chain size manipulation. Although suitable for ECM remodeling because of cellular interactions, its hydrophilicity does not favour cell attachment and tissue formation. In order to alleviate these deficiencies, conjugation to collagen and fibronectin can be performed to improve cellular interactions.<sup>37</sup>

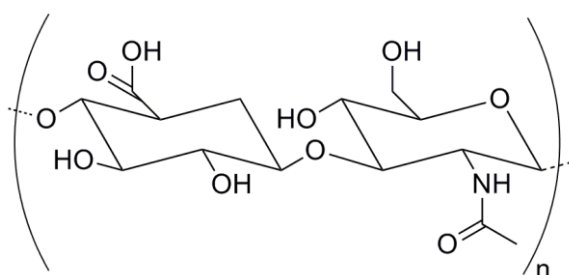


**Figure 2.3 – Chemical structure of hyaluronic acid.**

#### 2.2.4 Applications

Natural polymers are somewhat limited by the properties that they possess. In order to modify their properties, they must be changed in a way that does not incorporate synthetic materials. The advantage of natural polymers is their ability to interact within biological systems in a reproducible and predictive manner; changing their properties through a synthetic means may render these advantages obsolete. Chitosan has been found interesting for a variety of applications, primarily owed to its degradation and solubility, which can be tuned by substituting isobutyl at deacetylated sites without altering its bioactivity.<sup>38</sup> Chitosan does not exhibit foreign body reactions, thus minimizing inflammatory responses, making it attractive for a range of *in vivo* applications.<sup>39</sup> For stent applications, there currently is one major contribution that consists of a self-expanding chitosan stent.<sup>40</sup> The stent employs a highly de-acetylated version (slower degradation),<sup>41</sup> implanted into the vas deferens of rats, displaying

adequate self-expansion. Finally, chitosan has the ability to form a high charge density in weakly acidic solutions, producing cationic polymers. As a result, it can interact with anionic polymers, negatively charged mucous membranes and DNA making it applicable for mucoadhesives, bioadhesive drug delivery systems and for non-viral gene delivery vehicles, respectively.<sup>42-44</sup>

Although collagen does not interact with anionic materials, its properties, including enzymatic degradability and unique physico-chemical, mechanical and biological properties, make it an interesting material for a variety of biomedical applications.<sup>9</sup> Collagen is the main component of the extracellular matrix, presenting it as a strong candidate for TE/engineering applications. Because it is natural and abundant amongst biological systems, it acts as a substrate for cell attachment, proliferation and differentiation. Many applications involving spongy collagen matrices (Promogran<sup>®</sup>),<sup>45</sup> wound dressing materials (Biobrane<sup>®</sup> and Alloderm<sup>®</sup>)<sup>46</sup> and bilayer skin substitutes (Integra<sup>®</sup> Dermal Regeneration Template)<sup>47</sup> have been developed and FDA approved for treatment of ulcer wounds and thermal injuries. In addition, collagen has also been investigated for usage as delivery vehicles for small molecule drugs. Current products (Sulmycin<sup>®</sup>-Implant, Collatamp<sup>®</sup>-G and Septocoll<sup>®</sup>) focus on delivery of the antibiotic gentamicin, resulting in prolonged local exposure with minimal systemic infiltration.<sup>48</sup> However, the main source of collagen for biomedical applications originates from bovine, porcine and equine skin or Achilles tendons. The wide-spread use of these collagen-based biomaterials is therefore unforeseeable because of deficiencies and variations associated with immune responses to materials derived from different species. In order to make these applications realizable, human-sequenced collagen will have to be recombinantly developed.<sup>49</sup>

Lastly, HA has presented itself as a unique biomaterial due to its structure; it is a polysaccharide that is found in most, if not all, vertebrate tissues. HA is versatile, which can be owed to its varying roles in biological processes, including cell migration and differentiation control during embryogenesis, extracellular matrix organization and metabolism and regulation for wound healing and inflammation.<sup>50</sup> Because of these properties, HA has predominantly been studied for wound dressing, TE and drug delivery

applications. More specifically, HA promotes angiogenesis, thereby reducing inflammation<sup>51</sup> and its high degree of chemical functionality allows it to undergo crosslinking,<sup>52</sup> making it appropriate for regulating wound sites and to tailor its degradation rate for drug delivery. However, physical and biological limitations have made HA impractical as a biomaterial due to its low water solubility, rapid resorption, short residence time and anionic surface thereby prohibiting cellular attachment and tissue formation.<sup>53</sup>

## 2.3 Synthetic Polymers

### 2.3.1 Biodegradable

Biodegradable synthetic polymers have been receiving considerable interest as biomaterials; long-term biocompatibility issues with permanent implants has turned the focus towards temporary therapeutic devices for a variety of applications.<sup>9</sup> TE scaffolds, regenerative medicine, drug eluting stents for controlled drug delivery and gene therapy are some examples of emerging biomedical applications where biodegradable synthetic polymers are being investigated.<sup>54-56</sup> When considering degradable polymers for different biomedical applications, it is important to ensure that they are bioresorbable. The polymeric biomaterial is not only biocompatible, but upon degradation, the body can effectively process and remove monomers, oligomers and byproducts.<sup>57</sup>

#### 2.3.1.1 Poly(urethanes)

Poly(urethanes) (PURs) are an important class of polymers that have been used in a range of high-performance materials including films, coatings, adhesives, fibres and elastomers. Although they are biostable and have been extensively investigated for long-term medical implants, their good biological properties, biocompatibility and synthetic versatility has led to the development of biodegradable PURs. There are many different compounds that can be applied to form PURs (by means of a simple polyaddition reaction) therefore material properties are highly versatile.<sup>58</sup> Typical preparations of polyurethanes involve a polyester/polyether diol (soft segment), chain extender and a bulky diisocyanate (hard segment). The multiblock structure is therefore responsible for giving PURs their elastomeric properties.<sup>59</sup>

PURs were not considered to be thermoplastic until 1958, when diphenylmethane-4, 4-diisocyanate (MDI) was incorporated as the bulky diisocyanate.<sup>60</sup> However, in order to realize PURs as biodegradable polymers, common diisocyanates such as MDI and toluene diisocyanate (TDI) cannot be employed due to their inherent toxicity.<sup>9</sup> Incorporation of lysine diisocyanate (LDI) or 1,4-diisocyanatobutane (BDI) can alleviate these issues. Reacting LDI with polyester diols offers a range of applicable properties (Figure 2.4 for structures).<sup>61</sup> For example, peptide components in PURs allow

active moieties (ascorbic acid and glucose) to be introduced into the polymer thereby promoting cell adhesion, viability and proliferation.<sup>62</sup>

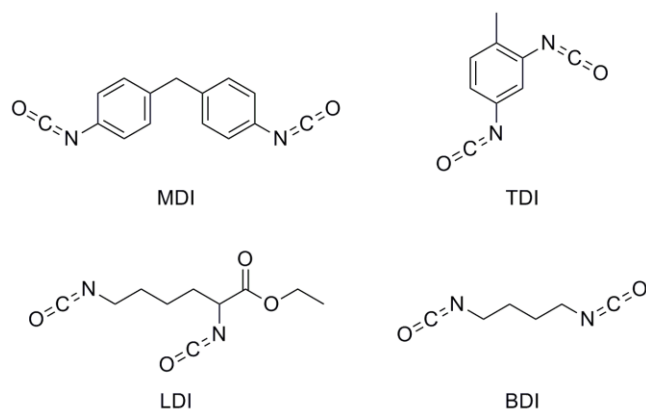


**Figure 2.4 – Structural representations of diisocyanates.**

PURs possess excellent mechanical properties, including high tensile strength and ultimate elongation due to their chemical structure, and because of this structure, can also be processed via extrusion, injection molding and calendaring.<sup>63</sup> The ease of processability makes PURs attractive for use as injectable biodegradable polymers. This has led to applications involving injectable hydrogels, which have been developed to alleviate issues with current surgical techniques. In addition, an injectable LDI-based polyurethane was developed (PolyNova<sup>®</sup>) for orthopaedic applications because of its good mechanical properties and fast self-setting as well as *in vivo* crosslinking ability. Finally, porous scaffolds for TE of bone and cartilage have been proposed by usage of PURs containing poly(caprolactone) PCL or poly(ethylene glycol) (PEG) segments due to superior control over crystallinity (by controlling soft segment MW) and mechanical properties.<sup>64,65</sup> PUR-based scaffolds have also been investigated for both *in vitro* and *in vivo* applications, such as analyzing cell density evolution [which was comparable to biocompatible poly(lactic-*co*-glycolic acid)]<sup>66</sup> and vascularization into dorsal skinfold chambers of mice.<sup>67</sup> Although the scaffolds did not appear to elicit any inflammatory responses, acidic degradation of PURs autocatalyzes the degradation process and byproduct production can lead to *in vivo* inflammatory responses.



### 2.3.1.2 Poly(ortho esters)

The development of poly(ortho esters) (POEs) produced biodegradable polymers higher hydrophobicity, thereby avoiding issues with bulk degradation in drug delivery applications.<sup>1,68</sup> By imparting hydrolytically sensitive backbones, this would limit degradation to very slow surface erosion in aqueous environments. There are four families of POEs, each with varying syntheses to improve on shortcomings of the preceding POEs (Figure 2.5).<sup>69</sup>

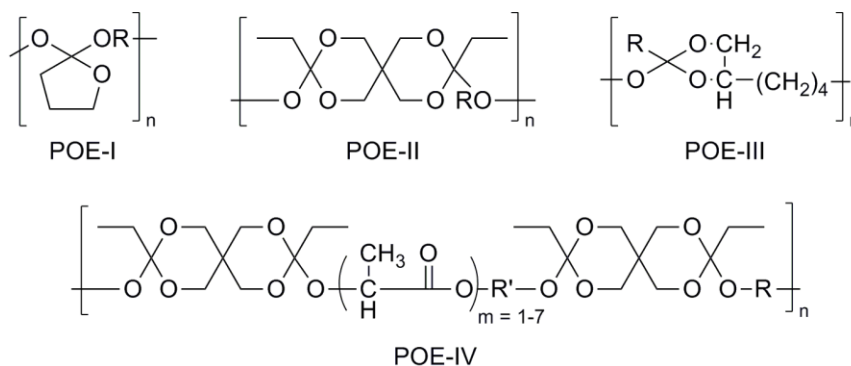


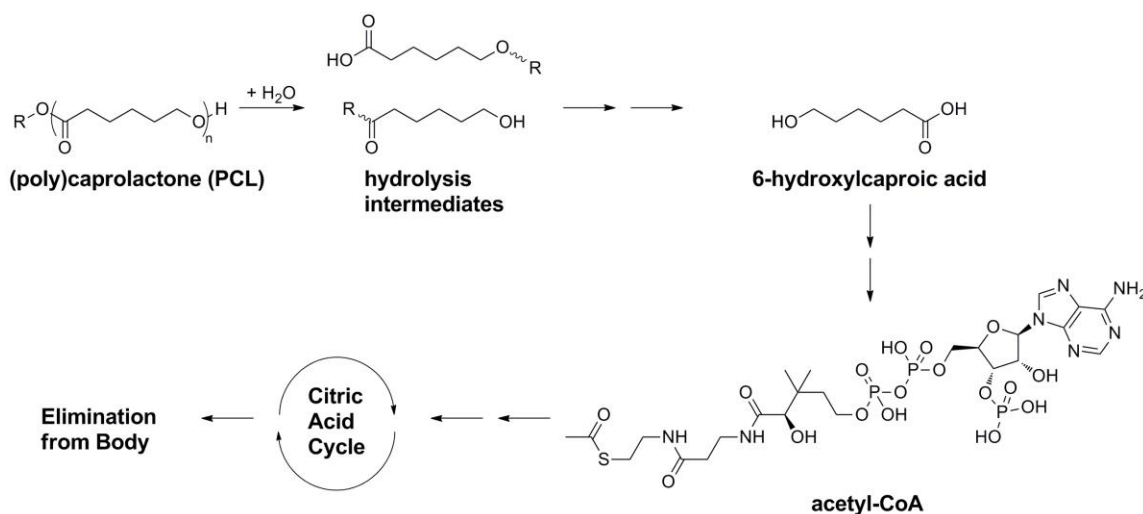
**Figure 2.5 – Chemical structures of various POEs.**

Because of versatility in their synthesis through incorporation of different diols, POEs possess varying degradation rates, levels of pH sensitivity, and glass transition temperatures.<sup>70</sup> For drug release applications, the rate of release depends on the rate of polymer hydrolysis. For example, the development of POE IV has led to the best control in terms of release profile for various therapeutic molecules.<sup>71</sup> With unprecedented control over degradation rate as well as good biocompatibility evaluation of POE IV, research has shifted towards using it as an injectable polymer for ocular applications, treatment of periodontal diseases and estrus synchronization in sheep.<sup>72</sup>

### 2.3.1.3 Aliphatic Polyesters

Polyesters are defined as thermoplastic polymers with hydrolytically labile aliphatic ester linkages throughout their backbone. This class of polymers is interesting due to its diversity and synthetic versatility. These polymers can be prepared from a large range of monomers through ring opening and condensation polymerization, resulting in materials

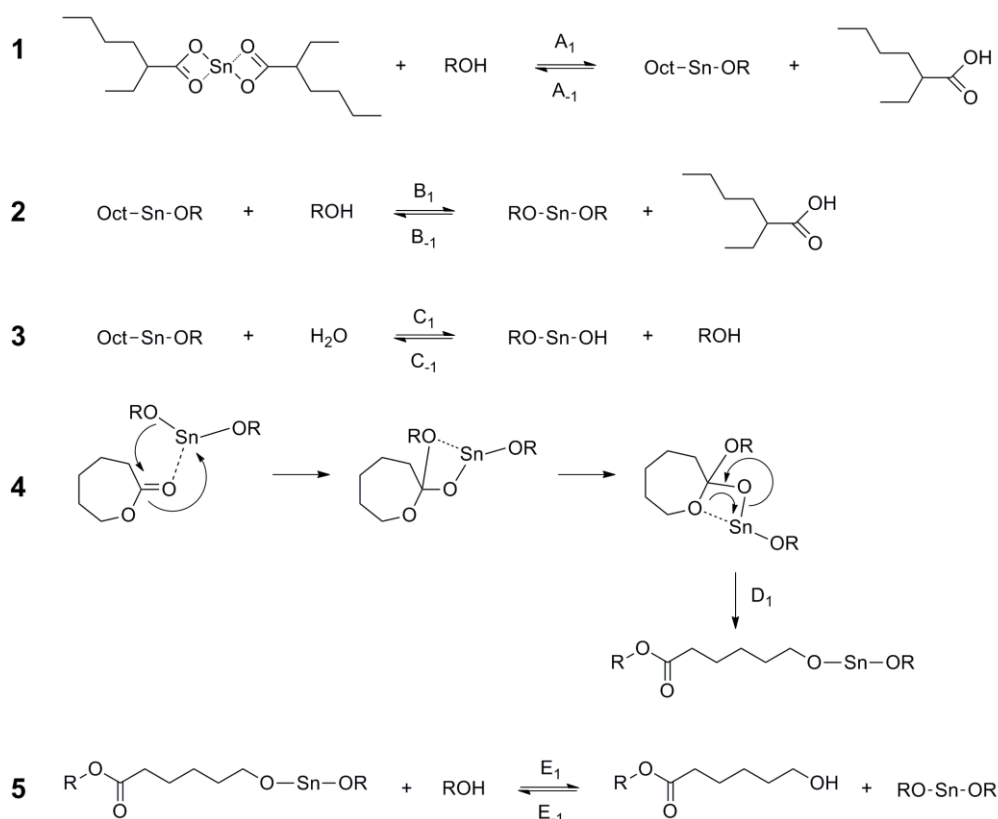
of very different properties. Furthermore, aliphatic polyesters are all biocompatible as well as bioresorbable and FDA approved for a variety of applications.<sup>73,74</sup> Although many polymers have been studied for their potential applicability as biomaterials, polyesters, such as poly(lactide) (PLA) and poly(caprolactone) (PCL) have recently been under extensive investigation due to their exceptional biocompatibility as well as good mechanical properties. In addition, both of these aliphatic polyesters have been shown to generate bioresorbable metabolites during hydrolytic degradation, establishing their high potential for replacing biostable polymers in time-limited applications. For example, during hydrolytic degradation, PCL breaks down into different constituents that are eventually eliminated from the body. It is first broken down into 6-hydroxyl caproic acid, followed by Acetyl coenzyme A, which finally enters the citric acid cycle and is excreted by the body (Scheme 2.1).<sup>75</sup> PLA is also advantageous in terms of degradation byproducts; they are metabolized into CO<sub>2</sub> and water, or are excreted via the kidneys.<sup>76</sup> These materials have therefore been heavily investigated for controlled drug release systems and as orthopaedic implants.<sup>77-79</sup>



**Scheme 2.1 – Hydrolysis of PCL to 6-hydroxylcaproic acid and acetyl coenzyme A intermediates followed by elimination from the body through the citric acid cycle.**

Both PCL and PLA are hydrophobic polymers that can be prepared via ring-opening polymerization (ROP) using a variety of anionic, cationic and coordination catalysts, or even via free-radical ROP.<sup>80</sup> The mechanisms of initiation, coordination/insertion of

monomer, deactivation and chain transfer for PCL with stannous octoate can be visualized in Scheme 2.2. First, an initiator bearing a hydroxyl-functionality (alcohol) is added to react with stannous octoate producing a stannous alkoxide species and ethylhexanoic acid (1). Next, further reaction with a second alcohol equivalent produces the stannous dialkoxide initiator (2); adventitious water will serve as a catalyst deactivator of either alkoxide initiator to a stannous alcohol derivative (3). Reaction of the stannous dialkoxide initiator with monomer by coordination-insertion generates the first actively propagating chain end, consisting of both the initiating alcohol fragment and active propagating centre (4). Either further propagation will occur to grow the PCL chain, or rapid intermolecular exchange of the stannous alkoxide moiety for a proton, thereby establishing a rapid equilibrium between activated and deactivated chain ends (5).



**Scheme 2.2 – Mechanism of stannous octoate polymerization of PCL: 1/2 – formation of stannous alkoxide initiator; 3 – deactivation of catalyst; 4 – coordination/insertion of monomer; 5 – chain transfer of active polymerizing centre to alcohol.**

PCL, as well as two of PLA's stereochemical forms (poly-D-lactide and poly-L-lactide) are semicrystalline materials, exhibiting glass transition temperatures ( $T_g$ ) of  $-60^\circ\text{C}$ ,  $55^\circ\text{C}$  and  $60-65^\circ\text{C}$ , and melting temperatures ( $T_m$ ) of  $59-64^\circ\text{C}$ ,  $150-170^\circ\text{C}$  and  $175^\circ\text{C}$ , respectively.<sup>81-83</sup> However, the third stereochemical form of PLA, poly-D,L-lactide (PDLLA), is amorphous and therefore does not exhibit a  $T_m$ , rather, just a  $T_g$  of approximately  $55-60^\circ\text{C}$ . In addition, poly-D-lactide (PDLA) is denoted as D due to its ability to rotate a plane of polarized light to the right (clockwise, dextrorotatory); conversely poly-L-lactide (PLLA) is denoted L as it rotates light to the left (counterclockwise, levorotatory) (structures in Figure 2.6).<sup>9</sup> Variations in transition temperatures will impact their chemical and physical properties, providing insight toward relative applicability in different biomedical applications.

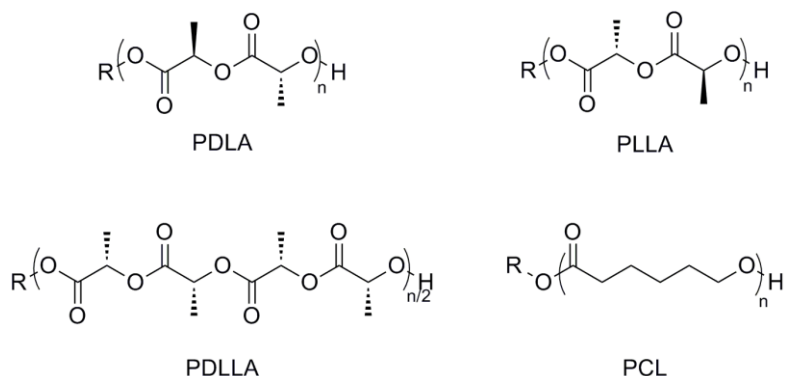


**Figure 2.6 – Chemical structures of PDLA (S-enantiomer), PLLA (R-enantiomer), PDLLA (racemic mixture) and PCL.**

Due to physical and chemical properties, these aliphatic polyesters have significantly different degradation rates. PCL has been shown to break down exceedingly slowly, with complete degradation requiring approximately a 3-4 year period.<sup>84</sup> Polymeric devices consisting of PCL first garnered interest for sustained drug release involving devices that were to remain active for over 1 year, and as slowly degrading suture materials (Maxon<sup>TM</sup>).<sup>82</sup> However, polyglycolides as well as polylactides became more popular for drug delivery vehicles as they display the ability to completely release an encapsulated drug over a few weeks and be fully resorbed in 2-4 months. Although PDLLA has been shown to exhibit increased degradation rates, it typically starts to show mass loss and fully erode within 12-16 months, whereas PLLA can take 2-5.6 years to degrade *in*

*vivo*.<sup>82,85</sup> Degradation of semicrystalline polymers such as PCL occurs in two stages when subjected to aqueous media. First, water diffuses into the amorphous regions, which are less organized and allow water to penetrate more easily. Next, hydrolytic degradation occurs from the edge to the centre of the crystalline domains, followed by intracellular degradation if the MW is less than 3000 g/mol. This explains why PDLLA degrades much faster as it lacks crystallinity.<sup>86-88</sup> The second stage of degradation confirms that PCL is resorbable, as polymer fragments are uptaken into phagosomes, whereby an intracellular mechanism completes the degradation process. In terms of *in vivo* degradation, PCL and PDLLA behave similarly.<sup>89</sup>

PCL's excellent biocompatibility also makes it attractive for 3D porous scaffolds in TE applications to direct the growth of cells and new bone at the site of implantation.<sup>76,90</sup> Moreover, its good rheological and viscoelastic properties render it easy to manufacture and manipulate while providing overall structure and support.<sup>91,92</sup> PCL's slow degradation and mechanical support are therefore excellent attributes for this application. The slow degradation coupled with bioresorbability ensures ample time for neo-bone/tissues to form at the site of implantation without complete fragmentation of the biomaterial. Along with scaffolds, PCL has also been employed in various TE applications including bone,<sup>93</sup> cartilage,<sup>94,95</sup> tendon and ligament,<sup>96</sup> cardiovascular,<sup>97</sup> blood vessel,<sup>98</sup> skin<sup>99</sup> and nerve.<sup>100</sup> PCL is a highly versatile resorbable polymer and although there are several FDA approved drug delivery and medical devices, an increase in TE applications should emerge due to PCL-composite structures and their superior mechanical and biocompatible properties.

PLA's advantages also manifest from its biodegradable nature as well as high strength and biocompatibility.<sup>101</sup> PLA's crystallinity depends on the ratio of D- and L-enantiomers used. However, combinations with as little as 12% D-lactide result in the amorphous PDLLA grade.<sup>102</sup> PDLLA is commonly used in the food packaging sector due to its ease of transformation (i.e. injection moulding and thermoforming), which also makes it attractive for usage in resorbable plating, artificial cartilage or bone, chemotherapeutic and pharmaceutical applications.<sup>103</sup> These applications require faster degradation, thereby portraying PDLLA's advantage over its crystalline counterparts,

PDLA and PLLA. Because of its faster degradation and moderate strength, PDLA is preferably developed as a drug delivery vehicle or a scaffolding material for tissue regeneration.<sup>9</sup>

By considering both PCL and PDLLA as possible bioresorbable polymers in this study, it will provide consistency when comparing results. Although PDLA has been shown to degrade more quickly,<sup>77,89</sup> degradation kinetics are based heavily upon MW, in that higher MW polymers will take longer to degrade due to an increase in chain length.<sup>104,105</sup> Figure 2.7 illustrates the degradation profile for PCL homopolymers with a linear/porous structure; linear PCL with an initial  $M_n$  of 30 000 g/mol elicited faster initial and overall decrease in  $M_n$  (decreasing to 30% of its initial  $M_n$  after one year).<sup>106</sup> Degradation is propagated due to hydrolytic degradation along the chain (or polymer backbone), via surface or bulk degradation pathways. Surface degradation is more predictable. The rate of hydrolytic cleavage, and therefore the production of oligomers and monomers, which diffuse into the surroundings, is faster than the rate of water infiltration into the polymer bulk. This does not cause a drastic change in MW, rather, an overall thinning of the polymer.

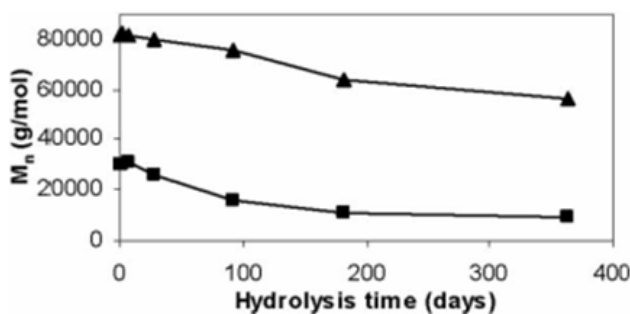


**Figure 2.7 – Molecular weight changes for a porous PCL structure (triangle) and a linear PCL structure (square). Reproduced with permission from Taylor & Francis, 2007.**

The current study involves the investigation of PCL and PDLLA grafted onto the IIR backbone. IIR is known for its chemical and oxidative stability. Therefore PCL chains will likely be localized within the IIR copolymer, thereby undergoing a reduced rate degradation profile. Tethering of these polyesters to the IIR backbone will result in

compliance, yet stability and rigidity, perhaps making these copolymers suitable for a variety of applications requiring good mechanical properties such as vascular prosthetics or intervertebral disc replacement.

## 2.3.2 PIB and IIR Copolymers

### 2.3.2.1 Background

Poly(isobutylene) (PIB) is a synthetic elastomer, which yields many desirable properties such as high elasticity, impermeability to gas and water, chemical stability and biocompatibility. Because of these properties, PIB and its copolymers with small percentages of isoprene (IP) (0.5-4mol%), commonly known as IIR, have been used in a variety of commercial products such as the inner tubes of automobile tires, the bladders of sporting equipment such as basketballs and soccer balls, lubricating oils, motor fuels, sealants, and even as a primary component in chewing gum.<sup>107</sup> Usage in these applications is also possible due to its low level of unsaturation, which provides a route for chemically crosslinking via sulfur-based curing. Crosslinking provides mechanical improvements as well as abrasion resistance, thereby enhancing its physical properties and bestowing suitability for different applications.<sup>108</sup> PIB and IIR are attractive due to their aforementioned properties and versatility, and their ability to be (co)polymerized via cationic polymerization.

IIR was initially investigated by Gorianov and Butlerov (1870), as well as Otto (1927); they found oily homopolymers of IB were successfully produced by usage of boron trifluoride. By the 1930s, I.G. Farben Company of Germany fabricated high MW PIBs, possessing rubber-like properties. The drawback of PIB was its inability to undergo vulcanization or modification due to its fully saturated structure. Although uncurable, homopolymers of PIB were commercialized from Badischer of Germany and Exxon Chemical Company as PANOL<sup>®</sup> and VISTANEX<sup>®</sup>, respectively. Additional research in the 1930s conducted by W.J. Sparks and R.M. Thomas of Standard Oil and Development Company (Exxon) allowed further development of IB into the first curable IB-based elastomer, by incorporating small amounts of a diolefin, IP, into the molecule. However, IIR was officially introduced and commercialized in 1942.<sup>109</sup> In addition, halogen

derivatives such as chloro- and bromo-butyl were introduced in the 1960s as commercially available products, which have greater variations in terms of vulcanization and can be cured with other general elastomers. Butyl polymers are considered specialty elastomers, eliciting the highest worldwide usage of all synthetic elastomers.

Versatility of PIB allows for the development of hybrid materials containing other polymers, thereby imparting new properties to PIB for specific biomedical applications. Demand for biomedical products is increasing in the western society due to the increasing population of the elderly. Diversifying PIB's usage toward the health sector is crucial to satisfy the demand for products that enhance life quality and longevity. Although PIB is a versatile polymer, approximately 80% of total PIB is directed toward the automobile industry. The current clinical use of PIB-based copolymers in vascular stent coatings, as well as its preclinical investigation in a number of other areas such as bone cements and intervertebral disc replacements suggests that PIB is a highly biocompatible and promising material for a range of biomedical applications.<sup>108</sup>

### 2.3.2.2 Synthesis of IIR

Commercial IIR grades such as poly(methylpropene-co-2-methyl-1,3 butadiene) or poly(isobutylene-co-isoprene) are prepared by copolymerizing high purity IB and IP via cationic polymerization at  $-100^{\circ}\text{C}$  in methyl chloride. A schematic diagram of a typical butyl plant can be found in Figure 2.8.<sup>110</sup> Monomers and methyl chloride are purified via flashing and stripping. Zinc or calcium stearate and antioxidants are added to prevent agglomeration throughout the polymerization process. Post-reaction, the PIB product is separated from the slurry, dried and processed. In addition, the reaction follows a generic approach to provide living-like conditions, making use of conventional Lewis acid initiation systems, but with the addition of a Lewis base. By employing Lewis acid coinitiators (or activators) such as aluminum trichloride ( $\text{AlCl}_3$ ), alkylaluminum dichloride and boron trifluoride ( $\text{BF}_3$ ) in methyl chloride or dimethyl sulphoxide (Lewis base moderators), it modifies the interaction between the carbocation active centre and counter-ion.<sup>111,112</sup> Moreover, without this modified interaction, the counterion would be too nucleophilic, causing the reactions to be terminated instantaneously.



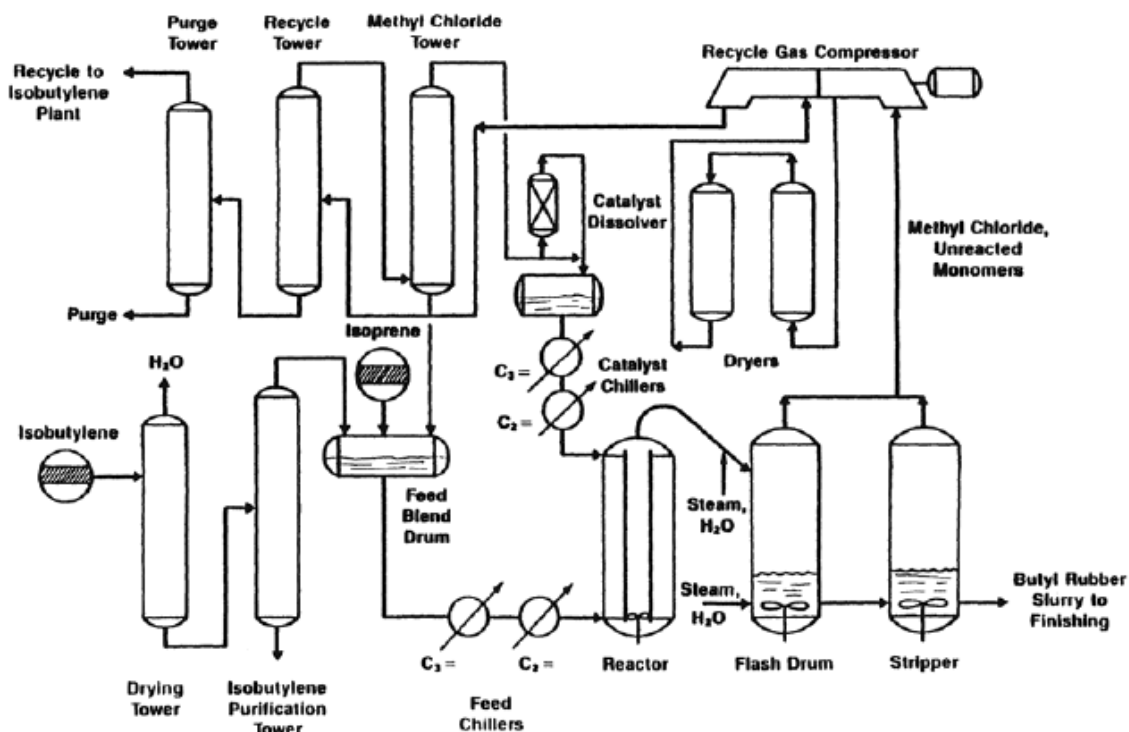


**Figure 2.8 – Commercialized IIR production: general IIR slurry polymerization (Reproduced with permission from John Wiley & Sons, 1990).<sup>109</sup>**

Polymerization of IB first involves the generation of a carbenium ion, which occurs due to reaction of IB monomer with a Lewis acid catalyst such as  $\text{AlCl}_3$  (Scheme 2.3). Carbocation stability causes propagation to proceed mostly in successive head-to-tail additions of monomer (either IB or IP) to the active centre.<sup>113</sup> For IIR synthesis, IP units typically enter the chain in a *trans*-1,4 configuration, as opposed to 1,2 and 3,4 modes of entry as evidenced by chemical analysis (Figure 2.9). The reaction is highly exothermic therefore polymerization can be controlled by decreasing the temperature. Methyl chloride is typically used as the reaction diluent with boiling liquid ethylene in order to remove excess heat.<sup>114</sup> Lastly, controlling factors such as temperature, solvent polarity and the presence of counterions can also tune the rate of propagation.

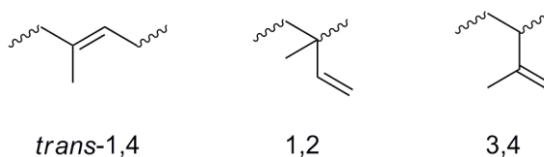
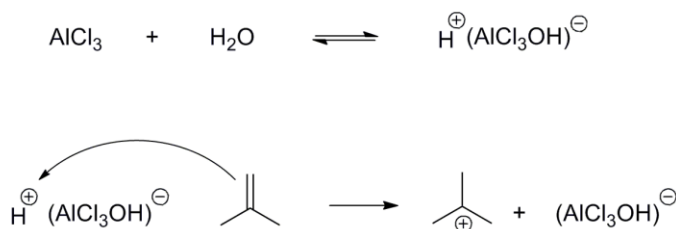


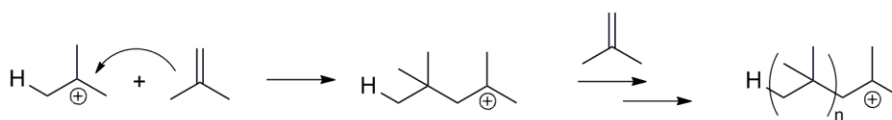
**Figure 2.9 – Isoprene unit enters chain predominantly in *trans*-1,4 configuration.**

Propagation continues until either termination or chain transfer occurs. Termination involves unimolecular rearrangement of the ion pair, causing the second last C-H bond to break and release a proton, generating a terminal alkene bond. Termination can also occur through alternate pathways such as formation of stable allylic carbenium ions, or by carbocation reaction with nucleophilic species including amines or alcohols. Control over termination allows for production of various MW IIR copolymers, capable of further modification. Lastly, chain transfer to a monomer unit is the typical mechanism governing polymerization termination (Scheme 2.3).<sup>115,116</sup> The monomer effectively abstracts a proton from the second last carbon (of the chain), resulting in a monomeric carbocation. Both unimolecular rearrangement and chain transfer termination mechanisms result in carbocation formation, thus propagating the growth of a new polymer chain. However, chain transfer may also occur to solvent, impurities and polymer chains resulting in branched polymers.

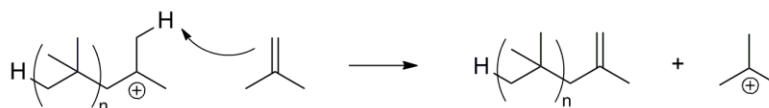
### 1) Initiation



### 2) Propagation



### 3) Termination



**Scheme 2.3 – Cationic polymerization of IB governed by initiation, propagation and termination.**

### 2.3.2.3 Physical and Chemical Properties of IIR

The discovery of IIR was preceded by the desire to transform PIB into a rubbery copolymer that allowed for low functionality, resulting from its low level of unsaturation. As a result, low-modulus vulcanized networks that resist ozonolysis and oxidation can be produced.<sup>117</sup> In addition, because of its oxidative, enzymatic and hydrolytic resistance, it is also biocompatible for long-term applications.<sup>118</sup> Its biocompatibility is advantageous for applications involving medical devices *in vivo* (vascular prosthetics, stents, implantable devices, etc.), to replace materials such as PURs that may degrade, leading to inflammatory and fibrotic reactions.<sup>119</sup> The long, fully saturated PIB segments also manifest physical properties such as low permeability to both gases and liquids, thermal stability, weathering, chemical and moisture resistance as well as vibration damping.<sup>120</sup> Very low permeability, making it advantageous for innerliner in tires, is attributed to the efficient intermolecular packing and high density of the PIB segment. In terms of air retention within tires, IIR demonstrated to be at least 8 times better than that of natural rubber (Table 2.1).<sup>109</sup>

**Table 2.1 – Air loss after automobile driving tests (Reproduced with permission from John Wiley & Sons).<sup>109</sup>**

Initial Conditions		Air Pressure Loss (psi)		
Inner Tube	Original Pressure (psi)	1 Week	2 Weeks	3 Weeks
Natural Rubber	28	4.0	8.0	16.5
IIR	28	0.5	1.0	2.0

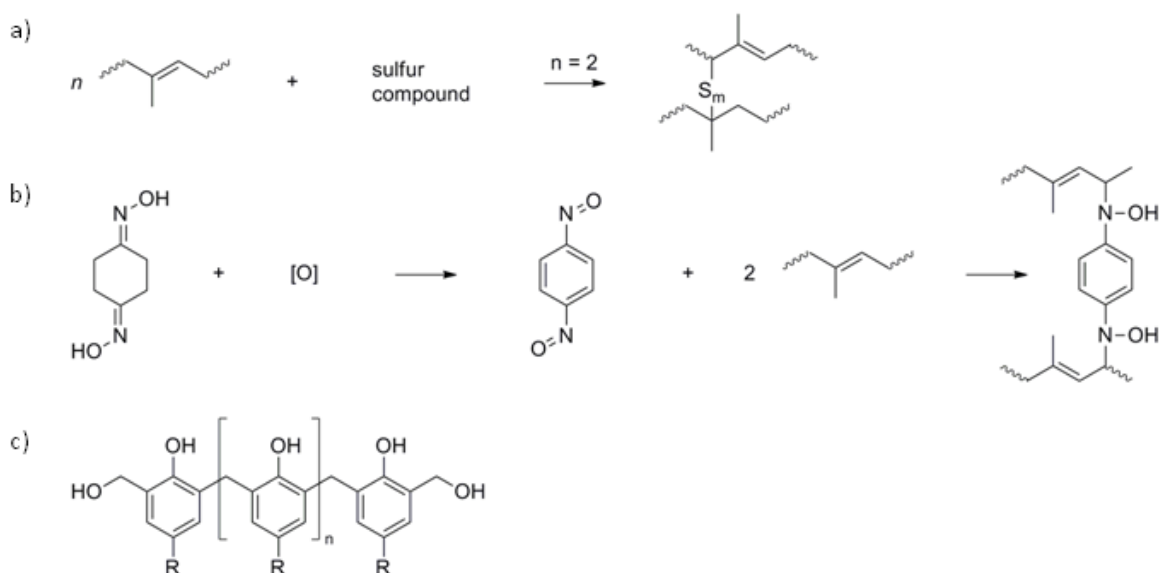
Moreover, PIB's compact and symmetrical intermolecular packing minimizes its intermolecular interactions, which is reflected by its viscoelastic properties.<sup>121</sup> Having two methyl side groups on every other chain carbon causes a delay in elastic response to deformation. This can also be described as high hysteresis. Perfectly elastic materials do not lose energy when a load is applied to them. However, viscoelastic materials do lose some energy, dissipated as heat, resulting in slight permanent deformations after a given stress is applied. This is also related to creep in that viscoelastic materials permanently

deform over prolonged periods of time due to the application of small stresses (strain rate dependent on time). These characteristics, along with IIR's high mechanical damping make it viable for various automotive applications including suspension bumpers and fan belts.<sup>121</sup>

In terms of chemical properties, IIR has a glass transition temperature of approximately  $-70^{\circ}\text{C}$  and is readily soluble in nonpolar solvents.<sup>122</sup> Although typical IIR exhibits IP contents ranging from approximately 0.5-4 mol%, it can be further increased to 7 mol% to examine the impact of increased functionality and unsaturation. IP acts as a strong chain transfer agent in the copolymerization of IB and IP, therefore conditions must be tuned in order to afford IIR with high mol% of IP. Moreover, the reactivity ratios of IB and IP monomers are similar, thus generating a randomly distributed copolymer. Rapid and somewhat uncontrollable polymerization rates, chain transfer and termination mechanisms contribute to IIR's high polydispersity indices (PDI), ranging from 2-4.<sup>123</sup> High PDIs indicate that IIR and copolymers have wide molecular mass distributions.

#### 2.3.2.4 Modifications of IIR

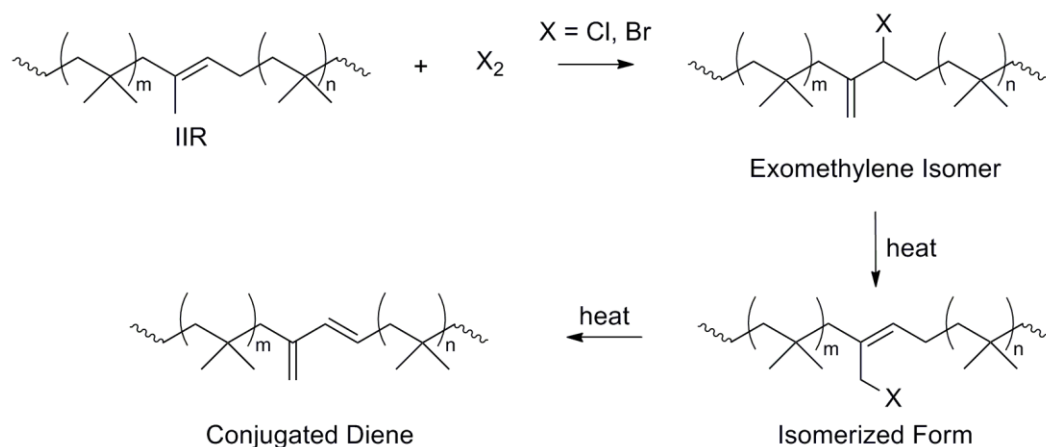
Although IIR has attractive properties and application potential, chemically crosslinking (vulcanizing) the elastomer improves abrasion resistance and mechanical properties. Commonly employed vulcanization methods include accelerated sulfur vulcanization, dioxime crosslinking or polymethylol-phenol resin curing. An example of sulfur-based crosslinking is depicted in Scheme 2.4a. Sulfur compound varieties consisting of thiurams, dithiocarbamates and thiazoles and concomitant temperatures of  $160^{\circ}\text{C}$  generate crosslinked products from highly unsaturated IIRs. Scheme 2.4b describes dioxime curing, where an oxidizing agent [O] oxidizes *p*-quinone dioxime, forming an active crosslinking agent, which can rapidly vulcanize at room temperature (RT). Lastly, Scheme 2.4c shows the general structure of a resin used for olefinic crosslinking. The method is dependent on the R group reactivity.



**Scheme 2.4 – Vulcanization of IIR: a) sulfur-based crosslinking; b) dioxime curing; c) general structure of resin capable of vulcanization.**

The discovery of IIR halogenations by Goodrich in the 1950s increased active functionalities and therefore produced versatile IIR derivatives.<sup>124-126</sup> While Goodrich commercialized a brominated butyl (bromobutyl, BIIR) derivative in 1954, Hycar 2202, Exxon researchers produced chlorobutyl (CIIR) and officially commercialized their product by 1961. Halogenations consisted of “dark” reactions, performed with a solution of IIR and elemental halogens (X) in hexane at approximately 40-65°C (Scheme 2.5). The goal was to create a halogenated IIR compound with only 1 halogen atom per isoprene unit (1:1 mole ratio of X to isoprene).<sup>127</sup> BIIR and CIIR possessed the attractive properties of IIR, as well as additional characteristics including enhanced cure properties (broader vulcanization techniques) and covulcanization with other high-unsaturation general-purpose elastomers.<sup>128,129</sup> With these improvements, halobutyl tubeless tire innerliners could be afforded. Typical addition reactions with halogen atoms result in Zaitsev configuration; however, the reaction of IIR with either Cl<sub>2</sub> or Br<sub>2</sub> results predominantly in substituted allylic halide structures, in this case, the exomethylene isomer (Scheme 2.5). This product is the most kinetically favoured, as a result of steric constraints from the dimethyl-substituted carbon. However, under thermal conditions, this product can rearrange to the X-methyl isomer due to low strength exhibited by the carbon-halogen single bond. Lastly, H-X elimination can occur producing conjugated

dienes, rendering the copolymer useless in terms of post-halogenation curing techniques.<sup>130</sup>

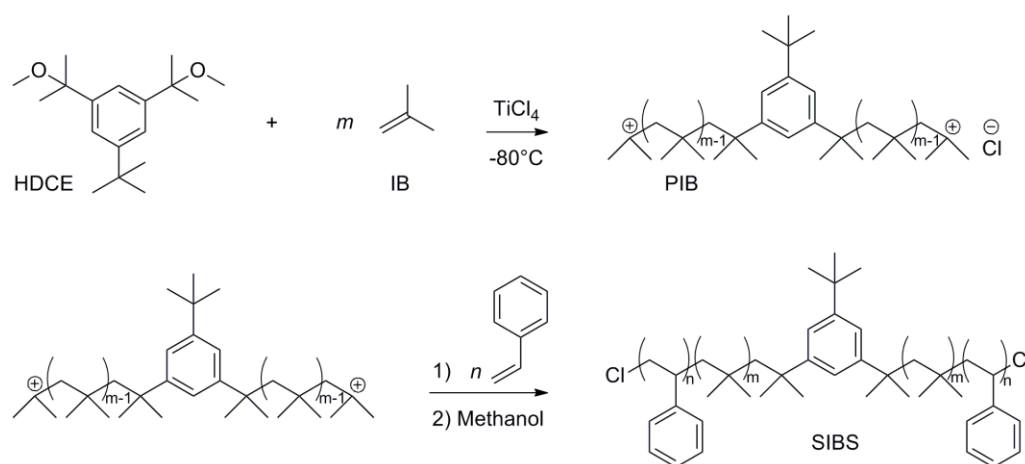


### Scheme 2.5 – IIR bromination followed by isomerization and HX elimination.

Chloro- and bromo- functionalities provide a greater variety in terms of curing methods. For instance, zinc oxide (ZnO) can be used to cure both derivatives, followed by simple extraction of Zn-X for post-purification.<sup>131</sup> CIIR can also be vulcanized via bis-alkylation or resin curing, producing an elastomer with increased heat resistance and elastic modulus (E). However, BIIR has broader vulcanization versatility due the higher reactivity of the C – Br bond allowing for straight sulfur cures, zinc-free cures and peroxide cures in decreased reaction times. In addition, it possesses a higher affinity for covulcanization with other unsaturated elastomers. Although chemical crosslinking of halobutyl does impart increased stiffness, hardness, abrasion resistance and tensile strength, harsh chemical-based crosslinking systems eliminate their potential for biomedical applications. Therefore, milder conditions involving modification of the backbone via installation of different chemical moieties, allows biologically acceptable avenues for altering chemical and physical properties of IIR.

IIR has been functionalized with small molecules such as acids,<sup>132</sup> esters,<sup>133,134</sup> amines,<sup>135,136</sup> and ethers.<sup>137</sup> However, it is of interest to tune chemical and physical properties via copolymerization or grafting, which allow a variety of polymers to be directly conjugated to the IIR backbone. This should facilitate desirable chemical characteristics to be expressed (originating from both polymers), resulting in interesting

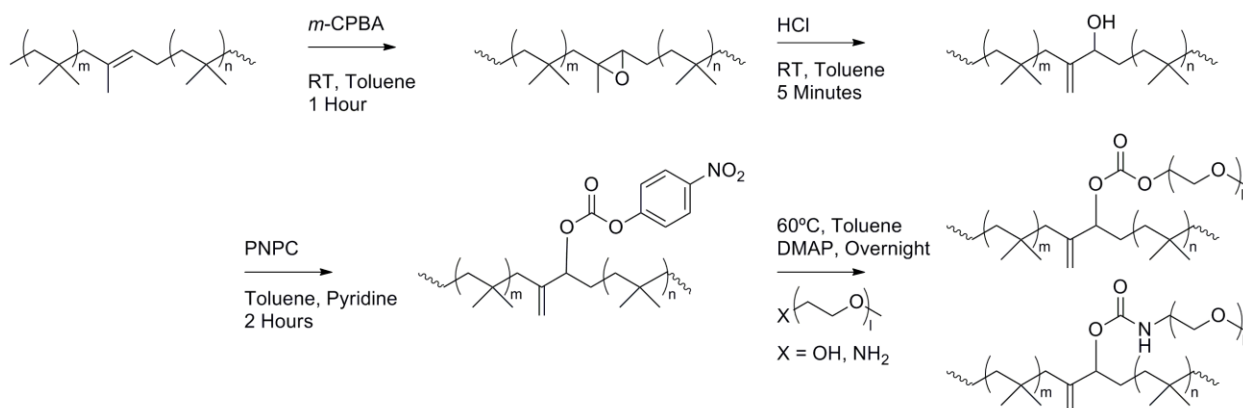
hybrid materials. Over the past 20 years, PIB has been copolymerized to afford various block copolymers. Poly(styrene-*block*-isobutylene-*block*-styrene), SIBS, which is a TPE, has been prepared by a living cationic polymerization method of PIB and styrene (Scheme 2.6).<sup>118,119</sup> More specifically, SIBS was synthesized by first utilizing a bifunctional initiator, 5-*tert*-butyl-1,3-bis(1-methoxy-1-methylethyl)-benzene (HDCE), for the cationic polymerization of IB in methyl chloride/hexanes at  $-80^{\circ}\text{C}$ . After reaching the desired MW of PIB, styrene was added and polymerized until termination via methanol addition. SIBS has demonstrated desirable mechanical (ultimate tensile strength and hardness) and stability properties in comparison to IIR owed to the styrene (glassy and hard) blocks. In addition, utilizing trifunctional or arborescent initiators can afford three-armed star SIBS block copolymers and PIB-based hyperbranched copolymers, respectively.<sup>123,138</sup>



**Scheme 2.6 – Reaction schematic elucidating SIBS production via bifunctional HDCE initiator.**

In order to induce a broad range of characteristics, a multitude of polymers including poly(methyl methacrylate) (PMMA),<sup>139-141</sup> PLA<sup>142</sup> and poly(ethylene oxide) (PEO),<sup>143,144</sup> have also been used to fabricate linear and star-branched block copolymers with PIB. Controlled polymerization conditions provide different molecular structures (di- and tri-block, star and arborescent), thereby affording a vast library of PIB-based copolymers possessing various properties.

IIR can also be functionalized via backbone grafting approach; directly attaching polymers at the IP functionality affords IIR copolymers with interesting chemical, physical and biological properties. In order to functionalize the unsaturated units of rubber, epoxidation can afford moieties that can undergo further chemical modification for various procedures. Zhang *et. al.* demonstrated epoxidation by means of hydroperoxide compounds, in conjunction with molybdenum compounds to catalyze the reaction.<sup>145,146</sup> However, reaction conditions required temperatures of approximately 90°C and durations of 10 hours.



### Scheme 2.7 – Synthesis of IIR-PEO graft copolymers.

In recent work, epoxidation of the isoprene functionality was performed at RT in the presence of *m*-chloroperoxybenzoic acid (*m*CPBA) for 1 hour, thus cleanly affording the epoxidized product with over 99% conversion.<sup>147,148</sup> This method not only required milder conditions, but also eliminated the presence of transition metal catalysts and prevented side-product formation. The epoxidized product was transformed via acidic ring-opening catalysis in under 5 minutes to generate clean formation of a hydroxyl (OH)-moiety. Interestingly, the product opposed Zaitsev's rule, evidenced by formation of the less-substituted alkene. By activation with *p*-nitrophenyl chloroformate (PNPC), PEO consisting of varying MWs could be grafted to specifically tune PEO weight percentage (wt%) in the IIR graft copolymers.<sup>147,148</sup> Although hydroxyl-terminated PEO could be used for grafting, PEO with amine-termini provided full conversion of the IP units, due to very high coupling efficiencies (Scheme 2.7). Mild conditions coupled with unprecedented control over graft copolymer fabrication and PEO content suggests the grafting-to mechanism possesses greater industrial applicability.



Kawahara *et. al.* also investigated graft copolymers consisting of styrene and deproteinized natural rubber (DPNR) in order to afford TPEs.<sup>149,150</sup> In this study, graft copolymerization was performed by employing *tert*-butyl hydroperoxide/tetraethylenepentamine initiating systems with DPNR to achieve grafting efficiencies between 70-95%. Although reasonable grafting efficiencies were afforded, control over MW of the poly(styrene) (PS) portion was difficult due to deactivation and chain transfer. In addition, the highest PS content attainable was 32wt%, which was attributed to the low concentration of active site availability for grafting ( $5 \times 10^{-4}$  mol/mol rubber compared to 2.2-7 mol% isoprene units for PEO-graft copolymers, Figure 2.10). The graph on the left of Figure 2.10 shows that a critical amount of styrene monomer is needed to maintain higher active grafting sites on the DPNR. Concentrations too low led to deactivation, while higher concentrations resulted in chain transfer. Whereas the graph on the right reiterates the importance of adding the correct concentration of monomer; lower feeds ensure that styrene is grafted to rubber particles as opposed to forming PS homopolymers or chain transfer products.<sup>150</sup>

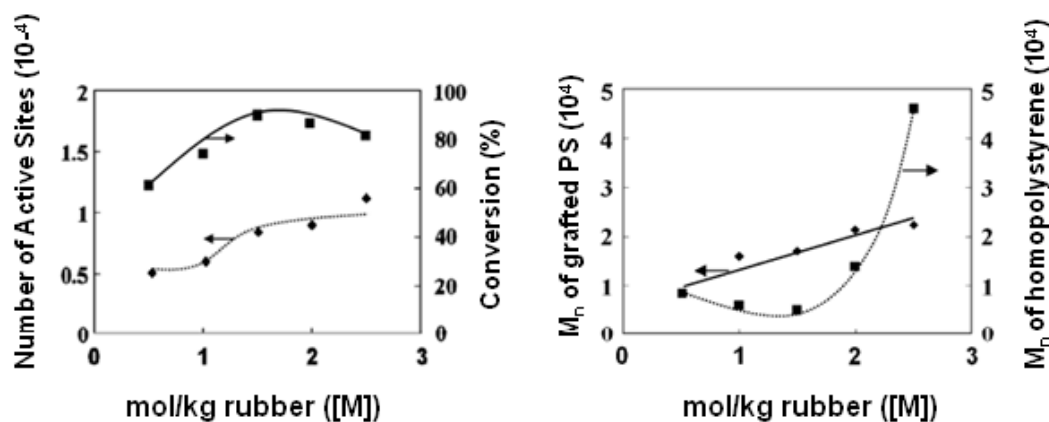


**Figure 2.10 – Monomer-concentration dependence on number of active sites and styrene conversion (left); monomer-concentration dependence on MW of grafted PS and MW of PS homopolymer (Biomaterials, 29, 2008, 448-460 © 2007 Elsevier Ltd. with kind permission from Springer Science and Business Media).**

## 2.4 Applications of IIR Materials

IIR's high impermeability and flex fatigue impart it with appropriate properties for use in tire fabrication, especially tire innerliners. The development of CIIR and BIIR butyl derivatives, as mentioned, led to increased curing rates and versatility as covulcanization with natural rubber (NR), butadiene rubber (BR) and styrene butadiene rubber (SBR) became possible, resulting in tires with increased durability. Desirable properties involving air and moisture impermeability and minimization of intercarcass pressure (which could cause belt edge separation and adhesion failures), have caused CIIR and BIIR to be used commercially.<sup>151</sup> BIIR is advantageous for innerliner fabrication due to increased adhesion to carcass compounds, better balance properties, lower density and costs and flex-cracking resistance. Finally, various blends of NR and BR, NR and CIIR, as well as SBR and BR have been used for tire black sidewall, white sidewall and tire tread applications, respectively. In addition to tire applications, IIRs are also applied in automotive hoses including coolant, fuel line and brake line hoses because of its resistance to higher temperatures in under-the-hood applications.<sup>152,153</sup> IIR's ability to dampen vibrations also makes it suitable for incorporation in dynamic parts. IIR has even been used in pharmaceutical applications such as IIR-stoppers and has been FDA approved for chewing-gum due to its biological inertness.<sup>154</sup>

PIB-based linear copolymers exhibit excellent biocompatibility, thus broadening their scope and applicability as potential biomaterials.<sup>108,155,156</sup> For example, PIB-copolymers are being developed as corneal shunts for the treatment of glaucoma,<sup>157</sup> as well as in synthetic aortic valves.<sup>158</sup> PIB-PMMA composites have been shown to have enhanced properties relative to commercial bone cements due to the incorporation of the elastomeric PIB into the glassy PMMA material.<sup>139,159</sup> However, limitations are related to void formation throughout the material. These deficiencies led to inconsistencies in the material itself, rendering it unsuitable for clinical use in bone cements. Multiarm PIB-cyanoacrylate (CA) copolymers have been reported as promising materials for intervertebral disk replacement due to the combination of CA chemistry and the viscoelastic properties of PIB.<sup>160,161</sup> Moreover, copolymers of PIB with hydrophilic polymers such as poly(*N,N*-dimethylacrylamide) or PEO have been used to form

membranes that can encapsulate cells while allowing the exchange of oxygen, nutrients, and secreted proteins such as insulin across the membrane.<sup>162</sup> PEO incorporation into IIR materials is also of interest due to PEO's inherent nature to exhibit protein resistance.<sup>163</sup> PIB-PEO copolymers could therefore be applied in applications where biofouling has proven to be problematic.<sup>117</sup> The level of protein adsorption resistance was investigated via fluorescent confocal microscopy (Figure 2.11).<sup>148</sup> Figure 2.11e and f, corresponding to IIR-PEO graft copolymers with PEO incorporation of 24 and 34wt%, showed no fluorescence, indicative of protein resistance. It is important to note that with increasing PEO content, water solubility of IIR-PEO materials also increases. Structural integrity could be compromised and may be problematic for potential biomedical applications.

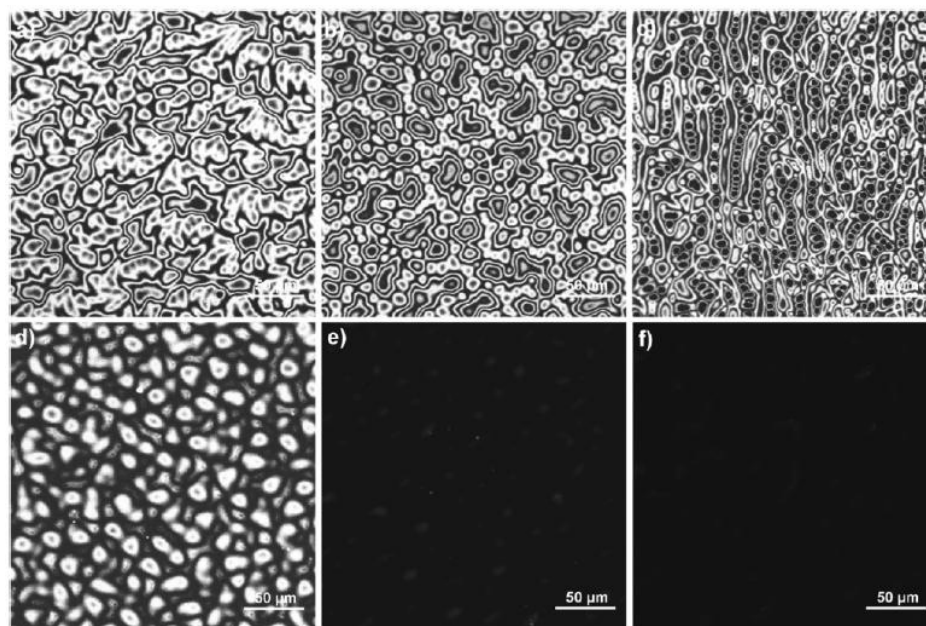


**Figure 2.11 – Fluorescence confocal microscopy images following adsorption of a rhodamine-fibrinogen conjugate. PEO content: a) 2%, b) 4%, c) 6%, d) 12%, e) 24% and f) 34% (Reprinted with permission from *Macromolecules* 2011, 44, 6405. Copyright (2011) American Chemical Society).**

PIB-PS copolymers consist of soft segment elastomer and glassy PS domains, resulting in TPEs (Figure 2.12).<sup>164</sup> These TPEs showed excellent properties, similar to that of IIR, whilst also exhibiting biostability and biocompatibility. With FDA approval, these copolymers have been used for coating drug-eluting coronary stents (DES) (Taxus® of Boston Scientific Co.).<sup>164</sup> SIBS has also been investigated for use as a

corneal shunt, with results showing a decrease in inflammatory response when compared to polydimethylsiloxane.<sup>165</sup> These advances have led to the development of the MIDI-tube, which has demonstrated high patency in rabbit test subjects for the treatment of glaucoma. SIBS is also viable for the production of intraocular lenses<sup>166</sup> as well as trileaflet heart valve replacements.<sup>167,168</sup> Its excellent mechanical properties as a TPE makes it an attractive candidate for the aforementioned applications, however, creep deformation may be problematic. Optimization of the polymer chemistry and resulting properties is still critical for many applications. For example, when SIBS was explored as a potential implant material in the urinary tract, significant attachment of uropathogenic species such as *E. coli* 67 was observed, indicating that the surface properties of the polymer were not ideal for this application.<sup>117</sup> Furthermore, there have been reported cases of stent coating delamination upon employment *in vivo*, indicating that the adhesion of PIB-PS copolymers to the metal materials could be strengthened.<sup>169-171</sup>

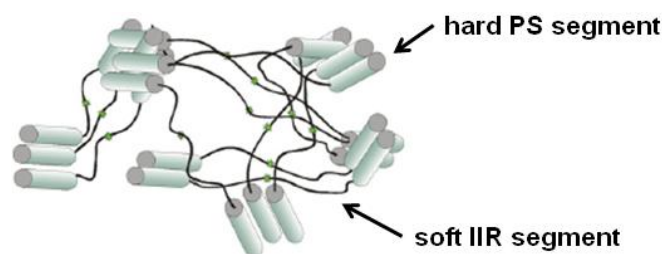


**Figure 2.12 – Cartoon representation of PIB-b-PS showing elastomeric entanglements (PIB) and hard segments (PS) (Reprinted from Biomaterials, 29/4, Pinchuk *et. al.*, Medical applications of poly(styrene-*block*-isobutylene-*block*-styrene) (“SIBS”) (448-460). Copyright (2008), with permission from Elsevier).**

## 2.5 Evaluation of Biomaterials

### 2.5.1 Chemical Characterization

It is standard to characterize new polymeric materials by a range of techniques including nuclear magnetic resonance (NMR) spectroscopy, size exclusion chromatography (SEC) and fourier transform infrared spectroscopy (FTIR) in order to confirm their chemical structures. NMR spectroscopy is a technique that allows one to obtain detailed information on the chemical structures of molecules. While NMR spectroscopy can be performed to probe any nucleus with a non-zero spin, one of the most commonly investigated nuclei is the proton. In  $^1\text{H}$  NMR spectroscopy, each signal is characteristic of a specific proton found in a given molecular structure. The precise resonance frequency is affected by electron shielding, which is dependent on the chemical environment. Therefore, this information is important in order to determine the chemical structure and purity of materials. Moreover, the intensity of each peak can also allow for quantification of a particular component in a sample. Specifically, by integrating copolymer peaks, the determination of PCL or PDLLA incorporation for each copolymer can be successfully calculated.

Gel permeation chromatography (GPC) is a type of size exclusion chromatography (SEC) that separates analytes based on hydrodynamic volume, thereby providing information about polymer chain length and in turn, MW. By utilizing packings comprising porous beads in a column, separation is achieved. Smaller analytes enter the pores, therefore increasing their retention time in the column, whereas larger analytes bypass the pores thereby eluting much faster. In conventional SEC, a number of calibration standards of known MW are run and their retention times are recorded in order to identify the relationship between retention time and MW. By relating the retention time of an unknown sample to the calibration curve, the unknown's MW can be determined. The SEC results will describe different MWs: weight average molecular weight ( $M_w$ ), number average molecular weight ( $M_n$ ), size average molecular weight ( $M_z$ ) and the viscosity molecular weight ( $M_v$ ). Polymers can then be characterized in terms of PDI:

$$PDI = \frac{M_w}{M_n} \quad 1)$$

**Equation 1 – Definition of polydispersity index where  $M_n$  is the total weight of the sample divided by the number of molecules (arithmetic mean) and  $M_w$  fairly accounts for the contributions of different sized chains.**

Fourier transform infrared spectroscopy (FTIR) involves the absorption of infrared light, and is typically performed in order to identify the chemical functional groups present in a sample. Since every sample is different, different bonds and molecules will lead to a very specific spectrum, or ‘molecular fingerprint’. The analysis produces an interferogram (all frequencies being measured at the same time), which undergoes a Fourier transformation, providing a frequency spectrum. The peaks correspond to the frequencies of vibrations between the atoms within chemical bonds. The variations in stretching are characteristic of specific chemical functional groups such as carbonyls, hydroxyls, or alkenes. In addition, peak intensity is directly related to the amount of a specific compound or materials, allowing for quantitative analysis.

## 2.5.2 Physical Characterization

### 2.5.2.1 Water Contact Angle

The measurement of the water contact angle (WCA) of a surface can provide insight into the hydrophobicity/hydrophilicity of a given surface, which can be crucial for various applications. A given surface at a specific temperature and pressure will exhibit a unique contact angle with a given liquid, which is affected by the surface energy and the interfacial energy between the liquid and solid (dictated by cohesion and adhesion forces).<sup>172</sup> The critical surface energy (or critical surface tension) characterizes the wettability of a material. Solids that possess high critical surface energies are more wettable as opposed to solids with low critical surface energies, which are typically not wettable by most liquids. WCA is measured by drop shape analysis, where the liquid interface meets a solid surface as depicted in Figure 2.13.

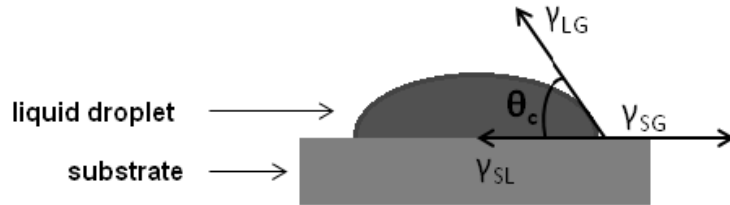


**Figure 2.13 – Contact angle measurement ( $\theta_c$ ) and interphase-energy between 3 phases (values in Young's equation found below).**

Although the results of this test will be used for qualitative analysis, the Young's equation can be used to find the surface energy of a solid:<sup>173</sup>

$$\gamma_{sg} = \gamma_{sl} + \gamma_{lg} \cos \theta \quad 2)$$

**Equation 2 – where  $\Theta$  = measured contact angle and  $\gamma$  is the surface tension of the solid-gas (SG), solid-liquid (SL) and liquid-gas (LG) interface.**

### 2.5.2.2 Atomic Force Microscopy

Due to advances in probe microscopies, techniques such as atomic force microscopy (AFM) can provide a wealth of information on the surface topography, morphology, and properties of materials.<sup>174</sup> AFM is advantageous over other techniques (such as scanning tunneling microscopy) as it can provide information concerning the nanomorphology of the bulk polymer. There are various AFM techniques including contact AFM, contact AFM in the light repulsive mode and lateral force AFM or friction force AFM. However, in the following study, tapping mode will be employed, which provides short-range forces that are still detectable, while minimizing the duration of tip-sample contact. The forces of tip-contact in tapping mode AFM are approximately 0.1-1 nN (in comparison to 5-500 nN for contact mode).<sup>175</sup> These low forces in combination with intermittent contact result in low lateral drag forces, thereby reducing damage of soft polymers.<sup>176</sup> This is particularly important, as the IIR-copolymers are relatively soft. Low forces will help minimize artifacts that could be produced when the tip contacts the material surface. In addition, because tapping is conducted normal to the surface, it decreases capillary and adhesion forces, providing better resolution as compared to static scanning AFM.



Tapping mode is conducted through use of a cantilever and tip (probe). Forces occur between the cantilever and the surface, which are determined by the resulting deflection of the cantilever beam. Moreover, a piezoelectric crystal causes the cantilever to oscillate near its resonance frequency (average of 300 kHz). The amplitude of oscillation decreases as the cantilever nears the surface, which is a result of energy loss manifested by Van der Waals and electrostatic forces. It is because of this decrease in amplitude that the surface features can be measured and identified. However, an electronic servo must be used in order to maintain the cantilever oscillation amplitude by means of a feedback mechanism (adjusts the tip-sample separation distance). The software automatically sets the frequency to maintain the lowest possible level of force on the sample. In doing so, the oscillation amplitude can be accurately measured by the detector and input into the controller electronics of the instrument. Both the topographical and phase images (detections) are produced simultaneously by converting the force of the tip contacting the surface into an analyzable image. These images can reveal subnanometer surface chemical resolution due to mechanical differences amongst various domains.<sup>177</sup> To obtain phase information, a phase shift is detected between the driving and actual tip response oscillation signals. When copolymers or blends are studied via AFM, one component displays lower surface energy and therefore typically dominates the top few angstroms of the surface.<sup>178</sup>

### 2.5.2.3 Scanning Electron Microscopy

Scanning electron microscopy (SEM) is a commonly used imaging technique for the determination of surface morphology, three-dimensional (3D) structures, and can also provide information on chemical composition. The scanning electron microscope utilizes a focused beam of accelerated electrons, thus generating a variety of signals at the surface of the test material. Signals that produce the 3D images consist of secondary and backscattered electrons. Secondary electrons show morphology and topography, while backscattered electrons show contrasts in composition of multiphase systems. Finally, the electron beam scans in a raster scan pattern (image capture and reconstruction), combining the beam's position with the detected signal to produce the final image.



### 2.5.2.4 Thermal Properties

Differential scanning calorimetry (DSC) is a thermal analysis technique used to measure heat capacity changes of a given material with respect to temperature for detection of glass ( $T_g$ ) and melt transitions ( $T_m$ ), crystallization, mesomorphic transition temperatures as well as phase changes and curing/crosslinking. Understanding thermal properties provides insight relating to the amorphous, semicrystalline or crystalline properties of a given material. Amorphous materials are those that are completely non-crystalline. Polymer glasses and rubbers make up the majority of such materials.<sup>113</sup> When amorphous materials are in the solid state, they are considered to be frozen polymer liquids that are inherently hard and brittle (at low temperatures). However, as the temperature increases and reaches the  $T_g$ , the polymer transforms to a rubbery material, gaining the ability to flow (non-frozen).<sup>179</sup> The glass transition is an important temperature as it dictates polymer properties. Temperatures lower than  $T_g$  result in a dramatic increase in stiffness relative to higher temperatures, as well as changes to the physical properties (heat capacity and thermal expansion coefficient) of an amorphous polymer. These physical properties will vary at temperatures surpassing the  $T_g$ . Polymers possess different  $T_g$ s, which are dictated by their chemical structure, molar mass, branching, chain flexibility, copolymerization and molecular architecture.

Crystalline or semicrystalline polymers possess the ability to crystallize (thermodynamically favoured to reduce Gibbs free energy,  $G$ , or kinetically when cooled quickly) when cooled below the melting point of the crystalline phase. Many factors affect the rate and extent of crystallization for a particular polymer such as rate of cooling, orientation in the melt, specific melt temperature, tacticity, chain branching and molar mass.<sup>180</sup> For crystalline polymers, atoms are covalently bonded into tightly packed, unidirectional macromolecular arrays. Unit cells are made up of repeating segments of polymer chains, with several segments of varying complexity in each unit. The polymer chains lie in one particular direction resulting in relatively weak bonding between the molecules, resulting in anisotropic physical properties. However, semicrystalline polymers are of particular importance; melt-crystallized polymers are never completely crystalline due to a large number of chain entanglements, thereby making it near

impossible to form an entirely crystalline polymer.<sup>181</sup> Semicrystalline polymers contain both crystalline and amorphous components due to irregularities in crystal formation. Lamellar crystals are separated from each other by layers of amorphous phase, with lamellae thickness dictated by interfacial energies,  $T_g$  and  $T_m$ , under-cooling and segmental diffusivity.<sup>182</sup> As with amorphous polymers, the transition temperatures of semicrystalline polymers are affected by chemical structure (stiffness, polar groups, side groups), molar mass and branching, as well as copolymer structure. In a copolymer, typically, only one of the polymers is crystallizable, causing the melt temperature to be impacted by incorporation into the copolymer. Main-chain stiffness is the predominant factor in determining  $T_m$  and  $T_g$ , resulting in a correlation that affects both of these properties. Typically, the value of  $T_g$  (K) is between  $0.5T_m$  and  $0.8T_g$ .<sup>183</sup> Control over these transitions is particularly evident in copolymers, thereby making these materials useful for influencing chemical and physical properties.

Thermal characterization can even allow one to make inferences regarding mechanical properties (Figure 2.14).<sup>184</sup> Rubbery materials are those that exhibit only glass transition temperatures due to their long polymeric chains and high degrees of flexibility/mobility, allowing them to undergo large deformations. In other words, the response of rubber is intramolecular; externally applied forces are transmitted to the long chains through linkages at their outer peripheries changing their conformations, thus causing each chain to act like an individual spring.<sup>185</sup> Long chains tend to alter their configuration rapidly, thus allowing typical rubbers to be stretched up to 10 times their original length. Removal of external forces leads to rapid restoration of original dimensions. However, when crystalline and glassy materials are subjected to external forces, deformations that cause two neighbouring atoms to be altered by more than a few angstroms will lead to unrecoverable deformations.

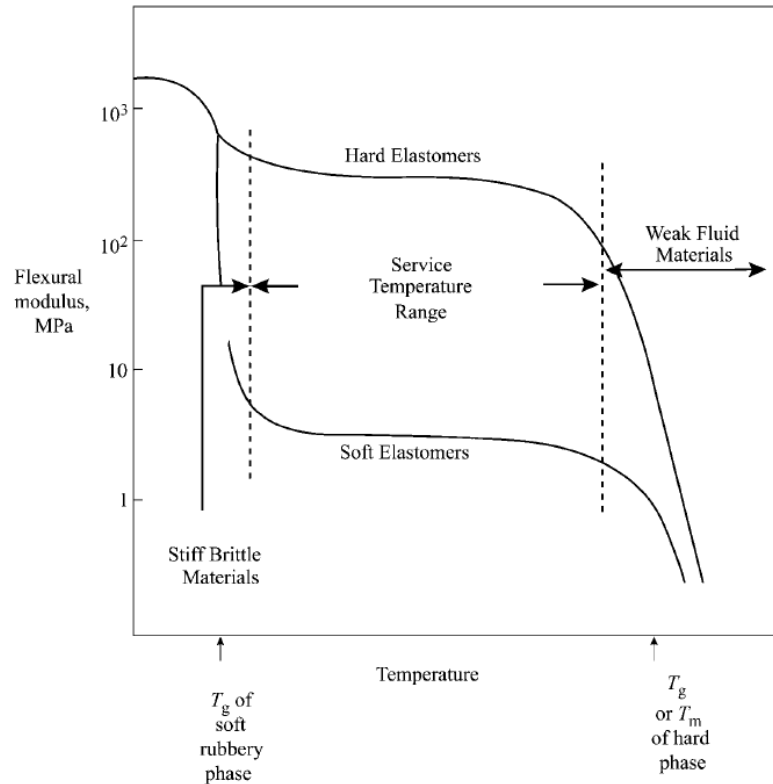


**Figure 2.14 – Temperature dependence of stiffness of typical thermoplastic elastomers (Reprinted from Handbook of Thermoplastic Elastomers, 1<sup>st</sup> Edition, Drobny, Jiri George, Introduction (1-7). Copyright (2007), with permission from Elsevier).<sup>58</sup>**

Materials of particular interest are TPEs, which are composed of a hard semicrystalline phase, and a soft amorphous phase. Phases are most commonly bonded chemically through block/graft copolymerization.<sup>7</sup> Performing DSC is therefore important to first determine  $T_g$ s and  $T_m$ s of polymers that may be used to make up a particular TPE. Each individual polymer typically retains most of its characteristics, with slight variations. The importance of the  $T_g$  and  $T_m$  relates to the physical variations of the elastomer phase. As shown in Figure 2.14, temperatures below the  $T_g$  of the elastomeric phase cause both phases to be hard, resulting in a stiff and brittle material. However, above the  $T_g$  of the amorphous phase, softening occurs, producing an elastic material with rigidity supplied by the hard phase, causing TPEs to behave similarly to vulcanized rubber. With increasing temperature, the hard phase will eventually melt, producing a viscous fluid. Performing DSC is pertinent to understanding the ideal service temperature

for TPEs which will be above the  $T_g$  of the rubbery phase, but below the  $T_m$  of the hard phase. Overall, TPEs are attractive when compared to vulcanized rubbers due to simpler and milder processing methods.<sup>58</sup>

In this thesis, investigating IIR-polyester graft copolymers will provide materials that can be potentially processed as TPEs. Moreover, these graft copolymers may belong to an important family of TPEs, polyester elastomers (PEE). These TPEs share similarities to polyurethane and poly(amide) TPEs.<sup>186</sup> Polyester elastomers, like other TPEs, resist deformation due to the presence of microcrystallites formed by partial crystallization of hard segments, which therefore function as physical crosslinks. Processing temperatures allow these crystallites to melt, yielding a polymer melt; such polymers can be shaped by moulding and retain their shape upon cooling as the hard segments recrystallize.<sup>184</sup> This aspect could be advantageous for various applications involving injectable thermosets or the fabrication of specifically shaped implants. PEEs are also highly versatile. Varying the ratio of hard to soft segment can result in materials ranging from soft elastomers to relatively hard elastoplastics.

### 2.5.2.5 Mechanical Properties

Tensile testing is considered to be the most fundamental type of mechanical testing that can be performed on a specific material. This testing mechanism provides useful information on the material's ultimate tensile strength (UTS), Young's Modulus (modulus of elasticity,  $E$ ), yield strength and elongation at break ( $\epsilon_b$ ). Identifying this information is particularly useful for research and development, engineering design and quality control and specification. The instrument itself utilizes a pair of self-aligning grips where the sample is placed and secured, ensuring that the sample is aligned with the direction of pull and to avoid possible slippage (Figure 2.15). Samples are typically stretched uniaxially until failure by gradually increasing the tensile load (breakage). Tensile testing machines therefore elongate the specimen at a constant rate, continuously and simultaneously measuring the instantaneous applied load and resulting elongations. The load-deformation characteristics are dependent on the specimen size.

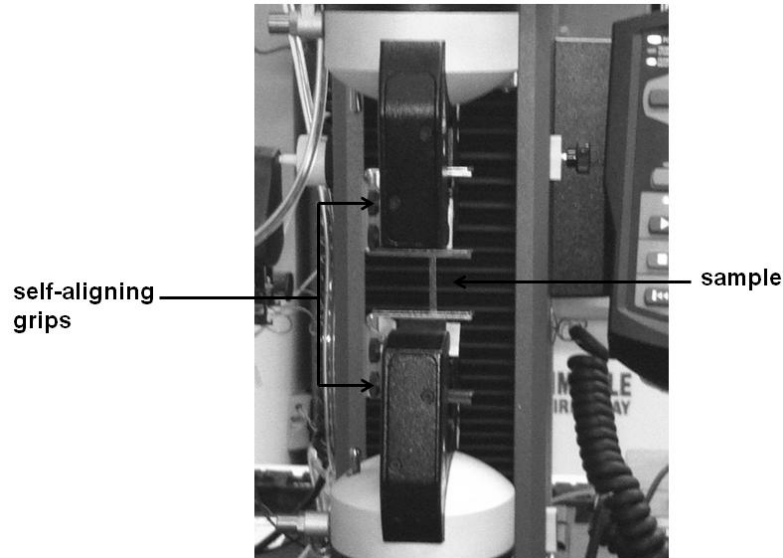


**Figure 2.15 – Instron (3300 series) tensile testing instrument.**

Load and elongation are normalized to parameters of engineering stress ( $\sigma$ ) and strain ( $\epsilon$ ). Stress occurs when a force ( $F$ ) is applied normal to the face of an element (Figure 2.16a). The force transmits through the element and is balanced by an equal force on the opposite side, establishing equilibrium. Strain is the response of materials to an applied stress, causing the given material to stretch from its original length,  $L_0$ , to a final length of  $L$  ( $\delta L = L - L_0$ ). Upon application of a given stress and strain response, elastic deformation occurs, which is described by Hooke's law, stating that stress is proportional to strain. Hooke's law allows the Young's modulus,  $E$ , to be defined for a material using simple uniaxial extension given by:

$$E = \frac{\sigma}{\epsilon} \quad 3)$$

**Equation 3 – Young's modulus determination for a material at a given strain and stress.**

However, this relationship only occurs in the linear portion of a particular stress versus strain trace resulting from a tensile stress. Within the elastic limit, a material will return to its initial shape upon removal of the applied stress. Once the limit is surpassed, permanent deformation will result. The modulus,  $E$ , can be considered to be a material's stiffness or resistance to elastic deformation. Higher moduli are measured in stiffer

materials.<sup>187</sup> Certain materials, particularly polymers, do not obey Hooke's law. When a uniaxial stress is applied, although there is stretching and elongation in the direction of the stress, this elongation causes constrictions (strains) to occur in the lateral directions ( $\epsilon_t$ ), perpendicular to the applied stress. In addition to axial stress, there exists stress parallel to the face of an object resulting in shear strain (Figure 2.16b) as well as equal tensile/compressive forces to all six faces of a cubic element, resulting in hydrostatic pressure stress (volume strain, or dilatation, Figure 2.16c). Therefore, as with E, there are the shear modulus (G) and the bulk modulus (K), showing linearity between shear stress and shear strain and hydrostatic pressure and dilatation, respectively:

$$\tau = G\gamma \quad 4)$$

**Equation 4 – Linear relationship relating the shear strain,  $\gamma$  to the shear stress,  $\tau$ .**

$$p = K\Delta \quad 5)$$

**Equation 5 – Linear relationship showing proportionality between the dilatation,  $\Delta$  and pressure, p.**

If the material behaves isotropically (strains are equal in lateral directions), a parameter termed the Poisson's ratio is defined as the ratio of lateral and axial strains:

$$\nu = - \frac{\epsilon_t}{\epsilon} \quad 6)$$

**Equation 6 – Definition of Poisson's ratio where  $\epsilon_t$  is the transverse strain and  $\epsilon$  is the axial strain.**

When an element is stretched axially in one direction, the element contracts in the lateral or transverse directions, resulting in a positive value for Poisson's ratio, typically in the range between 0.25 and 0.35 (for most materials).<sup>188</sup> Therefore the definition of Poisson's ratio (Equation 6) successfully relates all three moduli (E, G and K) to one another for an isotropic material as:

$$G = \frac{E}{2(\nu+1)}; K = \frac{E}{3(1-2\nu)} \quad 7)$$

**Equation 7 – Relation between Young's modulus (E), shear modulus (G) and bulk modulus (K).**

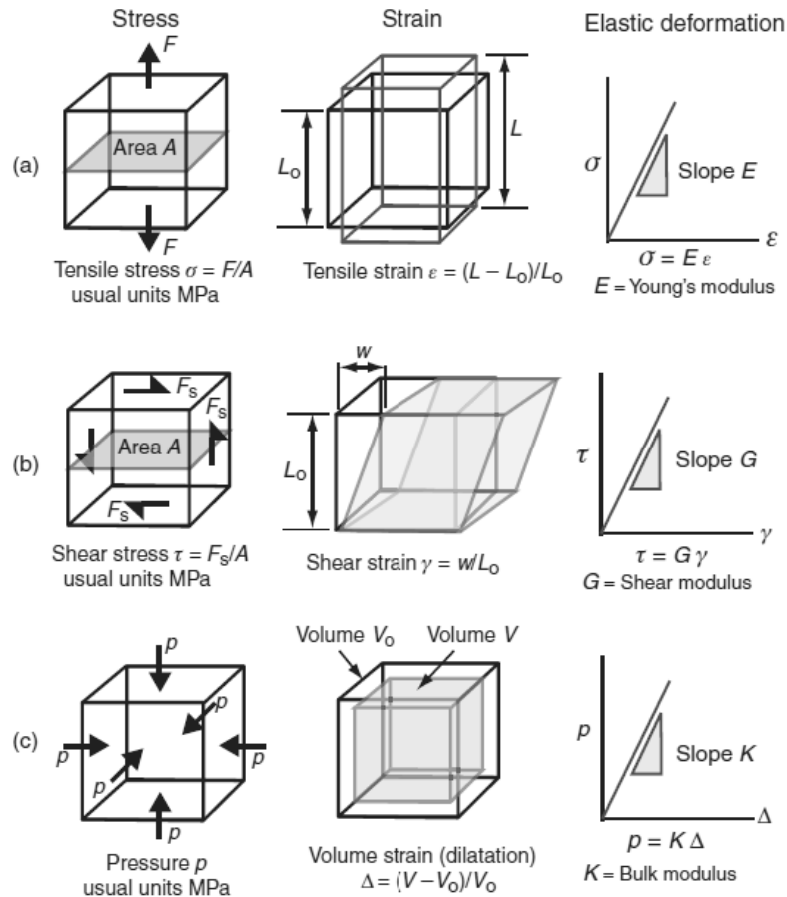


**Figure 2.16 – Definitions of uniaxial stress, strain and elastic deformation.** (Reprinted from *Nanomaterials, Nanotechnologies and Design: An Introduction for Engineers and Architects*, 1st Edition, Ashby, Michael F., Chapter 4 – Material Classes, Structure and properties. Copyright (2009), with permission from Elsevier).<sup>189</sup>

As shown in Figure 2.17, yield properties/ductility is measured using tensile tests by taking the material to failure. The yield strength,  $\sigma_y$ , depicts the stress at which the stress-strain curve (in the linear elastic regime) for axial loading deviates by a strain of 1% (for polymers). However, the behaviour beyond yield depends on the temperature relative to the polymer's characteristic  $T_g$ . Below the  $T_g$ , most polymers are brittle and

exhibit brittle fracture. At temperatures approaching the  $T_g$ , plasticity is possible and once the  $T_g$  is reached, cold drawing is achieved. This is a large plastic (permanent deformation) extension at constant stress during which molecules are pulled into alignment with the direction of straining, followed by hardening and fracture. At higher temperatures, thermoplastics become viscous and can therefore be moulded. Finally, plastic strain,  $\epsilon_{pl}$ , is the permanent strain that results from plasticity, defined as the total strain,  $\epsilon_{tot}$ , minus the recoverable, elastic part:

$$\epsilon_{pl} = \epsilon_{tot} - \frac{\sigma}{E} \quad 8)$$

### Equation 8 – Definition of plastic strain.

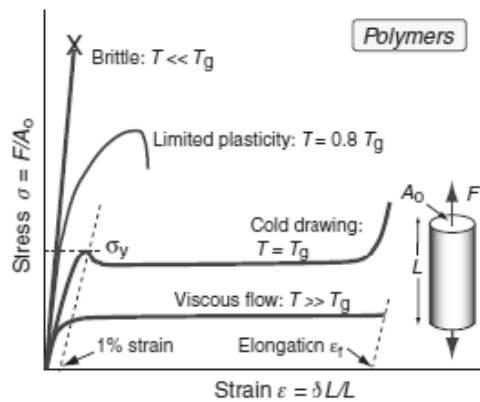


**Figure 2.17 – Stress strain curve for a polymer. Definitions of uniaxial stress, strain and elastic deformation. (Reprinted from Nanomaterials, Nanotechnologies and Design: An Introduction for Engineers and Architects, 1st Edition, Ashby, Michael F., Chapter 4 – Material Classes, Structure and properties. Copyright (2009), with permission from Elsevier).<sup>189</sup>**

Polymers obey Hooke's Law at low strains, therefore allowing the calculation of the Young's modulus by using appropriate software. However, with many elastomers and semicrystalline polymers, the linear portion is difficult to define. Because of this, moduli may be determined by tangent or secant methods. The tangent is the value of  $E$  at any point in a curve, whereas in the secant method, the curve is bisected, and  $E$  (the slope) is determined for the bisecting line.



Elastomers typically have very low Young's moduli, in the approximate range of 0.5-1 MPa, whereas semicrystalline polymers exhibit higher values for E and UTS. Figure 2.18a shows the broad range of moduli for a variety of material classes with large differences in density. Polymers and elastomers possess densities lower than metals or ceramics, as well as moduli below 10 GPa (elastomers specifically in the range of 1-10 MPa). Figure 2.18b depicts the yield strain of various materials. The yield strain ( $\sigma_y/E$ ) is the strain at which a material deviates from the elastic linear regime. It is important to note that elastomers, due to their extremely low moduli, display yield strains in the range of 1 to 10, the highest of all materials. This is important as a larger yield strain corresponds to greater resistance to brittle fracture, which is important for various biomedical applications.

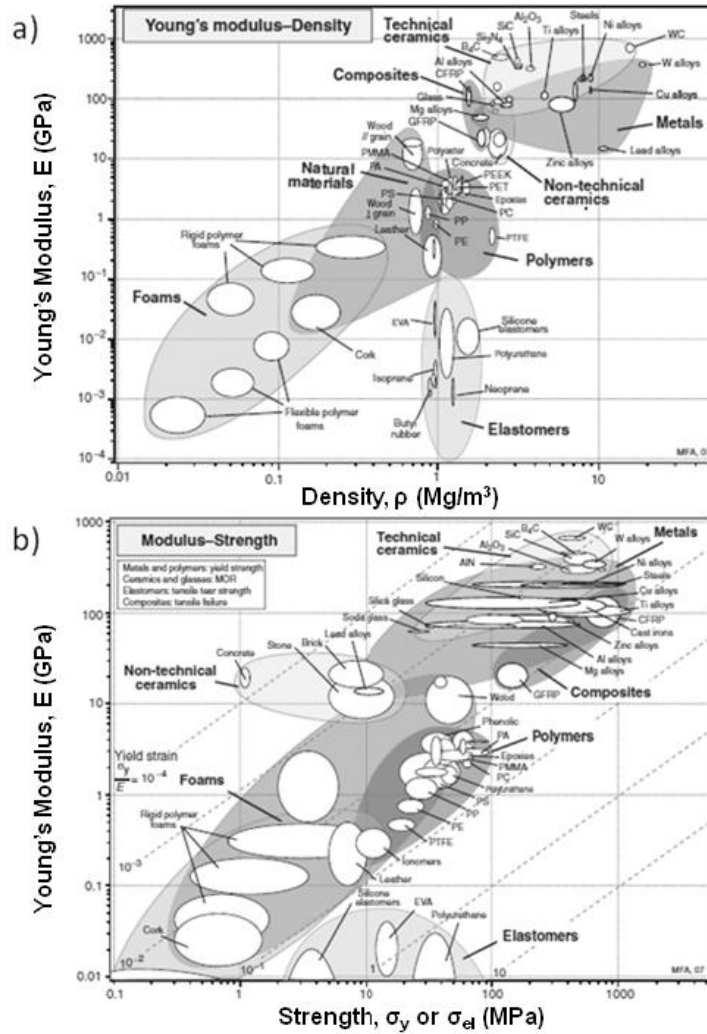


**Figure 2.18 – Material property charts showing: a) Young's modulus and its relation to material density; b) Young's modulus and material strength to defined the yield strain ( $\sigma_y/E$ ), where a material no longer behaves elastically. (Reprinted from *Nanomaterials, Nanotechnologies and Design: An Introduction for Engineers and Architects*, 1st Edition, Ashby, Michael F., Chapter 4 – Material Classes, Structure and properties. Copyright (2009), with permission from Elsevier).<sup>189</sup>**

Elastomers are unique because although they are not physically stiff, they are able to stretch out of the linear regime without resulting in permanent deformation. In contrast to elastomers, semicrystalline polymers are considered to be a mix of polymer crystals, randomly distributed throughout an amorphous matrix. If the amorphous phase is above its glass transition temperature, the polymer will be less brittle, therefore exhibiting a modulus of approximately 50-100 GPa.<sup>113</sup> An increase in crystallinity dramatically

affects mechanical behaviour of a given polymer. At lower degrees of crystallinity, such as those achieved by grafting PCL/PDLLA onto the IIR backbone, the crystalline domains throughout the amorphous rubber should behave as crosslinks, producing stiffness by increasing crosslink density. However, because PCL/PDLLA homopolymers have higher degrees of crystallinity than the copolymers, the resulting moduli will be a combination affected by both the amorphous and crystalline regions.

## 2.5.3 Biological Characterization

### 2.5.3.1 Cell-Material Interaction

Performing adequate assessment in terms of biological risks is inherently important when fabricating potential biomaterials. In order to properly assess biological safety, first, the toxicology of chemical constituents used in a potential biomaterial need to be scrutinized.<sup>190</sup> IIR, PCL and PDLLA are considered to be biocompatible materials; however, modes of preparation (various chemicals/solvents) of graft copolymers could potentially affect their biological, material and cellular responses. Since these materials are intended for use in a biological system, it is important to assess if they are biologically compatible with tissues, to minimize risk for a given patient.<sup>191</sup> In order for a device to be considered biocompatible, it must be able perform with an appropriate host response in a specific application.<sup>192</sup> Measuring biocompatibility is problematic due to the breadth of applications, which involve the interaction of different materials within different biological systems. However, in order to assess biocompatibility, material acceptance *in vivo* should be used to evaluate potential applications.<sup>193</sup> Furthermore, the International Organization for Standardization (ISO) has prepared a guideline document: Biological Testing of Medical Devices—Part 1: Guidance on Selection of Tests' (ISO 10933-1) to provide insight into testing methods that should be employed. Depending on whether the material will be in contact with the cardiovascular system, implanted, blood-interfacing, skin/bone-contacting, or other will impact the relevancy of specific testing methods.

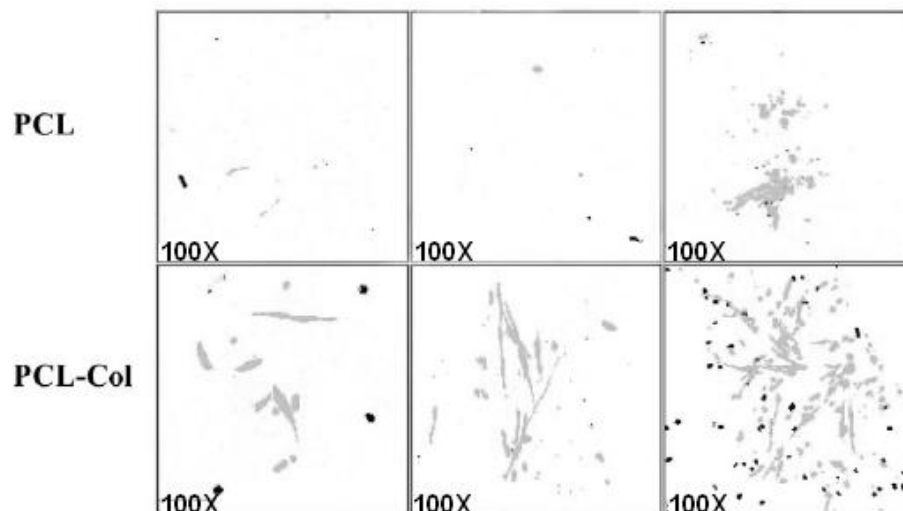


**Figure 2.19 – PCL and PCL-Col (collagen) materials: confocal scanning laser microscopies showing differences in cell proliferation on different surfaces (Reprinted from *Biomaterials*, 25/11, Cheng and Teoh, Surface modification of ultra thin poly ( $\epsilon$ -caprolactone) films using acrylic acid and collagen (1991-2001). Copyright (2003), with permission from Elsevier).**

It is fundamental to explore cytotoxicities of materials, as well as interactions of biosystems with materials at molecular levels. Investigating the interaction between mammalian cells and biomaterials via spreadability, adhesion and proliferation properties is particularly crucial.<sup>194</sup> Cells tend to communicate with their surroundings by means of cell-surface interactions involving the formation of focal adhesions as well as the clustering of integrin receptors.<sup>195</sup> Physical characterization techniques that analyze factors such as wettability, chemical composition<sup>196</sup> and mechanical<sup>197</sup> and topographical<sup>198</sup> properties can affect cell adhesion and therefore proliferation. Investigating cell spreading on surfaces is important as anchorage-dependent cells need to strongly adhere in order to differentiate and transfer signals and maintain cell homeostasis. Through investigation of human myoblasts cultured on PCL films, adherent cells did not spread and were consequently washed from the film. However, through surface modification to incorporate collagen (Figure 2.19), cells spread in all directions and experienced an increase in proliferation rate, thereby establishing a relationship between adhesion and cell survival capabilities.<sup>199</sup> Additionally, cells that maintain a circular shape typically do not display actin stress fibres within the cytoplasm, which are

critical when determining cellular health. Shin *et. al.* conducted studies by seeding Human Mesenchymal Stem Cells (hMSC) onto surfaces of Poly(L-lactide-*co*-E-caprolactone) (PLCL) and compared them to surfaces of PLCL conjugated with acrylic acid (AAc) and gelatin (Figure 2.20).<sup>195</sup> Cells on PLCL did not exhibit any spreading, but through surface modification, the morphology of the cells on the gelatin-AAc-PLCL displayed cells polygonally elongated in shape.

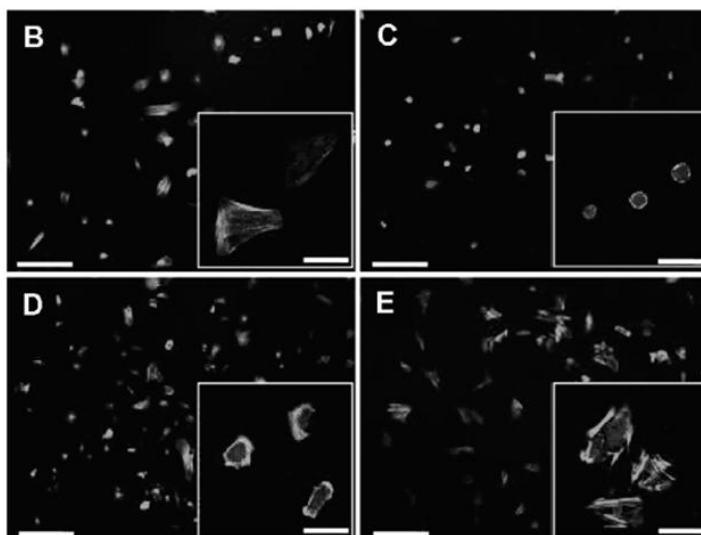


**Figure 2.20 – Morphologies of hMSCs cultured on various substrates: B) glass control; C) PLCL; D) AAc-PLCL and E) gelatin-AAc-PLCL. Scale bar = 200  $\mu$ m (Reprinted with permission from Shin, Y. M.; Kim, K.-S.; Lim, Y. M.; Nho, Y. C.; Shin, H. *Biomacromolecules* 2008, 9, 1772. Copyright 2008 American Chemical Society).**

C2C12, which is a murine myoblast cell line, possesses advantages including its ability to rapidly differentiate, excellent fusion and production of characteristic muscle fibre proteins.<sup>200</sup> Myoblasts, which are representative of either a muscle cell or fibre, are interesting to examine due to their end-to-end fusion configuration *in vitro*, producing morphologies and spatial arrangements in an elongated and predictable manner.<sup>201</sup> Dugan *et. al.* fabricated cellulose nanowhiskers (CNW) to understand the proliferation of C2C12 murine myoblasts, as well as the differentiation and fusion to form myotubes (muscle fibres).<sup>200</sup> Focal adhesions as well as the F-actin in the cytoskeleton were stained and imaged with confocal microscopy to determine if the morphology of CNW surfaces

affected cellular growth and attachment (Figure 2.21). The top line images show differences in morphology in that myoblasts on the glass coverslip were less spread when compared to CNWs (prepared at 500 and 6000 rpm); CNWs also exhibited vinculin (light specks), indicating adhesivity to surfaces. Morphology differences were attributed to surface roughness; roughness of various materials can affect cellular growth response.<sup>202</sup> Although stress fibres appeared on all surfaces, variations in focal adhesion orientation became apparent after 12 hours of incubation.

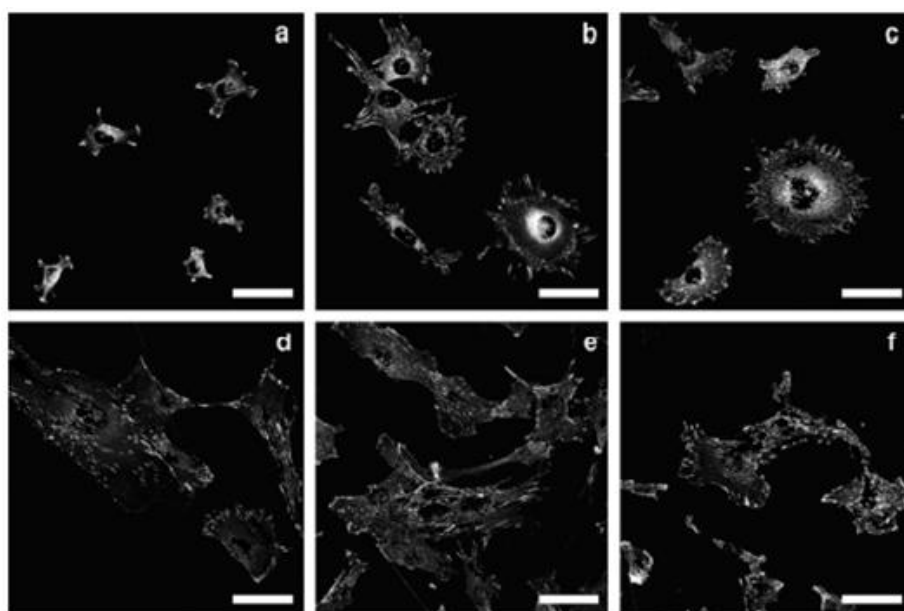


**Figure 2.21 – (a-f) Myoblasts stained for vinculin (light speckles), F-actin (outer periphery) and nuclei, scale bar = 50  $\mu\text{m}$ . (a) 4 h after seeding on glass coverslip control, (b) 4 h after seeding on C500 surface, (c) 4 h after seeding on C6000 surface, (d) 12 h after seeding on glass coverslip control, (e) 12 h after seeding on C500 surface, and (f) 12 h after seeding on C6000 surface (Reprinted with permission from Dugan, J. M.; Gough, J. E.; Eichhorn, S. J. *Biomacromolecules* 2010, 11, 2498, Copyright 2010 American Chemical Society).**

Finally, protein adsorption is a spontaneous occurrence with a high level of importance in biomaterials and biomedical science.<sup>203</sup> Although biofouling is undesirable, the adsorption of cell-adhesive proteins (such as vinculin and F-actin) may be needed to some extent depending on the intended application. This adsorption can be controlled in various ways such as modifying surfaces with polymer brushes (polymer chains attached to a surface),<sup>204,205</sup> resulting in stimuli-responsive signals such as

temperature, pH and light. Polymer brushes may be modified by attaching polymers that are known to adsorb proteins with polymers that are protein-repellent to finely tune overall adsorption.<sup>206,207</sup> Moreover, characteristic protein adsorption exhibited by polymers is dictated by their specific chemical structure. For example, a predominantly studied protein-repellent polymer is poly(ethylene oxide) (PEO). Its protein-resistant properties are owed to steric repulsion, causing the polymer to prevent proteins from reaching the substrate surface to adsorb.<sup>208,209</sup>

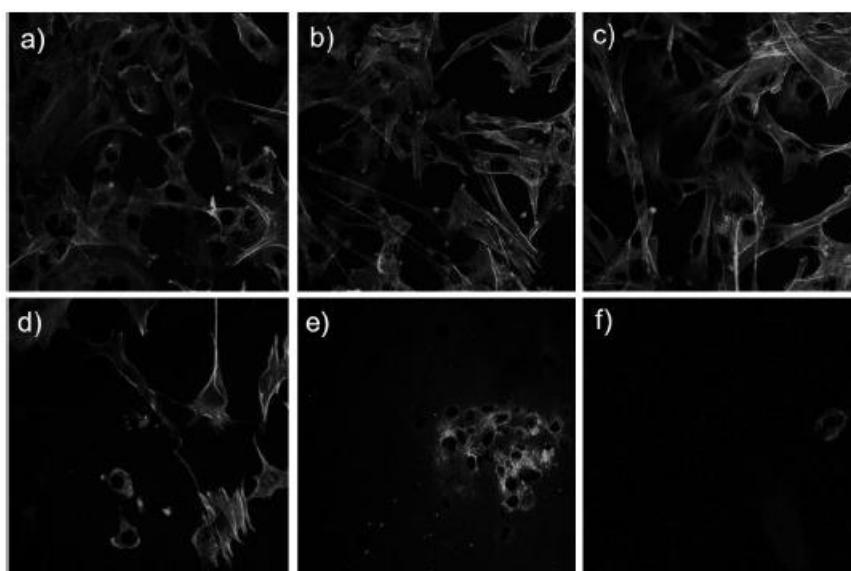


**Figure 2.22 – Confocal microscopy images of C2C12 cells adhered to control and copolymer surfaces: a) glass (control); b) IIR (control); c) 18wt% PEO ; d) 32wt% PEO; e) 65 wt% PEO; f) 83 wt% PEO. Nuclei (dark inner portion) and F-actin fibres (lighter periphery) with image area = 0.22 x 0.22 mm (Reprinted with permission from John Wiley & Sons, 2013).**

Factors including grafting density, length and conformation of PEO chains can also influence its surface resistance to proteins.<sup>210,211</sup> In particular, IIR-PEO graft copolymers have been fabricated for applications involving increased hydrophilicity and therefore emulsifying ability,<sup>212</sup> as well as varying PEO incorporation to confer resistance of the surface to proteins.<sup>147,148,213</sup> Proper growth and proliferation of cells on surfaces is believed to be dictated by the ability of proteins to properly adsorb to surface substrates. Recently, Karamdoust *et al.* showed that by increasing PEO incorporation into IIR-PEO

graft copolymers, reaching a critical PEO content (34 wt%, Figure 2.22d) caused a dramatic decrease in protein adsorption, evidenced by a decrease in cell adhesion.<sup>214</sup>



## 2.6 Thesis Objectives

The goal of this thesis is to synthesize IIR-polyester graft copolymers and to study their chemical, physical, mechanical and biological properties in order to gauge their potential as biomaterials. An advantage of this approach is that rather than using chemical crosslinking methods that are incompatible with biomedical applications, the thermal and mechanical properties of the polyester components may impart enhanced strength to IIR and other properties that are desirable for specific applications. In addition, the slow but eventual degradability of the polyester component may assist in the gradual environmental degradation of IIR materials, which are otherwise broken down only extremely slowly in nature.

The interest in IIR-polyester graft copolymers as potential biomaterials stems from the widespread interest in IIR for various biomedical applications. For example, current bone cement applications involve usage of poly(methyl methacrylate), which is inherently brittle.<sup>139,140</sup> To overcome this issue, toughening of bone cements can be accomplished with IIR-graft copolymer synthesis to impart impact- and fatigue-resistance properties. Similarly, PIB-CA materials are intended for intervertebral disc replacement, however, enzymatic attack on CA moieties causes the release of toxic byproducts. PURs are employed for usage in vascular grafts due to their elastomeric nature, but chemical and mechanical deficiencies led to inflammatory (and therefore occlusion) and crack manifestation, respectively.<sup>118</sup>

Therefore, incorporation of bioresorbable and biodegradable polyesters may eliminate issues associated with toxicity as well as the resistance of synthetic polymers to degradation for time-limited applications, including sutures and bone fixation devices.<sup>57,215</sup> Utilization of stable polymers can lead to undesirable inflammatory responses, as biological systems recognize them as foreign substances. However, degradable polymers offer advantages for therapeutic applications, specifically in medicine, surgery or drug delivery.<sup>9</sup> For time-limited applications involving degradation, bioresorbability is important as it describes materials with non-toxic byproducts that can be eliminated from the body through metabolic pathways.<sup>76</sup>

In order to synthesize the IIR-polyester graft copolymers, the aim will be the development of a simple synthetic method. This will make the final materials more attractive on an industrial as well as biomedical level. The exploration of both "grafting from" and "grafting to" methods will be described. Using the more successful "grafting to" strategy, a small library of graft copolymers is produced to provide insight concerning how varying weight percentages of polyester with respect to IIR affect chemical and physical properties. These are characterized chemically by a variety of techniques including NMR and IR spectroscopy, and SEC.

From differences in the chemical compositions of the materials, it is demonstrated that differences in physical properties arise. These are assessed and compared using techniques such as AFM, SEM, water contact measurements, and DSC. Tensile testing is used to elucidate changes in the mechanical properties of the materials as a function of their composition and degradation studies are performed to investigate their degradabilities. Lastly, although the literature suggests that IIR,<sup>216</sup> PCL<sup>82</sup> and PDLLA<sup>88</sup> are all biocompatible materials, the toxicities and cell adhering/proliferation properties of the new graft copolymers are studied in this thesis. Combined, this data set provides a basis of important information concerning the properties of these materials for further use in specific applications.

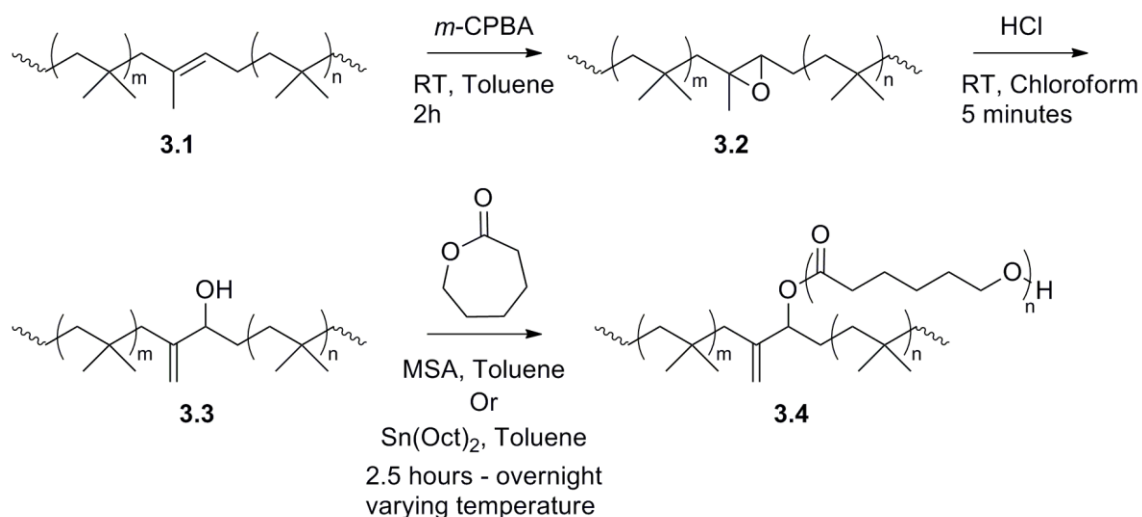
## Chapter 3

### 3 Results and Discussion

#### 3.1 Synthesis and Chemical Characterization of IIR-PCL Copolymers

##### 3.1.1 ROP of $\epsilon$ -caprolactone from the IIR Backbone

IIR-polyester graft copolymers via a "grafting from" approach was initially explored. The goal was to perform a ROP of  $\epsilon$ -caprolactone from the hydroxyl-moieties of the IIR derivative **3.3** (Scheme 3.1). First **3.3** was prepared as previously reported,<sup>147</sup> via epoxidation of commercially available IIR (RB-402) (**3.1**) to provide the epoxidized IIR derivative **3.2**, followed by ring opening under acidic conditions to obtain **3.3**. A library of graft copolymers were to be synthesized with varying weight percentages of PCL, as depicted in Table 3.1.



**Scheme 3.1 – Epoxidation followed by hydroxylation of IIR with 2.2mol% IP and subsequent ROP of  $\epsilon$ -caprolactone from IIR backbone.**

**Table 3.1 – Varying conditions to afford IIR and PCL graft copolymers by ROP of  $\epsilon$ -caprolactone from –OH moiety on IIR backbone.**

Target PCL wt% of Copolymer	Time	Catalyst Amount MSA or Sn (Oct) <sub>2</sub> (eq/OH Butyl)
75	6h - overnight	1-3
50	2.5h - overnight	1-2
25	3h - overnight	1-1.5
10	4h - overnight	1-1.2

The initial preparation of graft copolymers via polymerization from the IIR backbone hydroxyl moieties appeared successful.  $\epsilon$ -caprolactone monomer polymerized, as evidenced by the triplet corresponding to PCL at 4.06 ppm ( $-\text{CH}_2$  adjacent to oxygen), and IB peaks were visible at 1.12 and 1.40 ppm (Figure 3.1b). Moreover,  $^1\text{H}$  NMR spectroscopy also showed that the target PCL weight percentages (10-75 wt%, as per Table 3.1) were obtained, based on integration of the PCL triplet at 4.06 ppm with respect to the IB singlet at 1.40 ppm. However, it was later found that as the graft copolymers were initially precipitated into methanol, this solvent also caused all free PCL oligomers to precipitate. When the graft copolymers were precipitated in acetone, the free PCL remained soluble, leaving the purified graft copolymer. Acetone and similar solvents (2-butanone) solubilize PCL with MWs of 20 000 g/mol or lower, thereby providing a means to elimination of free homopolymer. Upon reprecipitation of the copolymers into acetone, it became apparent that the graft copolymer products mainly contained free PCL trapped within the rubber. Thus,  $\epsilon$ -caprolactone was preferentially undergoing homopolymerization, likely from adventitious water impurities, rather than from the hydroxyl functionalities along the IIR backbone. Therefore subsequent precipitations of graft copolymers resulted in a significant decrease in PCL content. This aspect was confirmed by taking additional NMR spectra of the copolymer material following acetone precipitation (Figure 3.1c). By integrating the aforementioned peaks associated with PCL and IB, a large decrease in PCL relative to IIR was revealed, in comparison to the initial spectrum (Figure 3.1b).

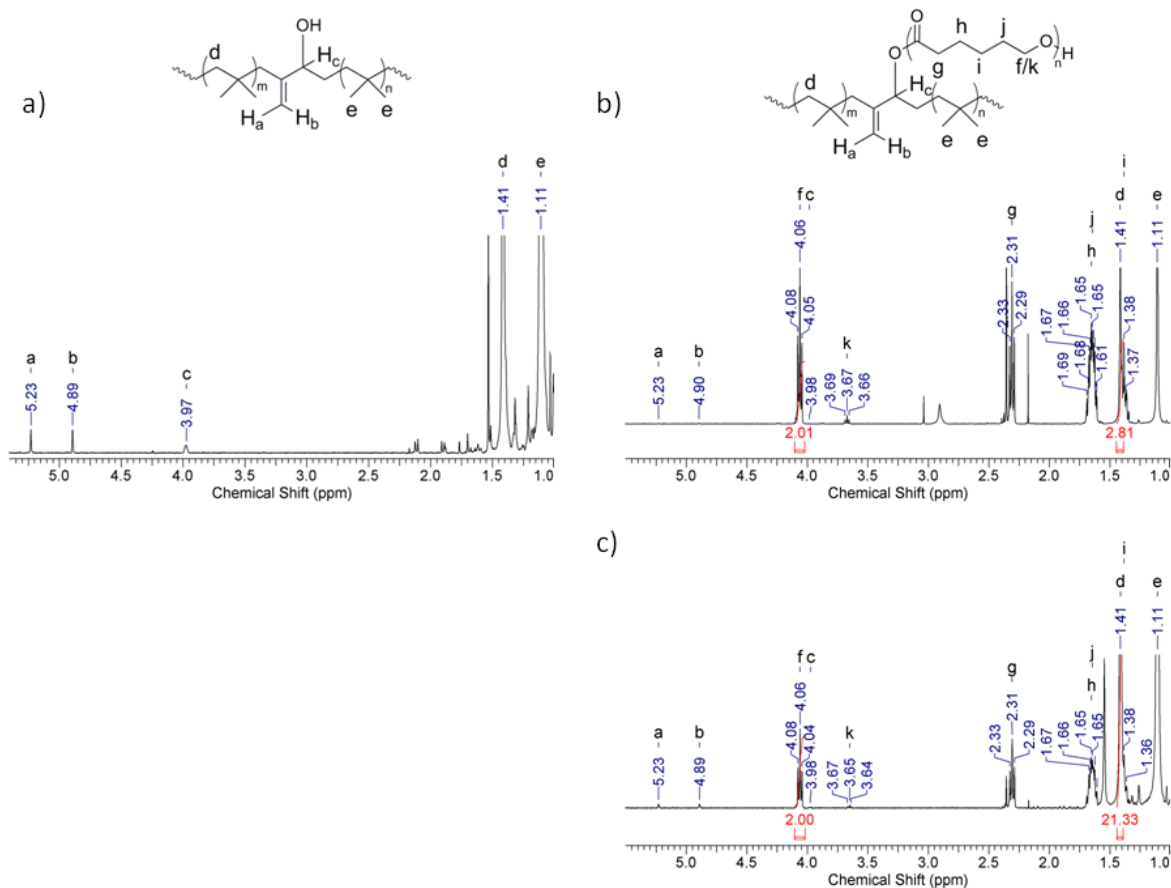


**Figure 3.1 – NMR spectra showing: a) hydroxylated IIR; b) 50 wt% IIR-PCL graft copolymer following methanol precipitation (label k denotes terminal methylene PCL); c) second precipitation in acetone of the same polymer from b), confirming a decrease in PCL content to 16 wt% (label k denotes terminal PCL methylene).**

Aside from  $^1\text{H}$  NMR analysis, issues with the ROP of  $\epsilon$ -caprolactone from hydroxyl moieties along the IIR-backbone were also confirmed by SEC and DSC traces. The aforementioned homopolymerization of  $\epsilon$ -caprolactone coupled with precipitations into methanol, caused SEC traces to display significant side peaks (at increased retention times), representative of a lower MW homopolymer, PCL (Figure 3.2, 50 wt% PCL). In addition, DSC traces also depicted two melting temperatures (Appendix F). These different  $T_m$ s signified the existence of two different species: PCL homopolymer and IIR-PCL graft copolymers. The lower  $T_m$  (43°C) belonged to the graft copolymer, as covalent attachment to IIR has been shown to decrease the melting temperature of semicrystalline polymers.<sup>147</sup> The higher  $T_m$  value of 53°C was attributed to PCL homopolymer. Free PCL

chains throughout the rubber matrix would provide larger crystalline domains, thereby showing an increased value of  $T_m$ . However, reprecipitation of graft copolymers into acetone markedly increased copolymer purity as free PCL chains were removed, producing copolymers with PCL successfully grafted to the IP functionality. This was confirmed by obtaining a second SEC (Figure 3.2, 50 wt% PCL post-purification) and DSC trace (Appendix F), elucidating a monomodal distribution and the existence of one  $T_m$ , respectively.

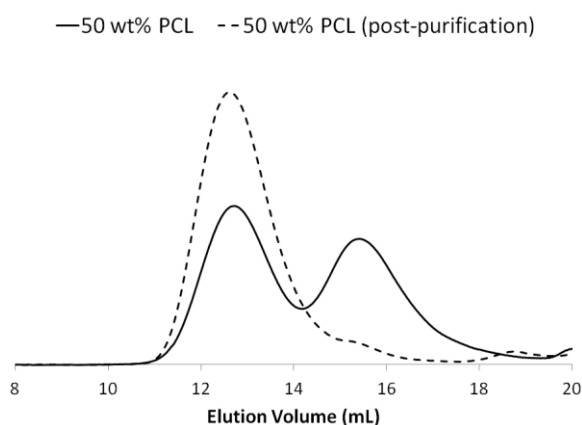


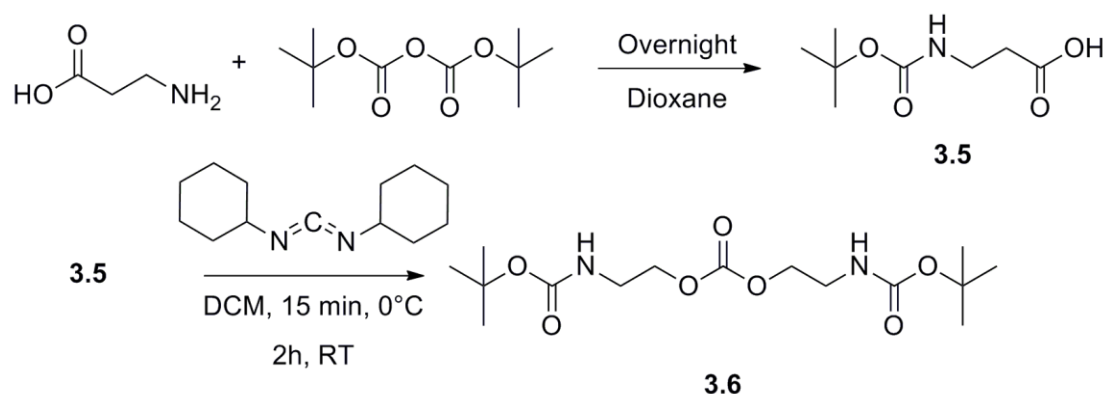
**Figure 3.2 – SEC trace for 50 wt% PCL shows free homopolymer. 50 wt% PCL (post-purification) trace reveals homopolymer removal achieved with secondary precipitation. Detection was based on differential refractive index.**

Issues with the synthesis of these copolymers stems from the preference of  $\epsilon$ -caprolactone monomer to homopolymerize, rather than copolymerize from the sterically hindered  $-OH$  moieties along the IIR backbone. Reaction conditions were varied (Table 3.1) in order to promote graft polymerization. However, the intended weight percentage incorporation was not achievable due to inconsistencies with grafting and the non-reproducible nature of the ROP.

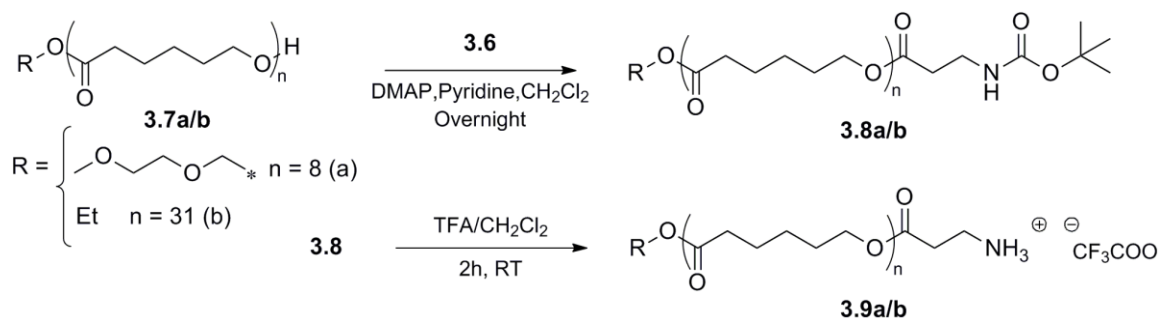
### 3.1.2 Grafting of PCL onto the IIR Backbone

#### 3.1.2.1 PCL Functionalization

Based on previous findings, in order to produce the target IIR-PCL graft copolymers, an alternative, “grafting-to,” synthetic approach was required. Recent success in grafting amine-terminated PEO to a IIR derivative having activated carbonates along the backbone, indicated the same approach should be pursued. The first step was to prepare an amine-terminated PCL. Using a previously reported method,<sup>217</sup> an anhydride derivative of di-tert-butyl dicarbonate (*t*-BOC)-protected  $\beta$ -alanine (**3.6**) was synthesized (Scheme 3.2). As shown in Scheme 3.3, commercially available PCL-OH (900 g/mol, **3.7a**, and 3500 g/mol, **3.7b**) was then reacted with **3.6** to provide the protected amine-functionalized PCL derivative **3.8a/b**, which was deprotected with trifluoroacetic acid (TFA) to provide the target amine-functionalized PCL **3.9a/b**. The synthesis of PCL-NH<sub>2</sub> was confirmed by <sup>1</sup>H NMR. The peak from the original PCL-OH polymer at  $\delta = 3.65$  ppm, representing the terminal methylene, shifted to 4.09 ppm upon reaction with **3.6** and finally to 4.16 ppm after deprotection, as shown in Figure 3.3 (for **3.7a**). Moreover, methylene peaks corresponding to  $\beta$ -alanine appeared at 2.51 and 3.39 ppm, as well as a methyl peak at 1.43 ppm belonging to the *t*-BOC group. The peak at 1.43 ppm disappeared upon deprotection, and the methylene peaks of the terminal  $\beta$ -alanine moieties shifted to 2.83 and 3.33 ppm, respectively. For functionalization of **3.7b**, see Appendix A.



**Scheme 3.2 – Synthesis of *t*-BOC-protected  $\beta$ -alanine anhydride.**



**Scheme 3.3 – Functionalization of PCL (3.7a/b) by first reacting with BOC-protected β-alanine (3.6) to produce the protected derivative (3.8a/b), followed by deprotection with TFA (n = 8 for 900 g/mol PCL, 3.7a, initiated with ethylene glycol derivative and n = 31 for 3500 g/mol PCL, 3.7b initiated with ethanol).**

In addition,  $T_g$  and  $T_m$  were provided by Polymer Source<sup>TM</sup> (Table 3.2). This information is important in order to observe how these temperatures are affected upon fabrication of graft copolymers. SEC traces (Figure 3.4) showed that reaction of **3.7a** and **3.7b** with BOC-protected β-alanine (**3.6**) and subsequent deprotection did not significantly impact MWs, indicating that polymer backbone integrity was maintained. This was especially important during TFA deprotection to ensure that ester hydrolysis did not occur.

**Table 3.2 – PCL thermal properties (provided by Polymer Source<sup>TM</sup>).**

Homopolymer	MW (g/mol)	$M_n$	$M_w$	PDI	$T_g$ (°C)	$T_m$ (°C)
<b>3.7a</b>	900	1872	2505	1.34	Not distinct	44
<b>3.7b</b>	3500	7621	9275	1.22	-64	63



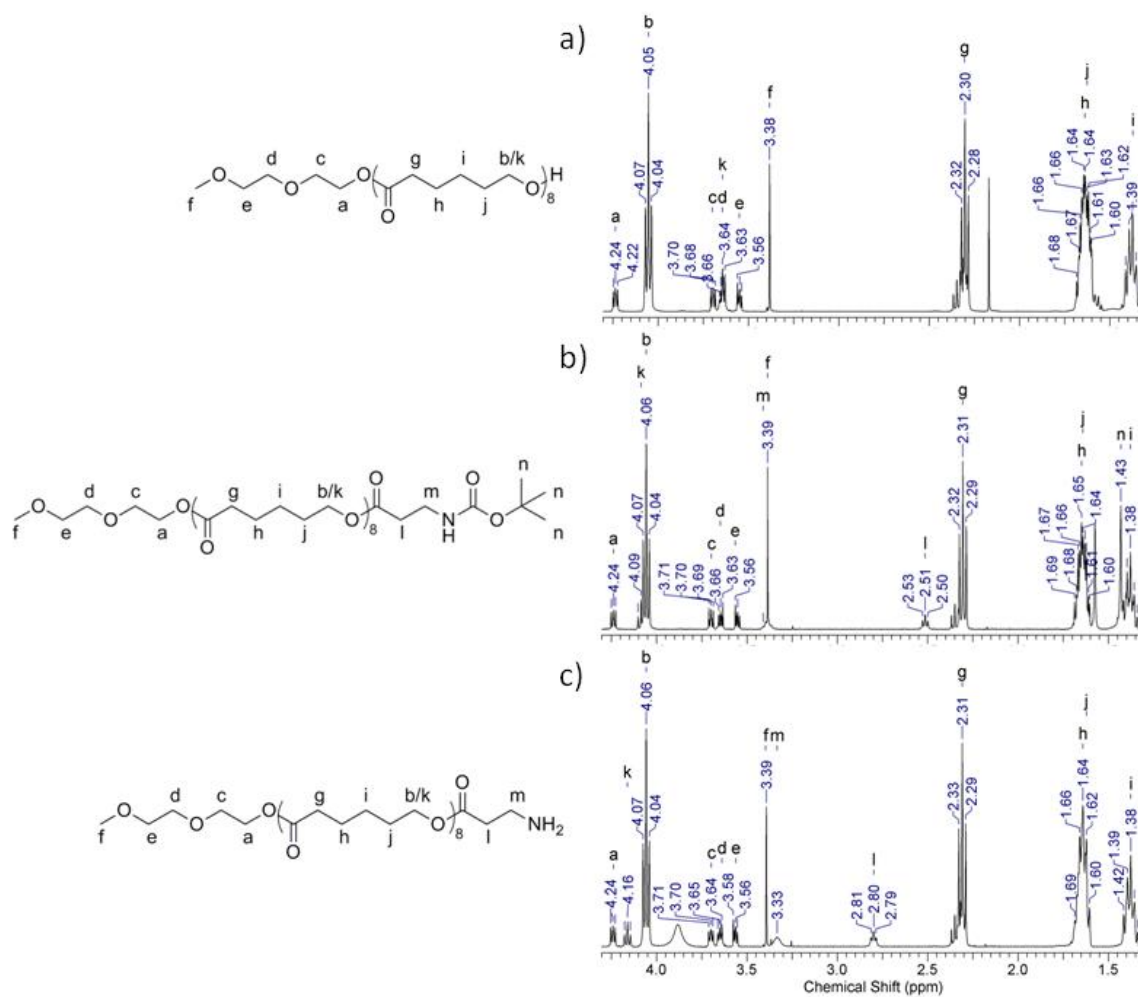


Figure 3.3 – PCL (900 g/mol) functionalization (with k referring to the terminal methylene): a) 3.7a; b) 3.8a; c) 3.9a.

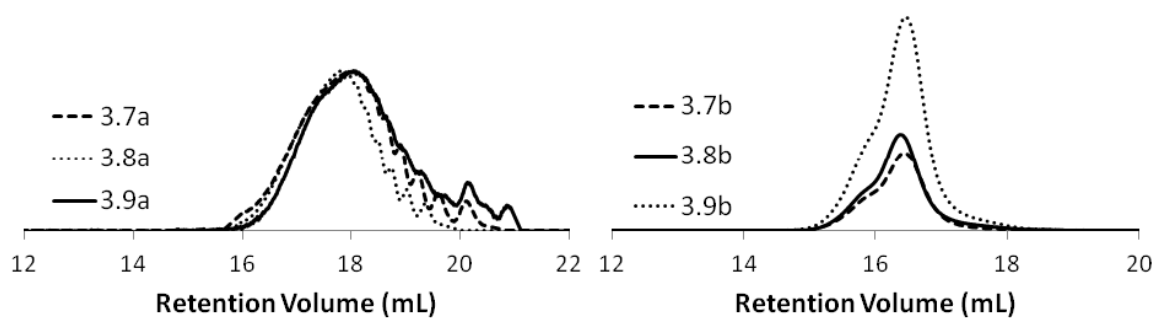


Figure 3.4 – SEC traces of PCL derivatives throughout the functionalization process: a) 3.7a – 3.9a (900 g/mol); b) 3.7b – 3.9b (3500 g/mol).

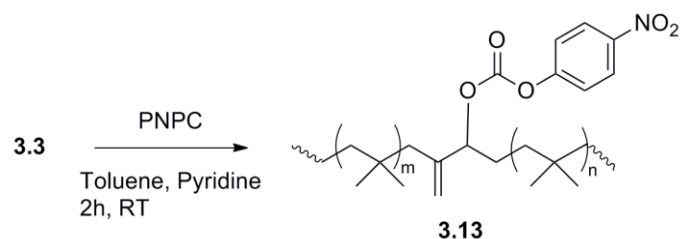
The synthesis of amine-functionalized PCL (**3.9a/b**) was also monitored by FT-IR in order to observe N-H stretching in the 3300-3500 $\text{cm}^{-1}$  region. In congruence with previously established work,<sup>218</sup> typical stretching and vibrations associated with the PCL homopolymer can be observed. Peaks at 2947 and 2866  $\text{cm}^{-1}$  are due to  $\text{CH}_2$  vibrations, the intense peak at 1728  $\text{cm}^{-1}$  is due to C=O vibrations,  $\text{CH}_2$  bending vibrations at 1472, 1420 and 1366  $\text{cm}^{-1}$ , C(O)-O vibrations at 1246 and 1171  $\text{cm}^{-1}$  and lastly, C-O vibrations at 1105 and 1047  $\text{cm}^{-1}$ . However, after reacting **3.8a/b** with BOC- $\beta$ -alanine, N-H stretching was observed at 3439 and 3393  $\text{cm}^{-1}$ , as well as -NHCO- amide bond-stretching at 1569  $\text{cm}^{-1}$ . Moreover, after deprotection with TFA, N-H stretching appeared as a single peak at 3445  $\text{cm}^{-1}$ . It was important to ensure that peaks signifying the presence of N-H stretching remained after deprotection, thereby confirming the successful cleavage of the BOC group, liberating the amine-functionality for subsequent copolymer fabrication (Appendix C for FT-IR traces).

### 3.1.2.2 Grafting of PCL to IIR

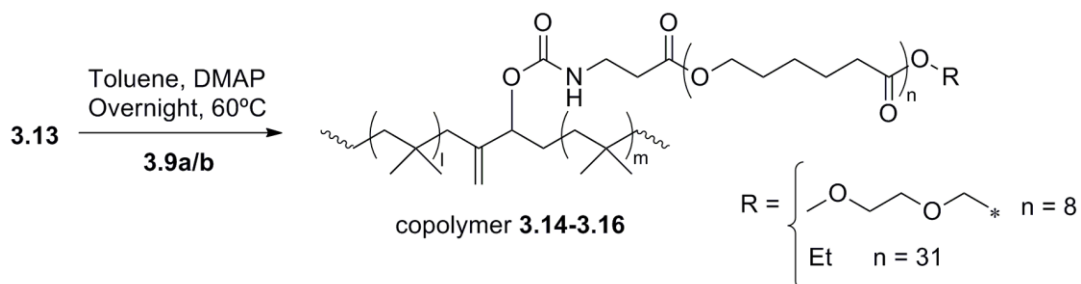
As shown in Scheme 3.4, IIR derivative **3.3** was activated with PNPC as per previous methods (**3.13**).<sup>147</sup> Following the Gillies group's protocol for the grafting of amine-functionalized PEO, the amine-terminated PCL **3.9a/b** was then reacted with the activated IIR derivative (**3.13**) in the presence of DMAP at 60°C overnight (Scheme 3.5). In order to purify each graft copolymer, redissolving in dichloromethane (DCM) with subsequent water washing and multiple precipitations successfully removed residual homopolymer (PCL) as well as impurities relating to 4-nitrophenyl carbonate. By precipitating into acetone, it ensured that PCL polymers were removed. Yields were typically in the range of 75-85%, with lower yields corresponding to graft copolymers with higher percentages of aliphatic polyester incorporation. Increasing the fraction of polyester incorporation could therefore increase the copolymers' ability to dissolve in acetone during purification.

Upon removal of ungrafted polyester homopolymers, the resulting graft copolymers were characterized by  $^1\text{H}$  NMR, FTIR, DSC and SEC. Conversion of the activated carbonates to carbamates upon successful grafting was revealed by shifts in  $^1\text{H}$  NMR peaks (4.8-5.3 ppm) corresponding to the exo alkene and the C-H in the  $\alpha$ -position

to the activated carbonate (Figure 3.5). In order to quantify PCL weight percentage, the  $^1\text{H}$  NMR peak corresponding to the PCL methylene triplet at 4.06 ppm ( $-\text{CH}_2$  adjacent to oxygen) was integrated and compared against the PIB methylene ( $-\text{CH}_2$ ) peak at 1.41 ppm.



**Scheme 3.4 – *p*-nitrophenyl chloroformate (PNPC) activated rubber synthesis.**



**Scheme 3.5 – Synthesis of PCL graft copolymers: 3.14 – 15 wt% PCL (n=8); 3.15 – 32 wt% PCL (n=31); 3.16 – 44 wt% PCL (n=31).**

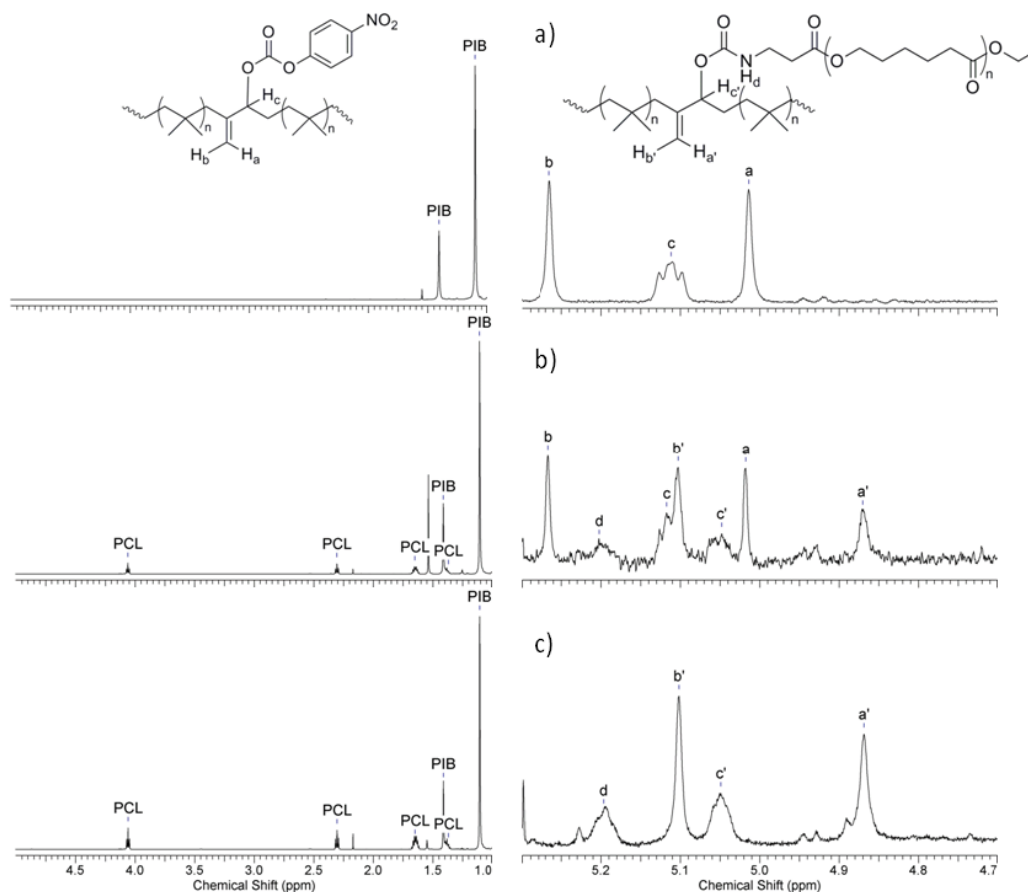


**Figure 3.5 –  $^1\text{H}$  NMR spectra ( $\text{CDCl}_3$ , 600MHz) of a) activated IIR; b) copolymer 3.15; and c) copolymer 3.16 showing how PCL content can be determined based on the relative intensities of PCL to PIB, as well as reaction conversion determination based on peaks from 4.8-5.3 ppm.**

The appearance of a side-peak in SEC traces would indicate the presence of free homopolymer. However, as observed in Figure 3.6, free PCL associated peaks did not appear at their corresponding higher retention volumes (as compared to graft copolymers) validating homopolymers were successfully grafted to the IIR backbone. However, performing SEC analysis on IIR graft copolymers has been found to be problematic.<sup>132,148</sup> Increasing PCL content should reflect an increase in MW, but this was not observed. Instead, graft copolymers with increasing PCL content eluted at higher volumes; polymers therefore behave anomalously on the column, as previously revealed in our group by light scattering analysis. The SEC traces were limited as characterization tools to ensure complete removal of ungrafted homopolymers, due to the inability to accurately

determine the MW data from these measurements. PCL content was controlled by varying the MW of homopolymer (900 and 3500 g/mol) as well as the number of equivalents relative to NPC groups (1.0 and 0.8 equivalents of 3500 g/mol PCL-NH<sub>2</sub>) to produce a small library of graft copolymers **3.14-3.16** (Table 3.3).

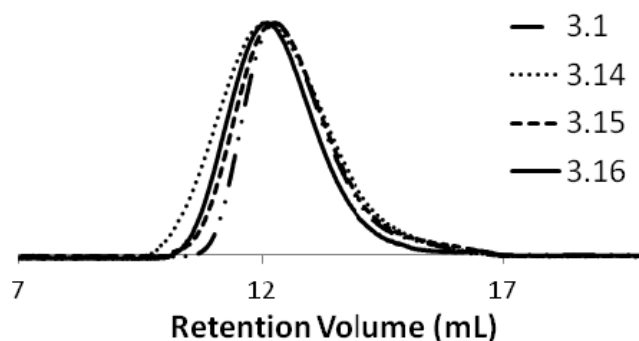


**Figure 3.6 – SEC traces for: ungrafted IIR (3.1) and each IIR-PCL graft copolymer (3.14-3.16).**

**Table 3.3 – IIR-PCL graft copolymers.**

Copolymer	PCL MW (g/mol)	Equivalent (PCL -NH <sub>2</sub> )	Functionalized Isoprene Units (%)	PCL Content (wt%)	Mw (kDa)	T <sub>g</sub> (°C)	T <sub>m</sub> (°C)
<b>3.14</b>	900	1.2	100	15	504	-67	none
<b>3.15</b>	3500	0.8	85	32	395	-65	44
<b>3.16</b>	3500	1.2	100	44	458	-62	50

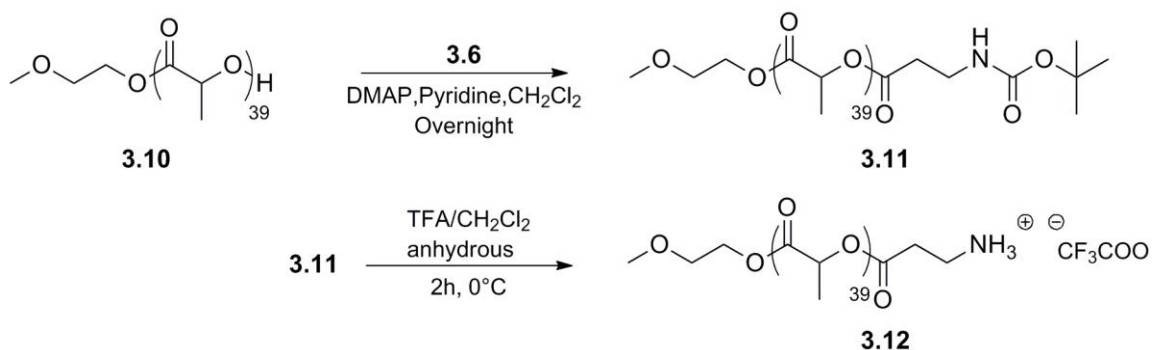
DSC measurements were also performed in order to determine T<sub>g</sub> and T<sub>m</sub> for each graft copolymer. The T<sub>g</sub>s of the graft copolymers were all very similar and were in the expected range for both IIR (-70 °C) and PCL (-64 °C). Previous studies where PEO-IIR graft copolymers were synthesized indicated that crystalline PEO homopolymer of 2000 g/mol, which displayed a T<sub>m</sub> of 58°C, was significantly reduced upon incorporation into the graft copolymer.<sup>148</sup> Similar trends were found in the current study. Copolymer **3.16** (44wt% PCL), combining PCL homopolymer of 3500 g/mol with an initial T<sub>m</sub> of 63 °C was decreased to 50 °C upon covalent grafting to IIR. Copolymer **3.15** (32 wt% PCL), with fewer equivalents of PCL (3500 g/mol) in relation to isoprene units exhibited a

further decrease in  $T_m$  to 44°C. Copolymer **3.14** (15wt% PCL), combining PCL homopolymer of 900 g/mol with an initial  $T_m$  of 44°C, resulted in no apparent  $T_m$  for the graft copolymer. Overall, the increase in melting temperature with increased PCL content can be attributed to the ability of the larger PCL domains within these copolymers to more readily crystallize in a manner that is similar to that of the homopolymer. DSC traces would also show the presence of free, ungrafted PCL chains. In this case, there would be an additional melting peak at the temperature for the corresponding PCL homopolymer (Appendix H). This extra melting transition was not observed here, confirming the purity of copolymers.

## 3.2 Grafting of PDLLA onto the IIR Backbone

### 3.2.1 PDLLA Functionalization

IIR-PDLLA graft copolymers were synthesized in a manner similar to that of the IIR-PCL graft copolymers. First, as shown in Scheme 3.6, a commercially available hydroxyl-terminated PDLLA **3.10** (2800 g/mol) was converted to the amine-terminated PDLLA **3.12** using the same procedure described above for PCL. The only apparent difference relates to the deprotection of PDLLA BOC-protected amine derivative **3.11** due to PDLLA's apparent sensitivity to water. Successful deprotection of PDLLA to afford the amine-terminated derivative (**3.12**) had to be performed using TFA under dry conditions at a temperature of 0°C for 2 hours. The sensitivity to water could possibly have caused the BOC protected  $\beta$ -alanine to be cleaved from the polymer terminus, and additionally, a reduced temperature could have had a kinetic effect on the reaction, thereby making it less favourable for the amine to be cleaved (when first attempted as per PCL deprotection conditions). In this regard, upon deprotection, a cyclic lactam was produced due to the cyclisation of the  $\beta$ -alanine amino acid. To reduce cyclisation, the polymer was redissolved in DCM and passed over a  $K_2CO_3$  plug in order to afford PDLLA-NH<sub>2</sub>. Although conditions were slightly different (as compared to PCL-NH<sub>2</sub>), the yields obtained were good and product purity was high.



**Scheme 3.6 – Functionalization of 3.10 by first reacting with BOC-protected  $\beta$ -alanine (3.6) to afford 3.11, followed by deprotection with TFA (3.12).**

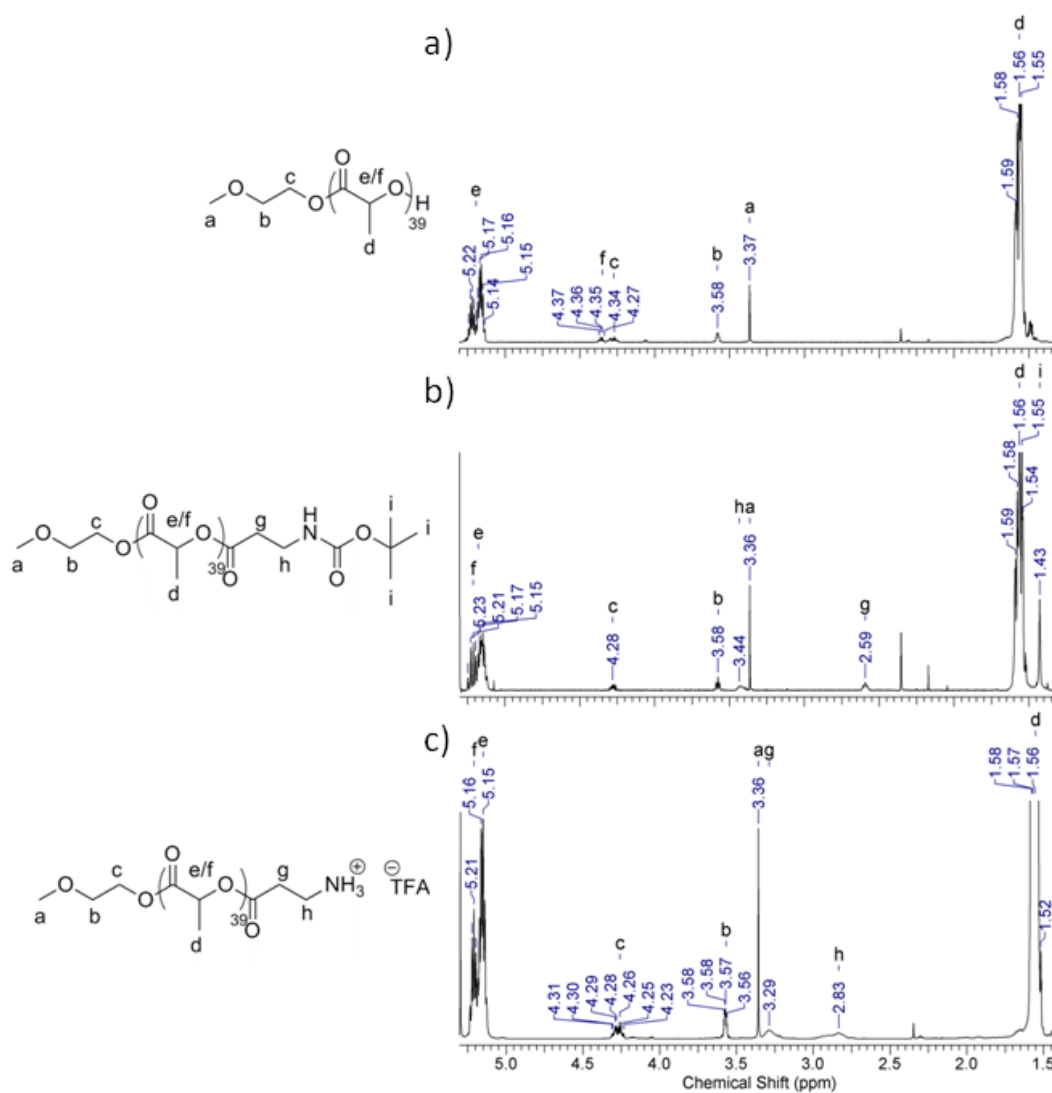


**Figure 3.7 – Schematic depicting PDLLA functionalization: a) 3.10 (2800 g/mol), starting material; b) 3.11, *t*-BOC protected  $\beta$ -alanine derivative; c) 3.12, amine-liberated derivative. In 3.10-3.12, f represents the terminal methylene.**

Successful synthesis of **3.12** was confirmed by  $^1\text{H}$  NMR spectroscopy. The terminal methine peak found at  $\delta = 4.36$  ppm shifted to the 5.23 ppm region (overlapping with the C-H  $\alpha$  to the carbonyl) where it also remained after deprotection. Furthermore, methylene peaks corresponding to  $\beta$ -alanine appeared at 2.53 and 3.42 ppm, as well as a methyl peak at 1.43 ppm belonging to the BOC group (Figure 3.7). In addition, SEC was also performed to ensure that there were no significant changes to the MW of the polymer during this process (Figure 3.8). Finally, FTIR was performed on **3.10**, **3.11** and **3.12** to



ensure the appearance of the peak corresponding to amine stretching in the  $3500\text{ cm}^{-1}$  region, indicative of successful conversion of  $-\text{OH}$  termini to  $-\text{NH}_2$  termini of the PDLLA polymer. Similar absorptions were observed in accordance with previously reported PDLLA spectra.<sup>219,220</sup> Vibration of the linear ester, carbonyl bands,  $\text{C}=\text{O}$  and  $\text{COO}$ , appears at  $1757\text{ cm}^{-1}$ ,  $1267$  and  $1134\text{ cm}^{-1}$ , respectively. In addition, characteristic  $\text{CH}_2$  vibrations can be observed at  $2997$  and  $2949\text{ cm}^{-1}$ . However, N-H stretching still appeared upon reacting with BOC- $\beta$ -alanine (similar to PCL functionalization) at  $3517$  and  $3435\text{ cm}^{-1}$  (with amide  $-\text{NHCO}-$  bond-stretching at  $1512\text{ cm}^{-1}$ ) and remained after deprotection as a single peak at  $3508\text{ cm}^{-1}$ , thereby confirming successful cleavage and liberation of amine-termini (Appendix C for spectra).

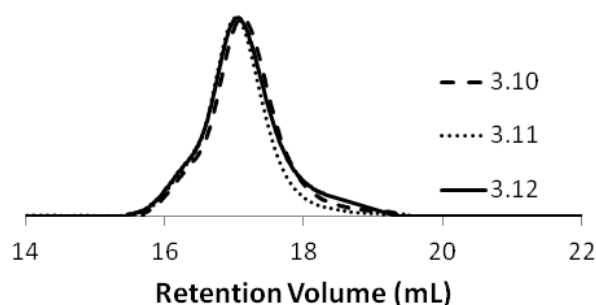
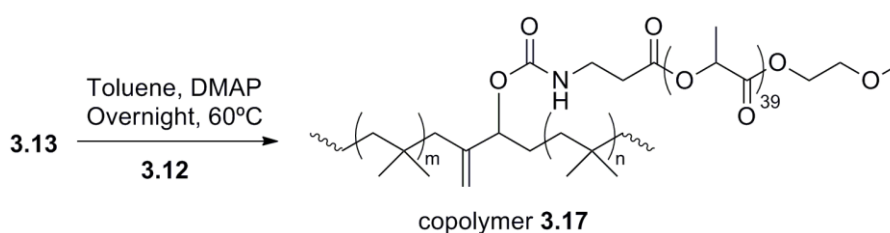


**Figure 3.8 – SEC traces elucidating functionalization of PDLLA 3.10-3.12.**

PDLLA starting polymer **3.10** was provided by Polymer Source<sup>TM</sup> and possesses a  $T_g$  of  $28^\circ\text{C}$  (Table 3.4). This information is important in order to observe how the glass transition temperature is affected upon graft copolymer synthesis. As was expected, PDLLA did not possess a melting temperature because of its structure; a racemic mixture of D-lactide and L-lactide results in an amorphous polymer.

### 3.2.2 IIR and PDLLA Grafting

Using a procedure similar to that used for the synthesis of the PCL-IIR graft copolymers, amine-terminated PDLLA **3.12** was reacted with the activated IIR derivative (**3.13**) to prepare graft copolymer **3.17** (Scheme 3.7). The product was purified by multiple precipitations into acetone. This not only successfully removed 4-nitrophenyl carbonate impurities, but also removed residual PDLLA polymers. Yields in the range of 85-90% were obtained. Graft copolymer **3.17** was characterized by  $^1\text{H}$  NMR, FTIR, DSC and SEC. In congruence with copolymers **3.14**, **3.15**, and **3.16**, conversion of the activated carbonates to carbamates upon successful grafting was demonstrated by the shifts in  $^1\text{H}$  NMR peaks (4.8-5.3 ppm) corresponding to the exo alkene and the C-H in the  $\alpha$ -position to the activated carbonate (Figure 3.9). PDLLA wt% was determined through integration of  $^1\text{H}$  NMR corresponding to the PDLLA multiplet from 5.13-5.23 ppm (-CH  $\alpha$  to carbonyl), compared against the PIB methylene singlet at 1.43 ppm (-CH<sub>2</sub>). The PDLLA content of copolymer **3.17** was found to be 30 wt% (Table 3.4). FT-IR spectroscopy showed strong peaks associated with CH<sub>2</sub> vibrations in the 3000 cm<sup>-1</sup> region, arising from both PIB and PDLLA, and an intense peak at 1700 cm<sup>-1</sup>, characteristic of the PDLLA C=O stretch (Appendix E). The purity of graft copolymer **3.17** was also demonstrated via SEC analysis; Figure 3.10 displays a monomodal distribution, thereby confirming the absence of free PDLLA homopolymer.



**Scheme 3.7 – Synthesis of PDLLA Graft copolymer: 3.17 – 30 wt% PDLLA.**

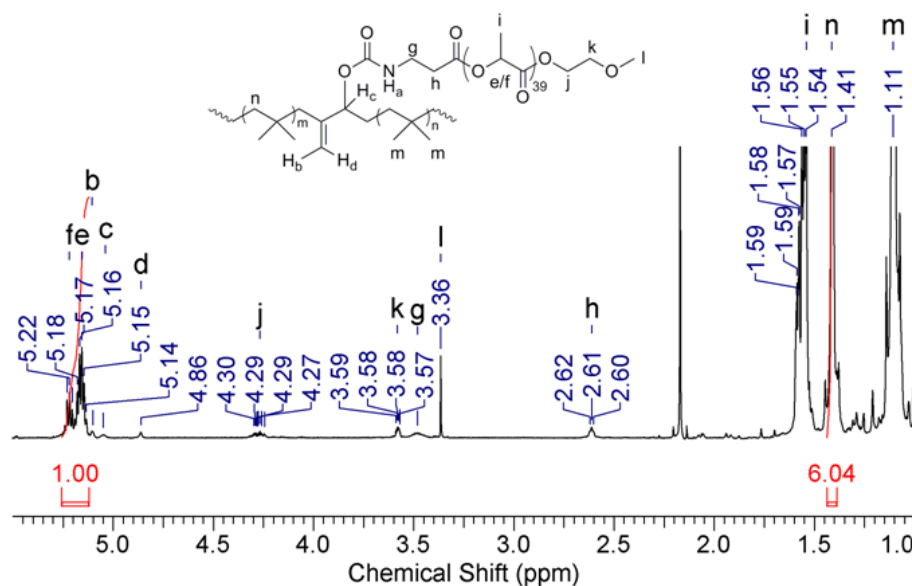


**Figure 3.9 – PDLLA content in copolymer 3.17: determined via integration corresponding to PDLLA multiplet from 5.13-5.23 ppm and PIB singlet at 1.41 ppm.**

**Table 3.4 – PDLLA homopolymer and IIR-PDLLA graft copolymer: PDLLA content and thermal properties.**

Polymer	PDLLA MW (g/mol)	Equivalent (PDLLA - NH <sub>2</sub> )	Percentage Functionalized Isoprene Units	PDLLA Content (wt%)	Mw (kDa)	T <sub>g,1</sub> (°C)	T <sub>g,2</sub> (°C)	T <sub>m</sub> (°C)
<b>3.10</b>	2800				4.7	28	none	none
<b>3.17</b>	2800	1.2	100	46	462	-63	23	none

DSC analysis was also performed on copolymer **3.17**. Contrasting with PCL, PDLLA, because of its amorphous nature, does not exhibit a T<sub>m</sub> (PLLA and PDLA are both semicrystalline and do show T<sub>m</sub>s), rather just a T<sub>g</sub> of approximately 28°C (Table 3.4). In accordance with copolymer **3.14**, the DSC trace of copolymer **3.17** exhibited a slight change in T<sub>g</sub> to -63°C from IIR's T<sub>g</sub> of -70°C. In addition, a T<sub>g</sub> corresponding to the PDLLA domains was observed at 23°C. This is a similar trend to what was observed with IIR-PCL graft copolymers, however, the T<sub>g</sub> of amorphous PDLLA (**3.10**) was affected. Upon incorporation into the graft copolymer, the T<sub>g</sub> of **3.10** was effectively reduced from 28°C to 23°C. Additionally, if present as a contaminant in the graft copolymers, the DSC traces would also show the existence of free, ungrafted PDLLA chains. In this case, there

would be an additional glass transition peak at the temperature corresponding to **3.10**'s  $T_g$  (Appendix G). This extra glass transition was not observed here, confirming graft copolymer purity.

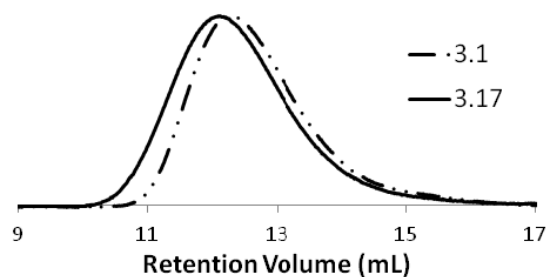


**Figure 3.10 – SEC traces of ungrafted IIR (polymer 3.1) and IIR-PDLLA graft copolymer (3.17).**

### 3.3 Preparation of IIR-PCL/PDLLA Blends

In order to observe the advantages that graft copolymers exhibit, physical blends consisting of IIR and polyesters were also prepared. In brief, these blends were prepared by dissolving IIR and either PCL or PDLLA in a common solvent, and then the solvent was removed. To replicate the polyester content of the graft copolymers, blends with IIR and 15, 32 and 44 wt% PCL as well as 30 wt% PDLLA were prepared and characterized by  $^1\text{H}$  NMR and DSC. DSC traces (Appendix I) for blends consisting of PCL (5000 g/mol) and IIR were found to exhibit the same  $T_{gs}$  ( $-66^\circ\text{C}$ ) and  $T_{ms}$  ( $50^\circ\text{C}$ ) regardless of PCL wt% incorporation. It is also interesting to note DSC traces for PDLLA (18 000 g/mol) blends and IIR. PDLLA homopolymer was provided by Sigma-Aldrich®, with a glass transition temperature in the range of  $38-42^\circ\text{C}$ . In this case, two  $T_{gs}$  were observed, one for IIR at  $-67^\circ\text{C}$  and the other corresponding to PDLLA at  $40^\circ\text{C}$  (Appendix I).

## 3.4 Physical Characterization of Graft Copolymers

### 3.4.1 Atomic Force Microscopy

The study of IIR-polyester graft copolymer films by AFM was of interest in order to gain insight into the phase separation and nanoscale morphologies of these polymers. In recent work, Zhang *et. al.* have demonstrated that breakout crystallization occurs when studying the thermal effects on block copolymers consisting of poly(butadiene)-*block*-PCL (PBD-*b*-PCL).<sup>221</sup> Breakout crystallization occurs when a crystalline portion that exhibits nanometer length scale domains is subsequently heated, thus transforming it into regularly alternating lamellae between the crystalline and amorphous layers. This successfully alters (or destroys) the melt mesophase, due to the crystallization of one block. Although the mechanism of breakout crystallization is poorly understood, it may occur when the crystallization driving force is enough to overcome the energy barrier due to the amorphous surroundings.<sup>222,223</sup> Furthermore, when considering PBD-*b*-PCL, it has been shown that PCL minority blocks do in fact break out into lamellar alternating structures with PBD.<sup>224</sup>

Therefore, because IIR-PCL copolymers are similar to PBD-*b*-PCL (amorphous and semicrystalline domains), AFM analysis could provide interesting images of copolymer nanoscale structure pre- and post-annealing. Although it would be of interest to understand the breakout kinetics (such as crystal coalescence and growth), AFM equipment involving real-time imaging was not available. However, differences in topographical and phase images could be analyzed, indicating that the development of crystallization did in fact impact the surrounding amorphous microdomain structures. In recent work, IIR-PEO graft copolymers exhibited micrometer scale patterns when spin-cast on to silicon wafer surfaces.<sup>147,148</sup> In this case, the patterning was attributed to kinetic factors such as the freezing of Marangoni instabilities, as well as phase separation (thermodynamically driven). In this sense, it would be interesting to study the pattern formation with IIR-PCL graft copolymers. Although PCL, like PEO, is semicrystalline, its inherent hydrophobicity could possibly affect the resulting surface morphology of copolymers.

Thin films of copolymers **3.14-3.17** were prepared via spin-coating a 3 wt% solution of copolymer in toluene onto silicon wafers. AFM showed that full surface coverage was achieved; topographical and phase images were obtained and analyzed. As shown in Figure 3.11, the surfaces were moderately rough at the nanometer scale. The average roughness was found using XEI software to be 1.45, 0.394, 3.09 and 0.203 nm for copolymers **3.14-3.17**, respectively.

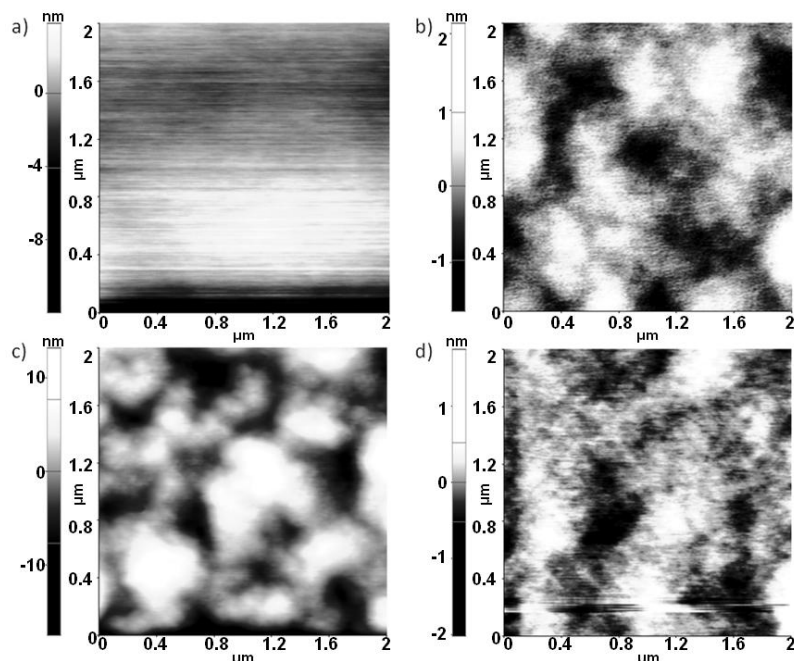


**Figure 3.11 – Topography of copolymers: a) 3.14; b) 3.15; c) 3.16; d) 3.17.**

IIR and PCL are both hydrophobic, but because they are chemically different, phase separation is possible under certain conditions. Consistent with the lack of  $T_m$  in DSC traces, no phase separation was observed for copolymer **3.14**, containing 15 wt% PCL (Figure 3.12a). However, upon increasing to 32 wt% PCL in copolymer **3.15**, some nanoscale patterning was observed (Figure 3.12b). By increasing the content of PCL further to 44 wt% in copolymer **3.16**, increased heterogeneity was observed (Figure 3.12c). From these results, it can be concluded that upon reaching a certain PCL content, the PCL can separate from the melt and overcome the surface energy of IIR, which tends to migrate to the top of the surface (lower surface energy). The repulsive energy from the chemically different polymers must be great enough in copolymer **3.16** for phase

separation to occur, thereby producing significant microstructures and surface patterning. In other words, free energy minimization during microphase separation therefore results in interesting patterning.<sup>225</sup> In the case of copolymer **3.17**, the image was suggestive of nanoscale phase separation, but well-defined patterns were not identified.

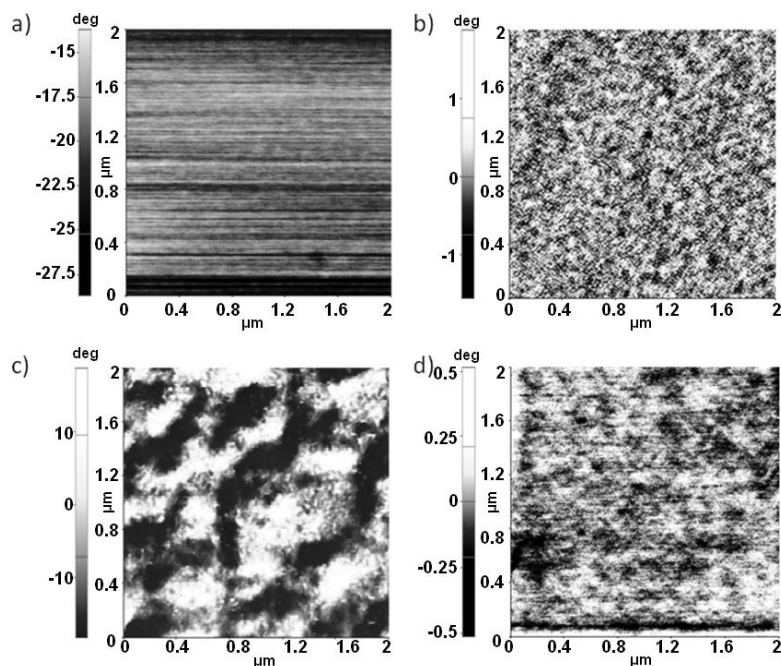


**Figure 3.12 – Phase contrast of copolymers: a) 3.14; b) 3.15; c) 3.16; d) 3.17.**

Upon annealing all of these surfaces, although partial organizing of PCL domains was observed in copolymer **3.15**, copolymer **3.16** displayed what appears to be a form of breakout crystallization (Figure 3.13d). Regular and alternating domains of PCL and IIR were formed on a nanometer scale. Perhaps the crystalline blocks were able to dissociate out of their microdomains and into the crystal growth front. In addition, the spin-coating process is kinetically driven, resulting in structures that are not thermodynamically favoured. However, annealing allows the copolymers to form their most thermodynamically favoured arrangement. Because the PCL chains are grafted at various points in the IIR backbone (due to 0.5-4 mol%), phase separation is restricted to nanoscale patterning. Therefore alternating lamellae of PCL form between IIR main chains. Further studies would have to be performed in order to determine the nucleation,



coalescence and growth, however, as a preliminary study, terraced crystalline structures did coalesce and form ordered structures upon crystallization of PCL domains.

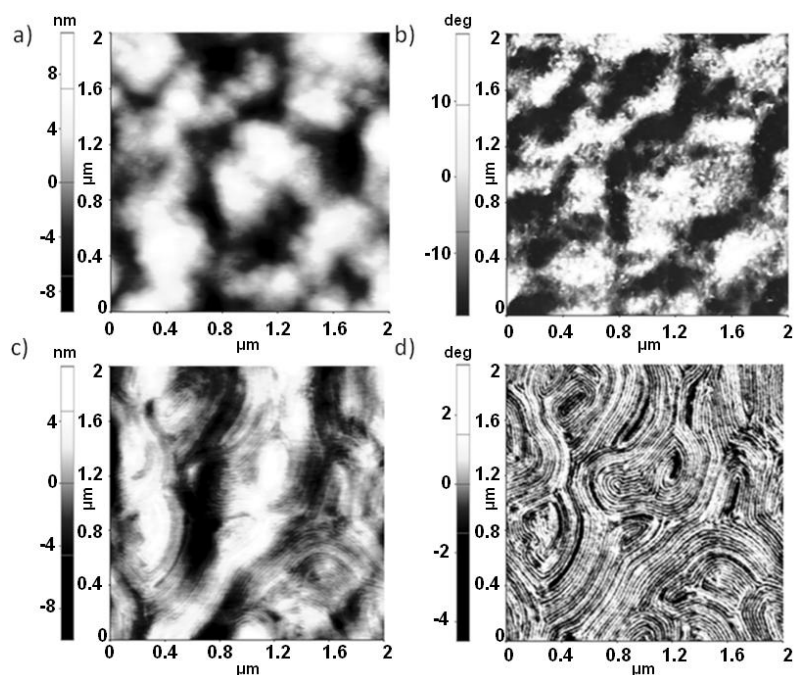


**Figure 3.13 – AFM analysis of copolymer 3.16. Before annealing: a) topography; b) phase contrast. After annealing: c) topography; d) phase contrast.**

Next, it was of interest to study the importance of the covalent grafting of PCL to the IIR backbone by imaging the physical blends of IIR with PCL and PDLLA. Topographic images proved that blended samples formed heterogeneous morphologies, characterized by the formation of micrometer-scale polyester aggregates. The dark spherical portions that can be observed in Figure 3.14, likely represent elastomeric particles dispersed throughout both polyesters in prepared blends. In congruence with Gheno *et. al.*,<sup>226</sup> acrylonitrile butadiene (NBR) with poly(vinyl chloride) (PVC) blends displayed spherical aggregates that increased in size with increasing soft segment, NBR. From Figure 3.14a, it is clear that the blend with the highest percentage of IIR (15 wt% PCL) displayed larger spherical elastomeric aggregates (on average) when compared to polymer blends with higher percentages of polyester. Moreover, in comparison to the graft copolymers, polymer blends (with comparable polyester incorporation) showed an increase in surface roughness to 5.78, 16.20, 4.78, 3.29nm for 15 wt% PCL, 32 wt% PCL, 44 wt% PCL and

30 wt% PDLLA blends, respectively. Likely, the covalent grafting of the polyester to the rubber confines phase separation to the nanoscale, rather than micrometer scale.

Physically incorporated polyesters can phase separate at any length scale and are not restricted by polymer dimensions. Knowing the composition of each blend also provided information pertaining to regions within each image. It appears that the darker regions are associated with the spherical elastomeric portions (depressions), forming by means of a coalescence mechanism.<sup>227</sup>

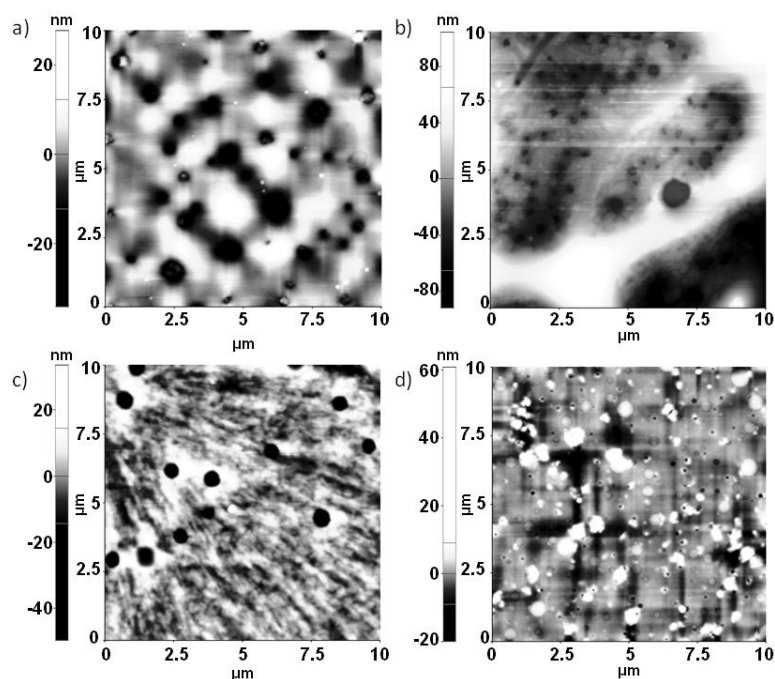


**Figure 3.14 – Topography images of IIR-polyester blends: a) 15 wt% PCL; b) 32 wt% PCL; c) 44 wt% PCL; d) 30 wt% PDLLA.**

Understanding the morphology in these blends was important in order to properly comment on the observed phase contrast images. In agreement with other rubbery-semicrystalline blend systems, darker regions are typically associated with softer, elastomeric portions.<sup>228</sup> It should also be noted that PDLLA does differ from PCL due to its amorphous nature. Because of this, PDLLA portions appear to represent darker spherical regions, resulting due to the agglomeration of PDLLA. When observing the phase contrast images in Figure 3.15a, b and d of 15 wt% PCL, 32 wt% PCL and 30 wt% PDLLA, respectively, there appear to be regions outside of the major patterning, which

are likely attributed to blend portions consisting predominantly of IIR. However, Figure 3.15c, corresponding to 44 wt% PCL blend does not exhibit these regions. Having reached a critical amount of PCL may have caused the crystalline portion to link itself, thus forming tightly packed domains. This phenomenon has also been observed with IIR/poly(butylene terephthalate) and liquid crystalline polymer blends in that increasing the crystalline portion to 75% resulted in the formation of agglomerates and fibril formation.<sup>227</sup> Lastly, consistent with the graft copolymers, PCL blends of 32 wt% and 44 wt% do appear to show lamellar patterning of larger PCL domains. However, increasing the weight percentage of the crystalline portion and allowing it more mobility caused an increase of patterning and overall complexity of observed phase contrast images.

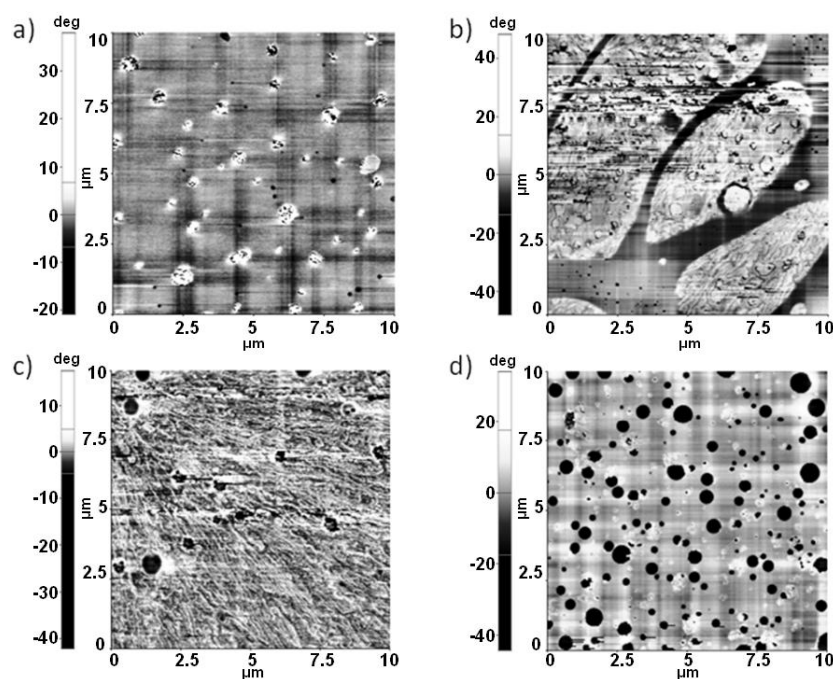


**Figure 3.15 – Phase contrast of polymer blends: a) 15 wt% PCL; b) 32 wt% PCL; c) 44 wt% PCL; d) 30 wt% PDLLA.**

### 3.4.2 Water Contact Angle Measurements

WCA evaluation is important when considering biomedical applications because biomaterials will likely come into contact with water, blood, or other bodily fluids. Understanding the material's hydrophilicity and therefore wettability could impact its use in certain applications. Table 3.5 illustrates the WCAs found for copolymers **3.14-3.17**, as well as PCL (900 g/mol, **3.7a** and 3500 g/mol, **3.7b**) and PDLLA (2800 g/mol, **3.10**) homopolymers. PCL-diol with a MW of 2000 g/mol has been shown to have a contact angle of approximately 79°. <sup>229</sup> Sessile drop analysis performed on PCL homopolymers showed similar contact angles of  $50.9^\circ \pm 1.77^\circ$  and  $70.8^\circ \pm 1.48^\circ$ , for PCL of 900 g/mol and 3500 g/mol, respectively (Table 3.5). However, increasing the MW of PCL shows increased contact angles; PCL of 80 000 g/mol has displayed contact angles of  $107^\circ$ <sup>230</sup> and  $114^\circ$ .<sup>218</sup> Lower contact angles for lower MW polymers can likely be attributed to the highly hydrophilic hydroxyl termini, which can have a larger impact in the context of lower MW polymers. With PDLLA, similar trends were observed. Higher MW PDLLA (125 000 g/mol) has been shown to have a static contact angle of  $95.28^\circ \pm 0.18^\circ$ .<sup>231</sup> **3.10** (PDLLA, 2800 g/mol) exhibited a lower contact angle of  $66.1^\circ \pm 1.97^\circ$  (Table 3.5).

**Table 3.5 – Contact angle of PCL and PDLLA homopolymers and copolymers.**

Homopolymer/Copolymer	Contact Angle (deg)
<b>3.7a</b>	$50.9 \pm 1.77$
<b>3.7b</b>	$70.8 \pm 1.48$
<b>3.10</b>	$66.1 \pm 1.97$
<b>3.14</b>	$92.1 \pm 0.68$
<b>3.15</b>	$91.5 \pm 2.30$
<b>3.16</b>	$94.1 \pm 1.38$
<b>3.17</b>	$91.0 \pm 1.50$

Upon grafting 3500 g/mol PCL to the IIR backbone, copolymer **3.16** showed an increase in contact angle to approximately  $94^\circ$ , whereas copolymer **3.15** showed an increase to approximately  $91^\circ$  (relative to PCL homopolymer). Copolymers **3.14** and **3.17** had very similar contact angles of  $92^\circ$  and  $91^\circ$  respectively. IIR has an approximate contact angle of  $91^\circ$ .<sup>232,233</sup> Therefore the contact angles of the graft copolymers were very similar to those of IIR. Although PCL and PDLLA homopolymers displayed lower contact angles, upon functionalization and subsequent grafting, their hydroxyl termini were no longer liberated. This would likely decrease their hydrophilicity, causing IIR to predominantly influence the contact angle.

Contact angles of approximately  $90^\circ$  are within the range of typical contact angles for various biomaterials.<sup>234,235</sup> Implanted biomaterials can be problematic for thrombosis formation and eliciting inflammatory responses, which are related to substrate wettability. Although thrombus formation occurs through a biological system known as the coagulation cascade, which is a healthy response of damaged tissues, thrombosis and occlusion are particularly problematic when polymers are used to synthesize vascular grafts.<sup>236</sup> Thrombus formation begins with protein adsorption onto the foreign substance and is more pronounced in terms of nonspecific protein binding onto highly hydrophobic surfaces. Contact angles around  $90^\circ$  have not been shown to cause nonspecific protein binding,<sup>237</sup> therefore confirming their potential application for vascular prosthetics. In order to confirm this, different techniques such as ellipsometry, quartz crystal microbalance with dissipation monitoring and surface plasmon resonance can be employed to determine protein adsorption.

### 3.4.3 Tensile Testing

Uncrosslinked IIR exhibits very low mechanical strength and low Young's Modulus. It was hoped that these properties could be improved through the incorporation of the polyesters. Therefore, the mechanical properties of the new graft copolymers were measured by tensile testing. The results of these tests are summarized in Table 3.6 and the corresponding stress-strain curves can be found in Figure 3.16. PCL and PDLLA have tensile strengths of  $3.9 \pm 0.34$  MPa (elongation at break ( $E_b$ ) =  $61 \pm 0.8\%$ ) and  $41 \text{ MPa} \pm 6 \text{ MPa}$  ( $E_b = 6.0\text{-}73.7\% \pm 4\%$ ), as well as Young's Moduli of  $83 \pm 9$  MPa and  $26.7 \text{ MPa} \pm 5 \text{ MPa}$ , respectively.<sup>79,238-241</sup> IIR has been shown to have E values of approximately  $0.20\text{-}0.5 \text{ MPa}$ <sup>242</sup> and a tensile strength of  $0.09 \text{ MPa}$  ( $E_b = 800\%$ ),<sup>243</sup> and it was of interest to determine how this was affected by grafting PCL and PDLLA to its backbone.

By covalently combining both PCL and PDLLA with IIR, it provided rubber-toughening, while also making the homopolymers more compliant by increasing their resiliency. PCL and PDLLA are quite brittle, as can be observed by their relatively low  $E_b$ s (i.e. brittle fracture). Graft copolymer synthesis allowed for a large increase in elongation (Figure 3.16). As per Table 3.6, graft copolymer **3.14** experienced a 15-fold increase in elongation whereas copolymer **3.17** showed a 42-fold increase (compared to ungrafted PCL and PDLLA). Increases in elongation prove an increased compliance, thereby decreasing brittle fracture that is experienced by the polyester homopolymers. Additionally, graft copolymers experienced dramatic increases in Young's Moduli relative to IIR, which can be owed to an increase in crystallinity (due to PCL and PDLLA). It was interesting to note that although copolymer **3.15** has a higher wt% of PCL incorporation than copolymer **3.14**, its stress vs. strain profile appeared to mimic that of elastomeric IIR more closely (Figure 3.17 for a general elastomer profile).



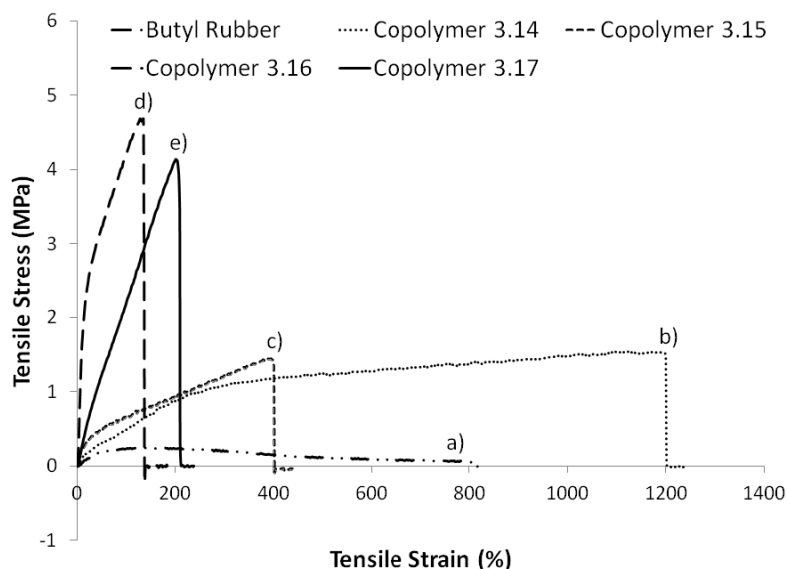


**Figure 3.16 – Stress-strain curve for: a) IIR; b) copolymer 3.14; c) copolymer 3.15; d) copolymer 3.16; e) copolymer 3.17.**

**Table 3.6 – Tensile data of graft copolymers and IIR.**

Copolymer	Polyester % in Copolymer	Young's Modulus E, at 50% Elongation, MPa	Young's Modulus E, MPa	Ultimate Tensile Strength (UTS), MPa	Elongation at Break ( $E_b$ ), %
<b>IIR</b>	0	$0.66 \pm 0.19$	$0.56 \pm 0.12$	$0.247 \pm 0.010$	$739 \pm 198$
<b>3.14</b>	15	$1.10 \pm 0.41$	$0.47 \pm 0.06$	$1.45 \pm 0.20$	$1216 \pm 182$
<b>3.15</b>	32	$1.14 \pm 0.27$	$0.74 \pm 0.15$	$1.24 \pm 0.13$	$447 \pm 65$
<b>3.16</b>	44	$9.57 \pm 1.13$	$21.66 \pm 5.90$	$3.92 \pm 1.03$	$165 \pm 29$
<b>3.17</b>	30	$3.07 \pm 0.47$	$2.90 \pm 0.43$	$4.00 \pm 0.86$	$251 \pm 52$

By grafting PCL onto the IIR backbone, elongation was increased at varying amounts depending on the weight percentage of PCL incorporation onto the IIR backbone. The acquired data follows the expected trend; increasing the percentage of PCL decreases its ability to elongate (relative to IIR), reaching a maximum decrease (7X) by graft copolymer **3.16**. Furthermore, E also increases from 0.47 MPa (copolymer **3.14**) to about 22 MPa (copolymer **3.16**). Copolymer **3.16** exhibits somewhat brittle fracture (as

it behaves similarly to PCL homopolymer, Figure 3.17 for semicrystalline polymer), whereas copolymers **3.14** and **3.15** display longer elongations and increased UTS (compared to IIR). In addition, the tensile strength at break ( $T_b$ ), or UTS, increased dramatically from copolymer **3.14** and **3.15** to copolymer **3.16** by inducing a small change in PCL content. Although it is difficult to conclude whether true TPEs have been produced, confirmation of this could be accomplished via cyclic loading tests.

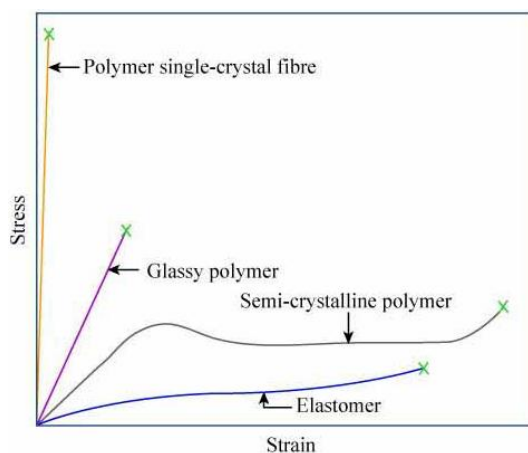


**Figure 3.17 – Stress vs Strain of a variety of materials (with permission to reprint from MIT OpenCourseWare, <http://flic.kr/p/66XeQc>).**

Lastly, it is interesting to consider the study by Xu *et. al.* where they investigated the influence of increasing the soft block in a PUR TPE.<sup>244</sup> TPEs with higher hard segment content (40-50% soft segment weight concentration, SSC) had higher moduli and larger initial linear portion, whereas increased soft segment TPEs (60-70% SSC) showed greater elastomeric behaviour and higher recoverability (Figure 3.18). Mechanical properties of TPEs are generally described as materials exhibiting high tensile strength and elongation of at least 2 times its original length.<sup>184</sup> Although the strengths of copolymers **3.14** and **3.15** were not significantly increased, they still display excellent elongation properties with partial physical crosslinking. Their greater elongation and better recoverability is owed to their more elastomeric behaviour. Comparatively, copolymers **3.16** and **3.17** possess higher strengths with moderate elongation. However, plasticization of the amorphous phase was still apparent. This is an inherent characteristic of rubbery elastomers.<sup>245</sup>



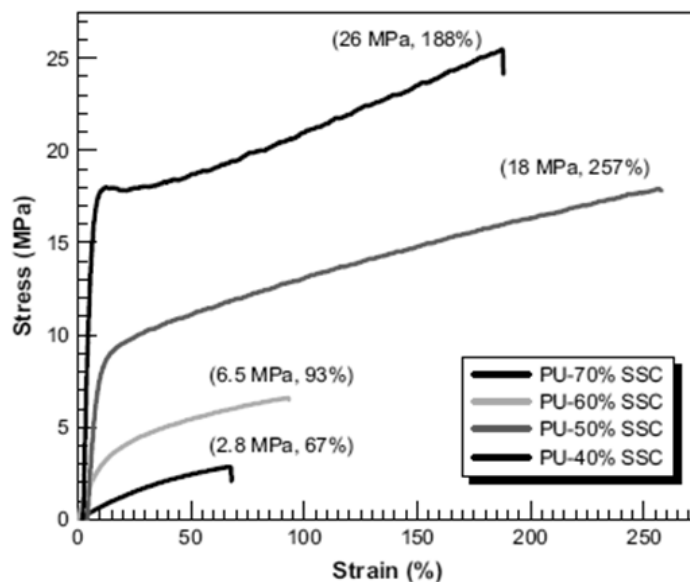


**Figure 3.18 – Thermoplastic PURs with varying soft segment contents. (Reprinted from Polymer, 49/19, Xu *et al.*, Morphology and properties of thermoplastic polyurethanes with dangling chains in ricinoleate-based soft segments (4248-4258). Copyright (2008), with permission from Elsevier).<sup>244</sup>**

From the AFM imaging, increasing to 44 wt% PCL in IIR copolymers induced phase separation. Therefore, one can infer that the microphase-separated structure of the IIR-PCL films enforced the mechanical characteristics, thereby imparting increased E and UTS. The PCL domains that exist throughout the IIR matrix provide a physical crosslinking mechanism, acting as fillers to strengthen the copolymer.<sup>243</sup> Copolymer **3.17**, when compared to IIR, also showed increases in Young's Modulus and UTS from 0.56 – 2.90 MPa and 0.247 to 4.00 MPa, respectively. Comparatively, it does show similar trends to PCL-based copolymers in that its overall strength is increased, however, copolymer **3.17** (30 wt% PDLLA) has almost the same UTS as copolymer **3.16** (44 wt% PCL). This is consistent with literature results in that PDLLA does display higher strengths than PCL. Overall, homopolymers of PCL and PDLLA are extremely brittle. For applications involving vascular grafts, compliance and a material's ability to stretch are of paramount importance.<sup>246</sup> Therefore graft copolymer synthesis effectively tunes and enhances the mechanical properties of IIR.

In biomedical applications, UTS and elongation are factors that govern suitability of a material for a given application. For example, elastomeric materials display physical properties that render them useful for implants involving soft or cardiovascular tissue.<sup>2,247</sup> The vascular wall consists of elastin, collagen and smooth muscle with Young's Moduli ranging from 0.3-0.6 MPa, 100-2900 MPa and 0.006 MPa, respectively.<sup>107</sup> Moreover, elastin and collagen exhibit tensile strengths 0.36-4.44 MPa and 5-500 MPa. Therefore for vascular stent applications, materials need to be extensible, allowing for vascular dilation and constriction. Although mechanical properties of different soft tissue can be mimicked by graft copolymers **3.14-3.17**, it is important to note that many complex factors dictate an effective vessel. For example, arteries are anisotropic, pulsatile, compliant and thrombosis-resistant. Because of these complexities, *in vivo* testing of possible prosthetics is critical when determining practical applicability.

Implantable materials need to reflect the mechanical behaviour (stresses/strains) of the tissues that they are either replacing or supporting. It is apparent from Figure 3.19 that the diversity of toughness and E values of biological tissues requires a range of biomaterials to be developed. Bone and tooth enamel require high moduli and moderate UTS, due to their high-strength but brittle characteristics. However, collagen-rich tissue such as intervertebral discs has moderate compliance and toughness because strength needs to be maintained at higher strains. Figure 3.19 also depicts soft tissues with varying levels of toughness and (lower) modulus combinations. However, successful clinical implants typically have extremely high UTS (10-100MPa), which is much larger than living tissue UTS (0.01-10MPa). Therefore, materials are needed with lower toughness and moduli for cartilage, cardiovascular tissue and orthopaedic soft tissue. Copolymer **3.16**, with a UTS of approximately 4 MPa and a Young's Modulus of 22 MPa could potentially serve as an implantable device for orthopaedic deficiencies, while copolymer **3.17** may be appropriate for softer cardiovascular tissue.

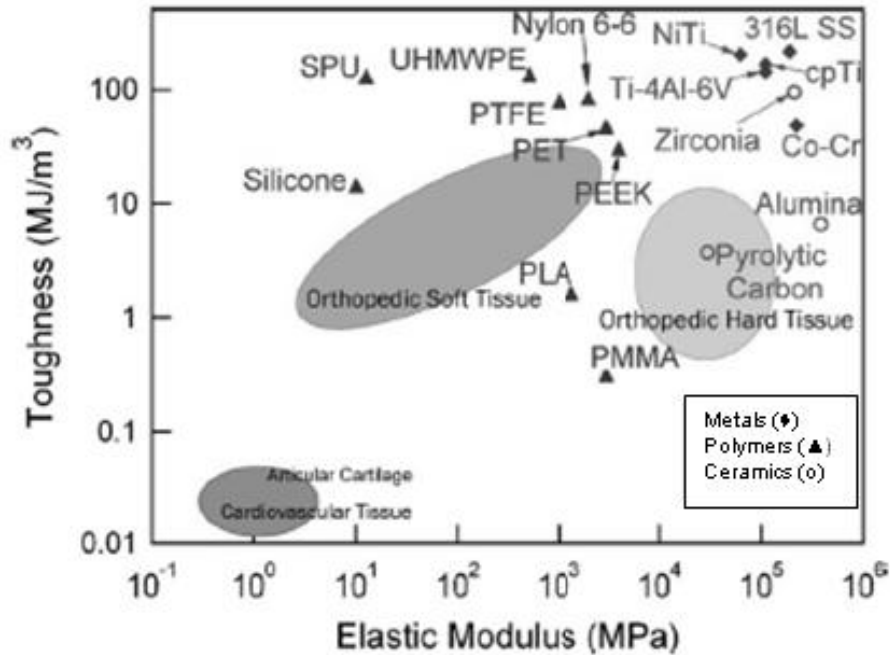


**Figure 3.19 – Toughness-Modulus plot for current implant materials and the mechanical regions for orthopedic hard tissue, orthopedic soft tissue, and cardiovascular tissue. (Reprinted with permission from Taylor & Francis, 2013).<sup>246</sup>**

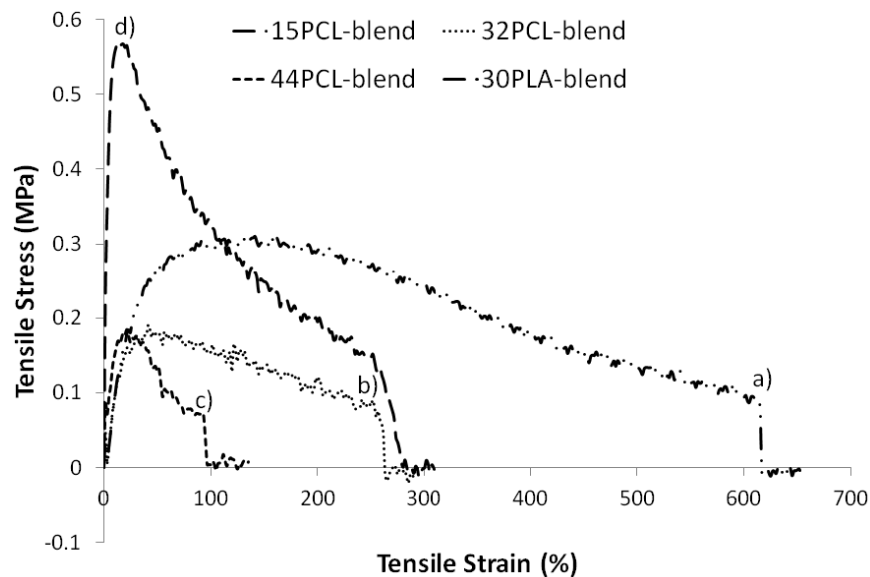


**Figure 3.20 – Stress-strain curve for: a) 15 wt% PCL blend; b) 32 wt% PCL blend; c) 44 wt% PCL blend; d) 30 wt% PDLLA blend.**

It was also important to demonstrate the superiority of covalent graft copolymer mechanical properties when compared to simple, physical blends. As revealed by AFM

imaging, not having PCL or PDLLA covalently linked to the IIR backbone resulted in free domains of polyester to be dispersed throughout the blend. Because domains were randomly dispersed, thereby causing a lack in consistent ordering or patterning, this manifested mechanical deficiencies, which were attributed to brittle PCL and PDLLA. These deficiencies are predominantly characterized by the blends' inability to withstand higher stress loads (Table 3.7). Moreover, the blends were much weaker when compared against their respective copolymer in terms of UTS. Figure 3.20 exhibits stress-strain plots for PCL (15-44 wt%) and PDLLA (30 wt%) blends, showing what appears to be an excess of noise, caused by the irregular composition of each blend. The blends' yield strengths are so high under tension that their yield strengths can never be reached because the materials fracture first (linear regime followed by fracture, no plastic deformation). In order to properly measure their yield strengths, unique tests that suppress fracture are needed. One that may be employed is referred to as the compressive crushing strength; however, this provides the elastic limit,  $\sigma_{el}$ , rather than the yield stress,  $\sigma_y$ .

**Table 3.7 – Tensile data of polymer blends.**

IIR – Polyester Blend	Polyester % Relative to IIR	Young's Modulus E, at 50% Elongation, MPa	Young's Modulus E, MPa	Ultimate Tensile Strength (UTS), MPa	Elongation at Break ( $E_b$ ), %
15 wt% PCL	15	0.79 ± 0.15	1.76 ± 1.57	0.28 ± 0.038	516 ± 114
32 wt% PCL	32	0.95 ± 0.18	2.29 ± 2.06	0.18 ± 0.025	271 ± 76
44 wt% PCL	44	1.20 ± 0.14	5.30 ± 2.33	0.18 ± 0.043	141 ± 52
30 wt% PDLLA	30	N/A	15.11 ± 4.51	0.62 ± 0.062	251 ± 74

As the tensile testing was performed on each blend, the sample seemed to fracture at the polyester domains; sample remained was still pulled in the axial direction due to IIR fibre attachment. The difference between many other studied IIR and thermoplastic polymer blends is typically the IIR is vulcanized prior to/during the blending process.<sup>248</sup> In these cases, blends showed an increase in UTS and E.

It can be concluded that the graft copolymers were superior in terms of their strength (compared to IIR and blend systems), which is an important property when considering materials for implantable biomedical devices. Although graft copolymers and blends were non-crosslinked (unvulcanized), the strength and rigidity added by the aliphatic polyester covalent attachment may serve as an appropriate avenue for avoiding harsh vulcanization conditions. This has been coined as 'green strength': the strength, cohesiveness, dimensional stability, and extensibility of rubber compounds prior to curing/vulcanization.<sup>228</sup> By avoiding vulcanization, graft copolymers may be considered viable candidates for *in vivo* applications.

### 3.5 Degradation Study of IIR-PCL/PLA Graft Copolymers

PCL and PDLLA have both been shown to degrade particularly slowly. Under physiological conditions, PCL has been found to degrade over a period of 3-4 years,<sup>84</sup> and PDLLA degrades over approximately 12-16 months.<sup>73,76</sup> IIR possesses high chemical stability, to the extent where it shows little to no degradation over several years. Because PCL and PDLLA were grafted onto the IIR backbone, it was expected that their degradation rates would be slowed. Since degradation rates were expected to proceed exceedingly slow, the focus of this study was therefore directed toward analyzing accelerated degradation rates by subjecting samples to 5M NaOH over a four month period.<sup>249-251</sup>

#### 3.5.1 Mass Evolution and Scanning Electron Microscopy

Interestingly, the accelerated degradation of copolymers **3.14-3.16** resulted in minimal weight loss, on the order of 0.5-1% change in weight (Figure 3.21, Appendix J). However, such minimal change in weight could be due to experimental discrepancies resulting from weight measurement, associated with the detection limit and low initial masses. In order to correct for this, future experiments should employ samples of larger masses. In order to correct for this, future experiments should employ samples of larger mass to realize greater differences pertaining to crude mass loss. However, these results were still quite significant when comparing to those of the control materials. Both IIR as well as PCL were studied under the same accelerated conditions to observe what affect the copolymerization of these materials had on their apparent degradation characteristics. The PCL control (MW approximately 5000 g/mol) fully degraded in less than 24 hours. In previous work, it has been found that the longer (and therefore higher MW) the aliphatic polyester was, slower degradation rates would therefore result.<sup>142,252</sup> Although mass loss was not apparent, the shorter PCL grafted chains of 900 g/mol (copolymer **3.14**) in comparison to 3500 g/mol (copolymers **3.15** and **3.16**) did show an increased rate of hydrolytic degradation, apparent in the subsequent SEC analysis section.

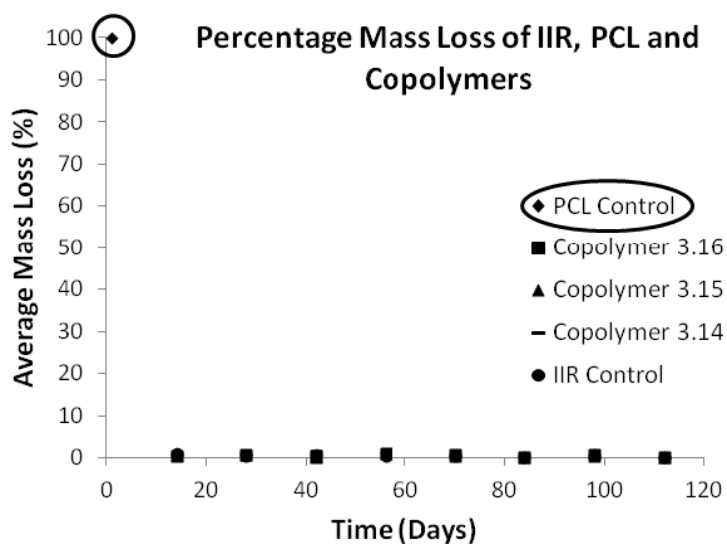


**Figure 3.21 – Mass loss of copolymers 3.14-3.16, PCL and IIR controls.**

The accelerated degradation of copolymer **3.17** was also studied to gauge if grafting of PDLLA to IIR exhibits accelerated degradation rates when compared to IIR-PCL copolymers. Due to time limitations, this study has only proceeded to the 2-month time point. Crude mass loss results were similar to copolymers **3.14-3.16** in that minimal weight loss, approximately 0.5-1.0 wt%, was observed (Figure 3.22, Appendix K for raw data). The same reasoning suggests that low perceived weight loss could be due to experimental discrepancies associated with the detection limit and low initial masses of testing materials. In congruence with PCL homopolymers, PDLLA showed complete degradation. However, full degradation was achieved in 5 days (compared to 24 hours), attributed to its higher MW (18 000 g/mol) than PCL (5000 g/mol).

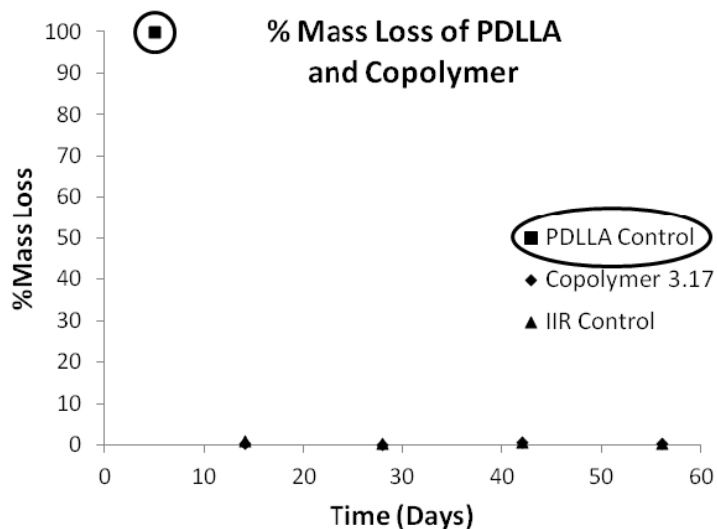


**Figure 3.22 – Mass loss of copolymer 3.17 as well as PDLLA and IIR controls.**

Next, when studying SEM results, PCL concentration appeared to significantly impact graft copolymer characteristics. As PCL wt% was increased, the obtained surfaces exhibited an increase in plasticity. It can be inferred that graft copolymers manifested partial TPE properties due to their excellent processability. When the discs were prepared via melt-pressing at elevated temperatures, the hard phase of the copolymers (PCL) would melt. However, upon cooling, the hard phase would solidify, producing copolymers with strength and elasticity. Copolymers exhibiting a greater portion of the hard phase therefore solidified into samples with reduced flowability, i.e. less elastomeric portion. Therefore copolymer **3.16** possessed higher plasticity resulting in flat and smooth topographies, which remained highly unchanged throughout the duration of the study (Figure 3.23d) and h)). Although copolymer **3.17** consists of PDLLA (not a semicrystalline “hard” phase), it does possess high UTS and E that are comparable to PCL. Perhaps these properties also caused copolymer **3.17** to have and retain smooth topographies over a 2 month period (Figure 3.24a and b). After just one month, IIR and copolymers **3.14** and **3.15** showed wrinkling, similar to their 4 month time points (Figure 3.23). Surface irregularities, however, were particularly pronounced for copolymers **3.14** and **3.15**, resulted in corrugated surfaces. This is perhaps attributed to the degradation of PCL. These findings also coincide with the notion of higher MW aliphatic polyesters displaying a decreased degradation rate. A higher degree of PCL incorporation and MW



for copolymer **3.16** (compared to copolymer **3.14**) suggests that there is a relationship between polyester concentration and the ability to maintain surface integrity.

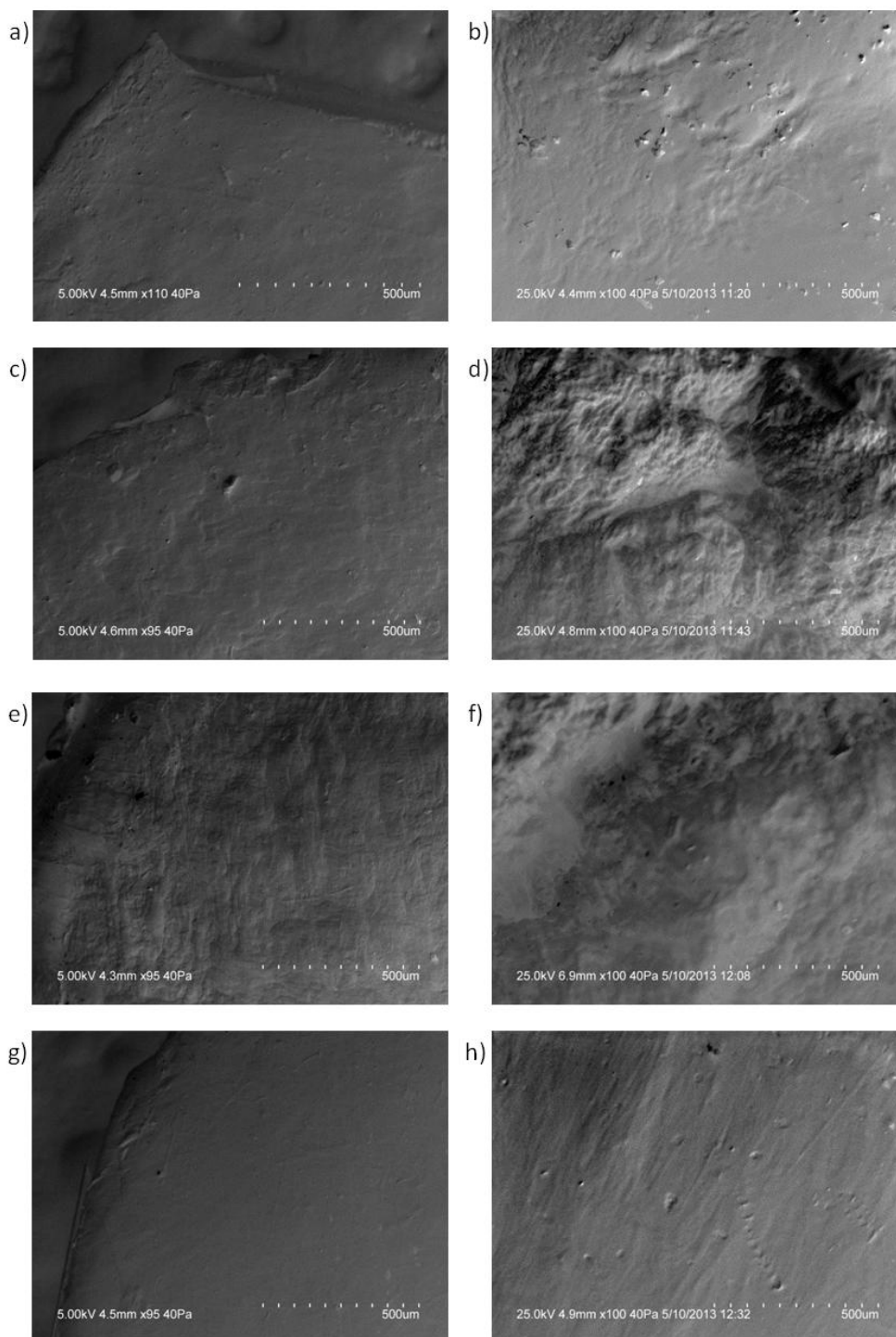


**Figure 3.23 – SEM imaging taken at 100X magnification under variable pressure mode at  $T_0$  and 4 months of: a) and b) IIR; c) and d) copolymer 3.14; e) and f) copolymer 3.15; g) and h) copolymer 3.16.**

Copolymers **3.14** and **3.15** and IIR displayed creep deformation resulting in sample wrinkling. Macroscopic images qualitatively portrayed the aforementioned sample deformation (Figure 3.25). As it can be seen, although there is no apparent weight loss, samples with higher amounts of IIR tend to shrink as they are subjected to an aqueous environment. Factors governing creep wrinkling can be attributed to differences in mechanical properties of IIR and PCL, resulting in smooth, shallow surface undulations due to uneven material expansion.<sup>253</sup> Moreover, wrinkling has been shown to relax the compressive strain in the hard layer (PCL), thereby reducing elastic strain energy.<sup>254</sup> Finally, the four month time point for copolymers **3.14** and **3.15** resulted in opaque materials, where the starting materials were more translucent. As PCL degraded, the crystallinity of the resulting degraded chains may have caused a decrease in sample transparency.

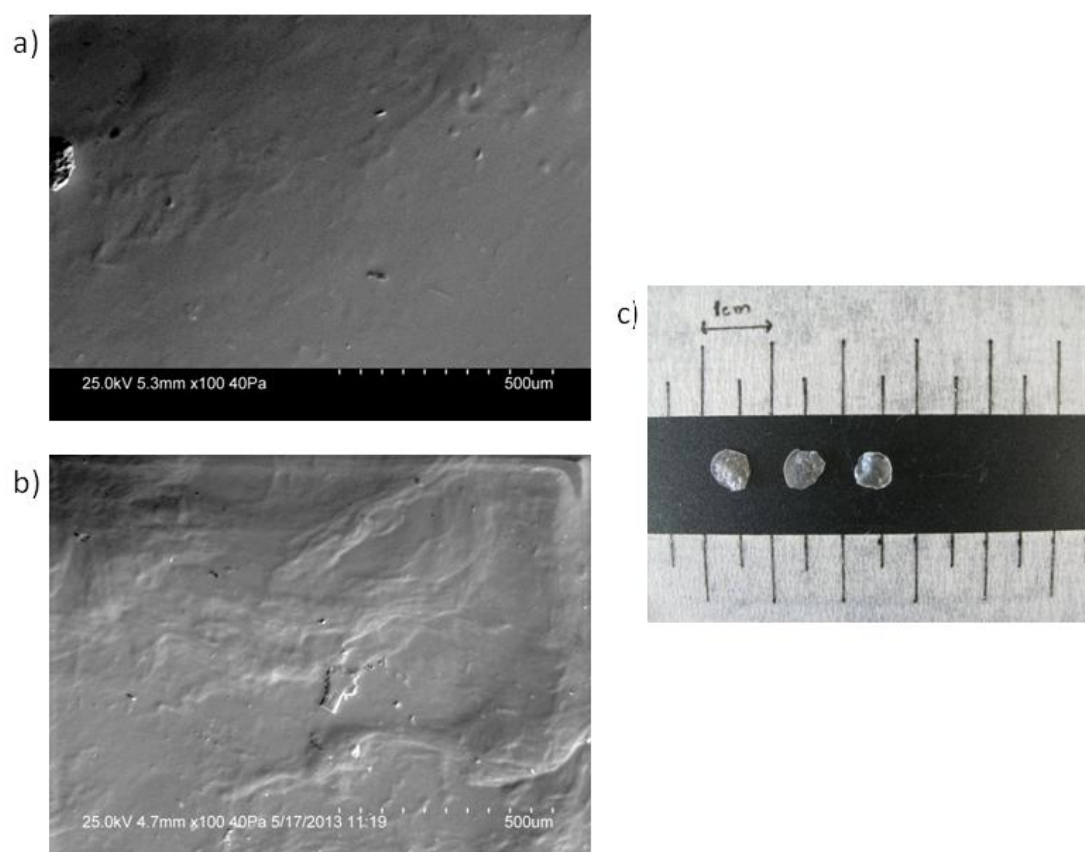


**Figure 3.24 – SEM imaging taken at 100X magnification under variable pressure mode at  $T_0$  and 2 months of: a) and b) copolymer 3.17. Macroscopic images of  $T_0$ -2 months of: c) copolymer 3.17.**

The macroscopic images are particularly interesting as there are some notable characteristics pertaining to copolymer **3.17** (Figure 3.24c) and **3.16** (Figure 3.25d). Wrinkling was almost negligible, along with maintenance of its translucent nature. These copolymers were not affected by creep deformation, which is favourable for different implantable applications such as vascular prosthetics. High amounts of degradation for such applications would not be favourable as they require mechanical strength and rigidity, along with structural integrity. Although copolymers **3.16** and **3.17** do not have as much strength or toughness as PIB-PMMA block copolymers, it is this decrease in rigidity yet structural integrity that makes them more suitable for soft-tissue-based applications (wound healing, sutures, intervertebral disc and articular cartilage repair).<sup>246</sup>

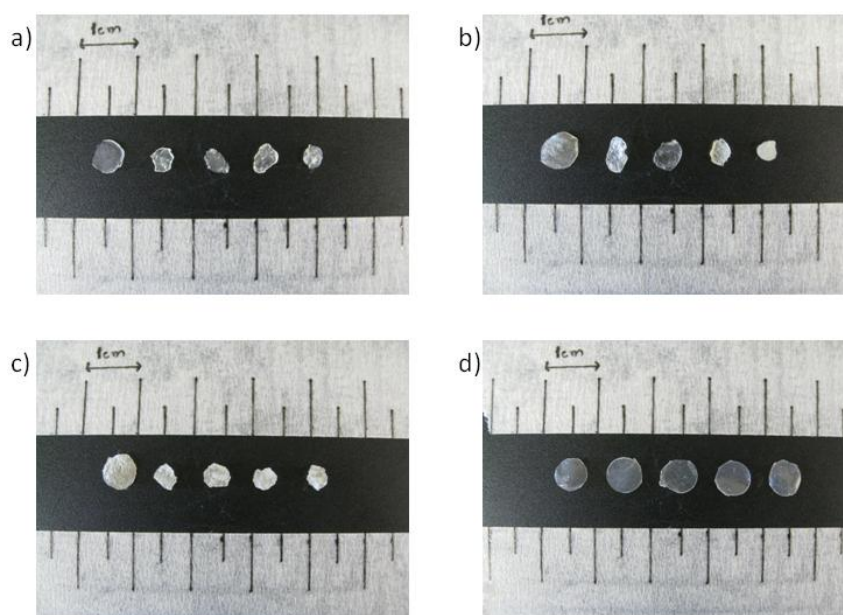


**Figure 3.25 – Successive macroscopic images representing  $T_0$ , 1 month, 2 months, 3 months and 4 months of: a) IIR control; b) copolymer 3.14; c) copolymer 3.15; d) copolymer 3.16.**

There is a large interest in TE applications therefore synthesizing materials incorporated with biodegradable chemistries and materials that can withstand strains of up to 100% is highly favourable.<sup>255,256</sup> It is the combination of the ability to maintain mechanical integrity, elongation strains and appropriate strength that makes a material suitable as a shape memory polymer (SMP). Although SMPs can be synthesized across a wide range of polymer chemistries including poly(methacrylates/acrylates), aliphatic

polyesters and PURs, there are several degradation and mechanical related issues.<sup>257-259</sup> Original SMPs were based upon polymers such as PLA, PCL and poly(glycolide), with subsequent methacrylation to allow for free-radical polymerization, procuring crosslinked networks for drug delivery applications.<sup>260</sup> These SMPs suggested that although initial degradation did not affect material properties, degradation at amorphous regions increased crystallinity (and therefore E), thereby increasing brittle behaviour. However, degradation at the crystalline domains softened and decreased the modulus of the materials, resulting in structural deficiencies. Therefore, copolymers **3.16** and **3.17**'s ability to maintain their structural integrity with average elongations at break of 165% and 251% respectively (Table 3.6), demonstrates their applicability for applications requiring structural maintenance and resiliency. A decrease in rigidity and maintenance of structural integrity is the greatest accolades a polymeric device for such specific biomedical applications can therefore possess. *In vivo* conditions would have to be further examined as this may compromise structural integrity (cyclic mechanical loading and biochemical attack). Although these resulting deficiencies are more critical for polymers containing hydrophilic sensitivities, hydrophobic polymers may still experience a loss in toughness due to internal crazing effects or gradual surface hydrolysis.<sup>261</sup> However, PCL and PDLLA reinforced with IIR provide adequate water penetration resistance.

### 3.5.2 Size Exclusion Chromatography

In addition to crude mass loss measurements, SEC was also performed on polymeric materials at each time point. Even though there were no significant changes in mass, hydrolytic degradation under accelerated basic conditions may have affected copolymer MW profiles. Observing changes in MW will provide further insight toward understanding copolymer properties and applicability as biomaterials. The graphical representations shown in Figure 3.26 depict the change in  $M_n$  and  $M_w$  over the 16-week study period for copolymers **3.14-3.16** and 8 week period for copolymer **3.17**. Figure 3.26a shows that the  $M_n$  of IIR (control), copolymer **3.16** and copolymer **3.17** remained highly unchanged, which is attributed to IIR's chemical stability and copolymer **3.16** and **3.17**'s increased polyester concentration.

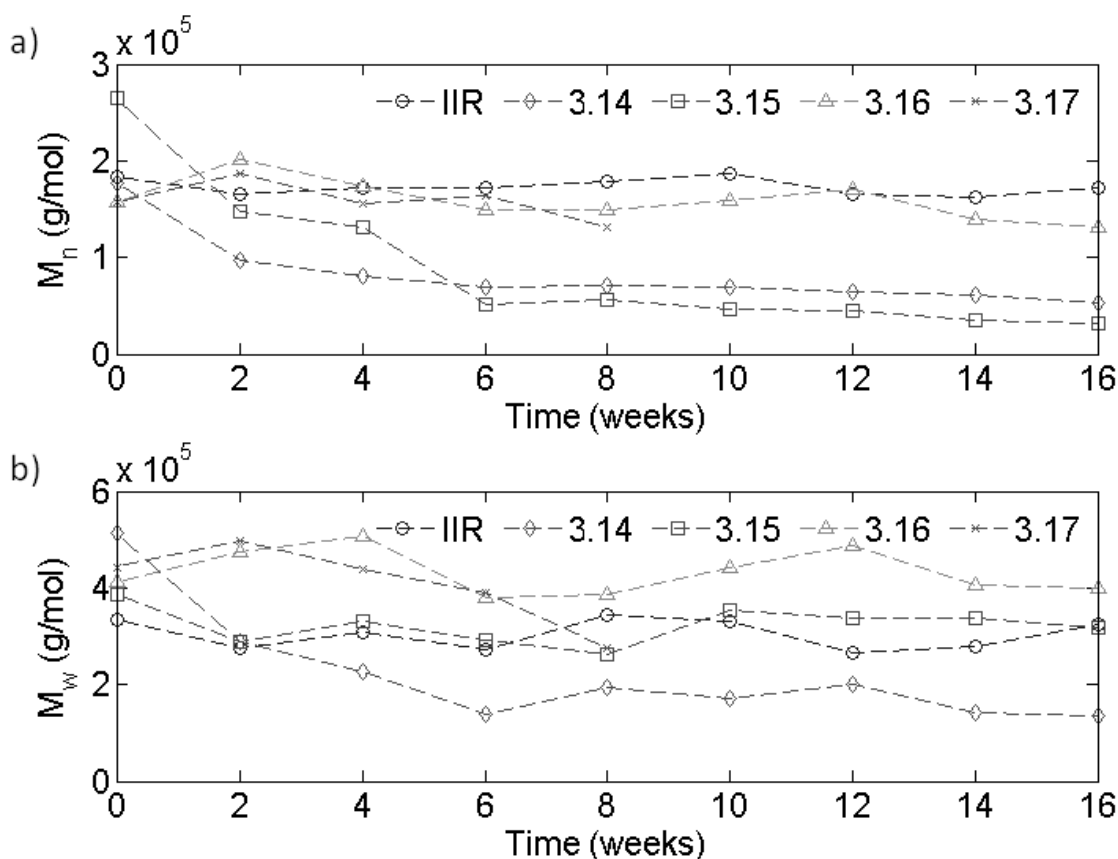


**Figure 3.26 – MW data for IIR control as well as copolymer 3.14, 3.15, 3.16 and 3.17: a) change in  $M_n$ ; b) change in  $M_w$ .**

Copolymers **3.14** and **3.15** showed gradual decreases in  $M_n$  values (Figure 3.26a). In congruence with this finding, Figure 3.27b shows a significant shift in the MW profile of copolymer **3.14**. Lower MW polyester chains will degrade faster; copolymer **3.14**, prepared with the lowest MW polymer (900 g/mol PCL), therefore exhibited the largest decrease in MW. Since it was prepared with lower MW PCL, cleavage of PCL chains underwent further degradation, resulting in oligomers that possibly diffused out of the polymer matrix (absence of lower MW side-peak in SEC traces). A simultaneous decrease in  $M_w$  was also realized, causing a dramatic but controlled decrease in MW profile.

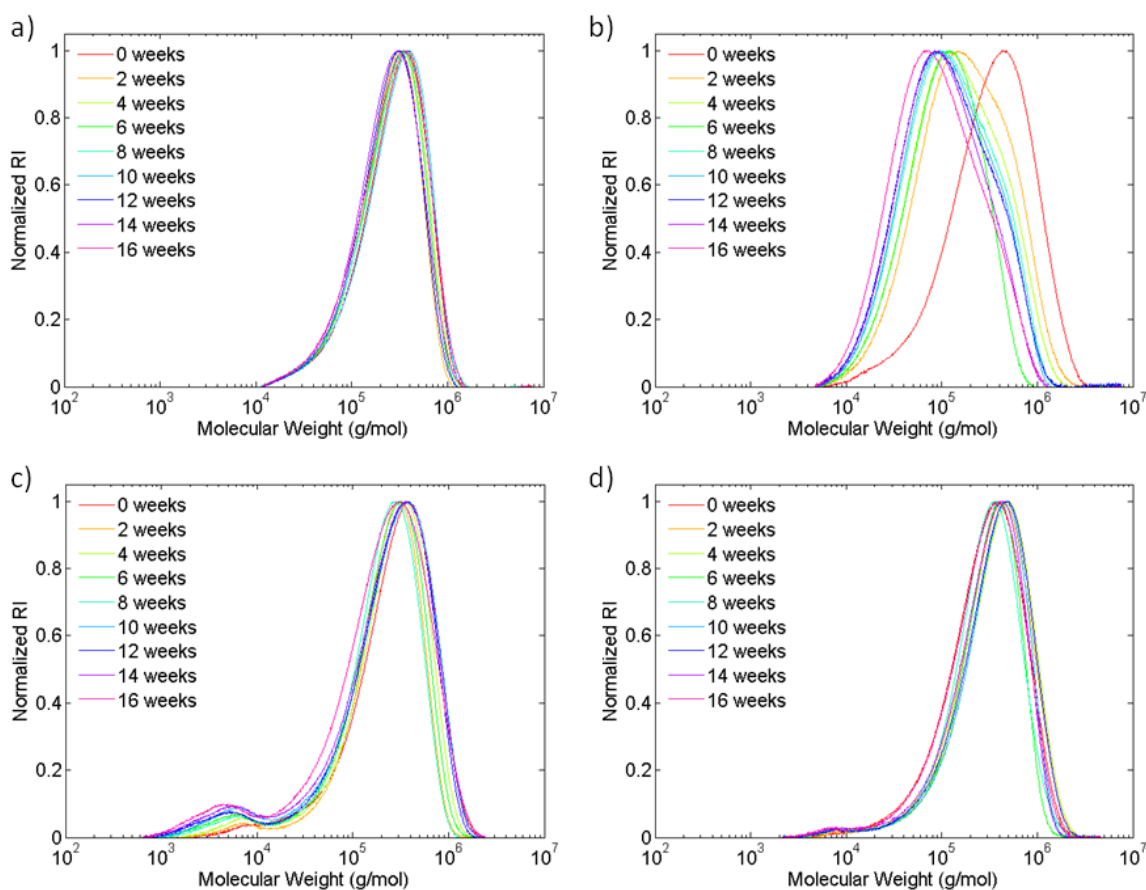


**Figure 3.27 – MW profiles elucidating each time point over the 4 month study period for: a) IIR control; b) copolymer 3.14; c) copolymer 3.15; d) copolymer 3.16.**

Even though copolymer **3.15** did show a decrease in  $M_n$ , its  $M_w$  did not show a corresponding decrease, causing the main peak (attributed to IIR) to remain stationary



(Figure 3.27c) causing a significant increase in PDI. This behaviour is attributed to the shedding of the lower MW PCL side chains and the formation of a bimodal polymer distribution.

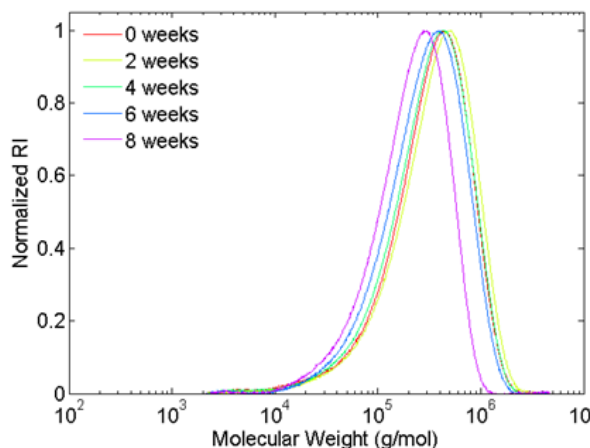


**Figure 3.28 – MW profile elucidating each time point over the 2 month study period for copolymer 3.17.**

Copolymer **3.16** did not show a significant decrease in either  $M_w$  or  $M_n$ , which is attributed to higher PCL concentrations. Miao *et. al.* showed that increasing the level of PCL and therefore crystalline domains in triblock copolymers of PCL and poly(sebacic anhydride) resulted in slower degradation profiles in both physiological and basic conditions.<sup>262</sup> Therefore in this thesis, increasing PCL content relative to IIR may be the determining factor for decreased degradation. Conversely, increasing amorphous domains allows water to penetrate and degrade materials easier. Because of this, degradation of IIR-PDLLA copolymer **3.17** was hypothesized to display an increased weight loss and change in MW due to PDLLA's amorphous state. However, Figure 3.28 showed that its MW profile remained relatively constant over the first 8 weeks of the study.

Degradation of PCL can occur via surface or bulk processes. However, a combination of these pathways may have influenced IIR-PCL copolymer degradation.<sup>90</sup> Prediction of erosion pathways is particularly complicated when grafting polyesters that typically abide by bulk erosion (where degradation is unpredictable and starts spontaneously) onto IIR (one that does not show degradation).<sup>263</sup> Although mass remained almost constant for all samples,  $M_n$  did decrease for copolymers **3.14** and **3.15**,

indicative of PCL chain cleavage and subsequent oligomer formation.<sup>264,265</sup> Chain scission was homogeneous for copolymer **3.14** causing a homogenous decrease in MW (bulk degradation). It is interesting to note, however, that **3.16** (44 wt% PCL incorporation) showed little to no change in MW. This is similar to surface degradation in that water cannot penetrate the polymer, causing the hydrolysed byproducts to diffuse rapidly into the media, resulting in limited water penetration to the copolymer matrix. As a result, degradation will occur purely at the surface, causing the polymer to thin while leaving the MW intact. However, under base-accelerated conditions, autocatalysis at the surface would not occur. Therefore the high concentration of PCL combined with stable IIR caused water penetration to be negligible resulting in minimal degradation.



## 3.6 Bioassays and Compatibility

### 3.6.1 Cell Growth on Polymer Films

The evaluation of cell growth on copolymer surfaces was performed by studying the adhesion and topology of C2C12 murine myoblast cells on films of copolymers **3.14-3.17**, and comparing them to the same cells grown on selected control surfaces. Although this method is qualitative, observing cell morphology is an essential screening method for cytotoxicity and cell compatibility at the initial analysis stage.<sup>191</sup> Observation of how the cells behave in terms of adhesion and viability gauges cellular response, which can be confirmed via the MTT (3-(4,5-dimethylthiazol-2-yl)-2,5-diphenyltetrazolium bromide) cytotoxicity test.<sup>191,266</sup> To prepare the films for these studies, copolymers **3.14-3.17** were prepared as 3 wt% solutions in toluene with subsequent drop-casting onto glass coverslips, followed by sterilization.

Seeding myoblasts onto polymer surfaces and comparing cell proliferation to glass, IIR, PCL and PDLA homopolymers, allowed for direct comparisons between substrate and cell morphology. After allowing an incubation period of 48 hours, cells were stained with DAPI (4'-6-diamidino-2-phenylindole dihydrochloride) and Alexa Fluor 568 phalloidin in order to visualize nuclei and actin protein fibers of the cytoskeleton, respectively. Observation of the cytoskeleton structure is crucial. Scrutinizing cellular spread and resulting morphologies provides qualitative comparisons between copolymers and control substrates to assess cellular health.<sup>267</sup> In addition, cells were also counted on each surface for a quantitative measure. In order to do so, surfaces were prepared in triplicate for each sample and 3 images were taken at random locations to determine cell density. Utilizing cellc12 and Matlab 9 numerical values were obtained. By averaging these values, determining standard deviations, and performing ANOVA statistical measurements (Prism), confirms whether cell densities are/are not significantly different between each surface. Figure 3.29 shows representative images from the control samples (a-d) as well as from each copolymer (e-h). In this regard, one can clearly evaluate the results on a qualitative and quantitative basis.

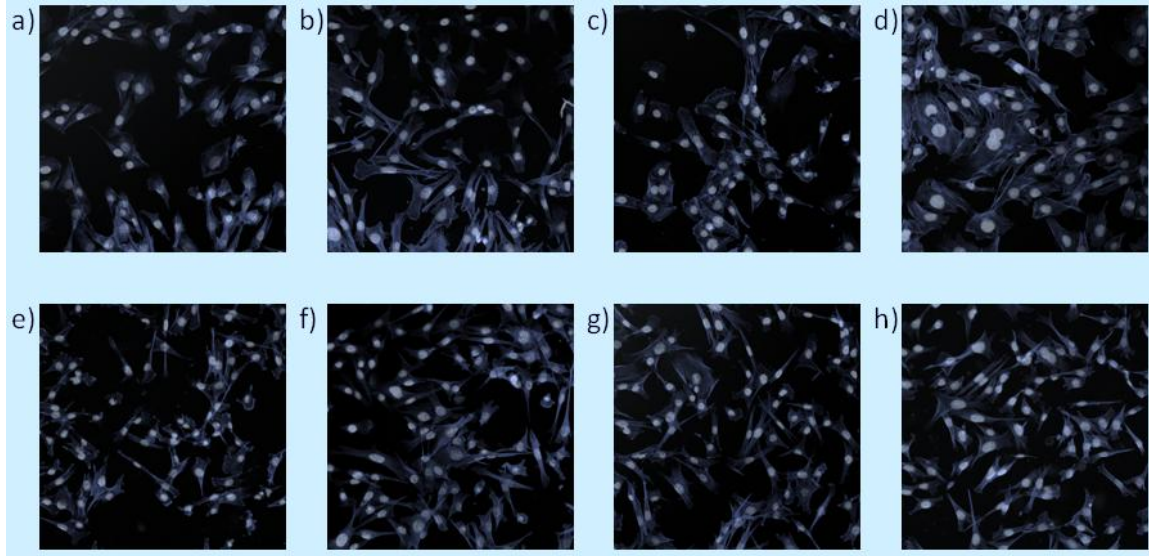


**Figure 3.29 – Growth of murine myoblast cells on: a) glass; b) IIR; c) PCL; d) PDLLA Cell imaging of copolymers: e) 3.14; f) 3.15; g) 3.16; h) 3.17.**

Qualitatively, the spread of the cytoskeletons for graft copolymers in Figure 3.29 are comparable to those of the controls. A healthy cytoskeleton effectively spreads across the surface, ensuring proper adhesion of the cell to the test material. However, on the glass coverslip, as well as PDLLA and PCL controls, cells generally appeared smaller and less well-spread. Differences in morphology may be owed to differing degrees of surface roughness; smoother surfaces (such as the controls mentioned) lead to differing focal adhesions. It has been previously reported that uneven biomaterial surfaces (with higher surface roughness) can cause cells to grow differently, thereby affecting their surface response.<sup>202</sup> In addition, recalling that the surfaces of copolymers are somewhat hydrophobic (about  $90^\circ$ ), this may also impact the differences in cell adherence when comparing between PDLLA, glass coverslip and PCL controls (much more hydrophilic). More hydrophobic surfaces seemed to result in cells that were more flat, bipolar or tripolar in morphology, and also formed lamellipodia (actin projection on mobile edge), which is suggestive of high mobility and strong adhesion.<sup>266</sup> This may be in part attributable to the rapid adsorption of proteins from the cell culture media onto the more hydrophobic surfaces, providing an ideal surface for cell adhesion. Stress fibers were also imaged on all surfaces, implying that cell growth and proliferation was successfully demonstrated and that actin cytoskeleton organization occurred. Actin stress fibres are

typically associated with strong focal adhesions, which could be tested via vinculin labeling (major protein associated with focal adhesions). However, although cells were found to be more rounded on surfaces with slightly higher hydrophilicity, increasing the incubation time did result in increased cell elongation and therefore adhesion. Since C2C12 murine myoblast cells proliferate quickly (doubling in approximately 27 hours), some confocal images (such as Figure 3.29e) featured cells that displayed tips deeply stained by the dye, indicative of dynamic contact. Overall, actin filaments were observed on all tested surfaces. This linear polymer microfilament is important for cellular functions such as mobility and contraction of cells during division, thereby confirming the existence of healthy, proliferating cells.

Quantitatively, unhealthy cell specimens would result in much fewer cells adhering to the substrate if conditions were unfavourable for proper attachment. Figure 3.30 reveals the average density of cells on each surface, which ranged from 270-400 cells/mm<sup>2</sup>. ANOVA tests confirmed that there were no significant differences between the results for the different surfaces. Control substrates such as glass are considered to be reasonably good substrates for cell growth, indicating that the graft copolymers provide favourable conditions as well. These results are crucial in determining cell adhesivity properties for potential implantable biomaterial applications. This importance is related to surgical implantation of different medical devices in that local tissue injury resulting from insertion of vascular grafts, heart valve sewing cuffs and annuloplasty rings, affects both thrombosis and inflammation at the site. Both of these processes are also known to contribute to healing of tissue into and around the device.<sup>268</sup> Ensuring that a monolayer of endothelial cells can form on the surface of vascular grafts, for instance, can prevent thrombosis and allow for faster healing times.<sup>108</sup> Moreover, this preliminary test also suggests that copolymers will provide a non-toxic environment, which will be confirmed via the MTT cytotoxicity assay.

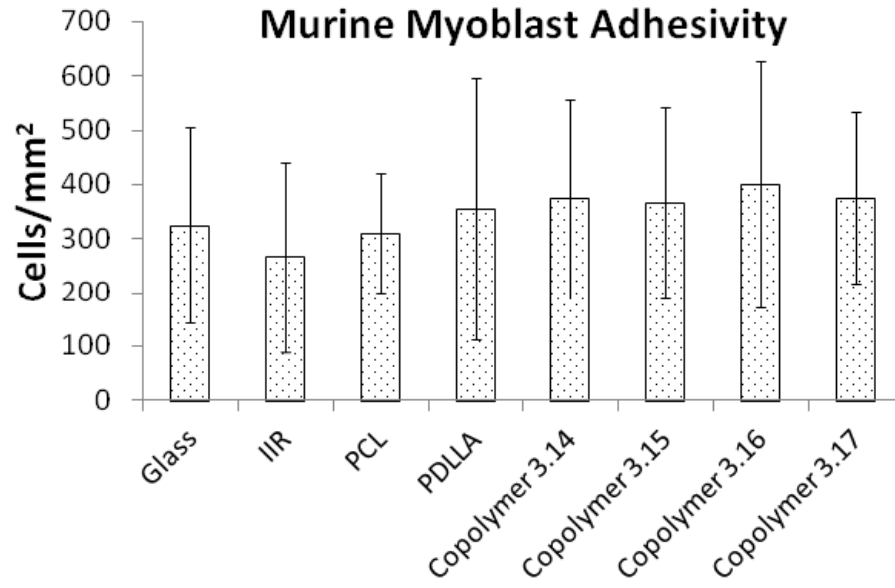


**Figure 3.30 – Cell adhesivity quantified by determining average cell concentrations for each substrate.**

### 3.6.2 MTT Toxicity Assay

Performing cytotoxicity testing is also considered a pre-screening test; it is essential to carry out in order to quantify the number of cells that will remain viable upon incubation with potentially toxic biomaterial leachables. Fatal leachables may diffuse out of a material, thus causing a toxic environment, which is detrimental to cell proliferation. This test allowed for quantification of cell growth and differentiation associated with controls [glass, IIR, PCL, PDLLA and high density poly(ethylene)] and copolymers **3.14-3.17**. A slight adaptation of ISO 10993-5, 'Biological Testing of Medical Devices – Part 5: Tests for Cytotoxicity, in vitro method, tests on extracts,' was used as a quantitative means for determining cell viability. The 'extract' method was used in order to determine toxic effects that could possibly be generated by the biomaterials. In congruence with the American Society for Testing and Materials, approximately 80 mg of the material was used for each test. Melt-pressing the material into a uniform surface and cutting into 1 cm<sup>2</sup> pieces maintained surface area exposure for reproducible and reliable results. The culture media was used as an extracting medium at 37 °C for 24 hours prior to testing, as this allows sufficient time for possible leachables to enter the surrounding media. The cells were then incubated in serial two-fold dilutions of the leachate with fresh culture media. After 24 h incubation time with cells, a standard MTT cell viability assay was performed. In this case, a reduction of cell viability by more than 30% relative to control cells exposed only to fresh culture media is considered to be a toxic effect.

The results of the MTT assay are shown in Figure 3.31. Positive and negative controls were included in each of the tests. High density poly(ethylene) (HDPE) was used as the negative control, as it does not elicit cytotoxic effects. Sodium lauryl sulfate (SDS) was used as a positive control to cause cell lysis, thereby compromising its integrity and health. Although PCL, PDLLA and IIR polymers are known to be biocompatible, investigating copolymer cytotoxicity and comparing between controls is highly relevant. As indicated in Figure 3.31, neither the negative control (HDPE) nor graft copolymers **3.14-3.17** exhibit any significant cytotoxic effects. However, toxicity of SDS was confirmed at the expected concentrations of 0.2-0.10 mg/mL.



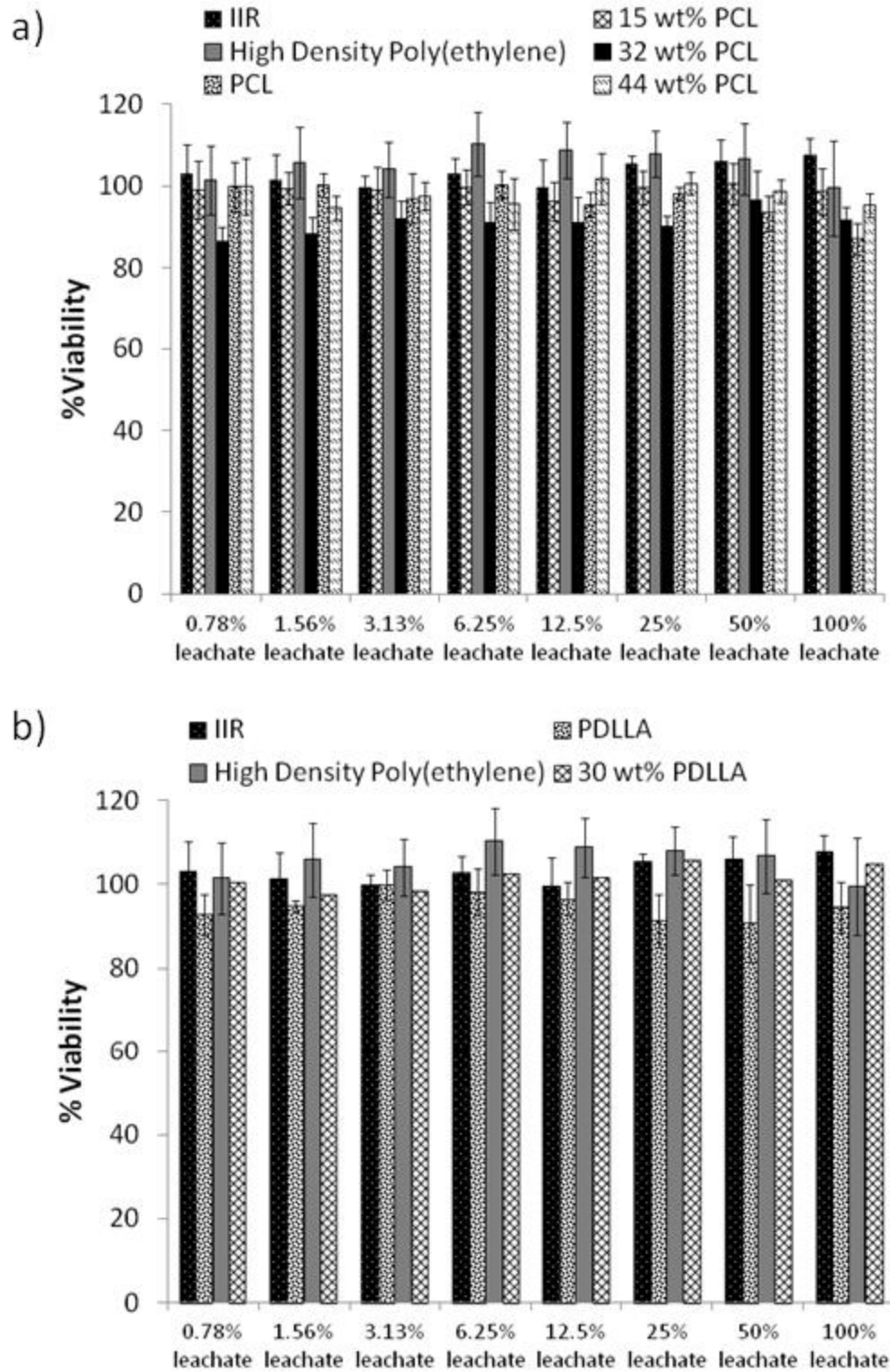


Figure 3.31 – MTT cytotoxicity assay performed on: a) graft copolymers 3.14-3.16; b) graft copolymer 3.17.

## Chapter 4

---

### 4 Materials and Methods

#### 4.1 General Procedures and Materials

IIR 402 with a  $M_w$  of 395kDa and a polydispersity index (PDI) of 2.44, as measured by size exclusion chromatography (SEC), composed of 2.2mol% isoprene units was kindly provided by LANXESS and was converted to the activated derivative (**3.13**) by the previously reported method.<sup>147</sup> Hydroxy-terminated PCL (MW = 900 Da and 3500 Da) and PDLLA (MW = 2800Da) were purchased from Polymer Source (Montreal, Québec). Silicon wafers were purchased from University Wafer (Boston, Massachusetts). Cell culture materials were purchased from Nunclon® and Invitrogen. Solvents were purchased from Caledon, PNPC was purchased from Alfa Aesar (used as received). *m*-chloroperbenzoic acid was dissolved in toluene and dried with  $MgSO_4$  before use. Pyridine and  $\epsilon$ -caprolactone monomer were distilled over  $CaH_2$  before use. All other chemicals were purchased from Sigma Aldrich and used without further purification unless stated otherwise. Dry dichloromethane and toluene were obtained from an Innovative Technology (Newburyport, USA) solvent purification system based on aluminum oxide columns.  $^1H$  NMR spectra were obtained in  $CDCl_3$  at 600 MHz using Varian Inova spectrometers. NMR chemical shifts are reported in ppm and are calibrated against residual solvent signals of  $CDCl_3$  ( $\delta$  7.26). Coupling constants (J) are reported in Hz. The percentage of functionalized isoprene units was determined from  $^1H$  NMR, based on the relative integrations of the signals at 5.03 and 4.87 ppm coinciding to the alkene adjacent to the activated carbonate and the PCL/PDLLA carbamate product, respectively. The PCL and PDLLA content in weight percentage was determined by  $^1H$  NMR, based on the relative integrations between the peaks at 4.03ppm (PCL methylene), 5.19ppm (PDLLA methane) and 1.12ppm (isobutylene). Differential scanning calorimetry (DSC) was performed under a nitrogen atmosphere on a Q20 DSC TA instrument at a heating/cooling rate of 10 °C/min from -100 to + 100 °C. The  $T_g$  and  $T_m$  were obtained from the second heating cycle. SEC was performed in tetrahydrofuran (THF) using a Viscotek GPCmax VE 2001 GPC Solvent/Sample Module equipped with a

Waters 2489 UV/Visible Detector, Viscotek VE 3580 RI Detector and two PolyPore (300 mm x 7.5 mm) columns from Agilent. The calibration was performed using polystyrene standards. FTIR was performed on a Bruker Optics TENSOR 27 series FT-IR, OPUS 7.0, via transmittance (%) with a background scan of 16 and a sample scan of 128, recording wavenumbers from 500-3700 $\text{cm}^{-1}$ .

## 4.2 Graft Copolymer Synthesis and Chemical Characterization

### 4.2.1 Synthesis of Polymer 3.8a

Following a previously reported literature,<sup>148</sup> a round-bottom flask equipped with stir bar was charged with PCL homopolymer of 900 g/mol (**3.7a**) (0.40 g, 0.44 mmol, 1.0 equiv.), 4-(dimethylamino)pyridine (DMAP) (0.20 g, 1.64 mmol, 3.7 equiv.) pyridine (0.10 g, 1.29 mmol, 2.9 equiv.) and dichloromethane (DCM) (7 mL) under dry conditions. BOC-protected  $\beta$ -alanine anhydride (**3.6**) (0.39 g, 1.1 mmol, 2.5 equiv.) was charged into a separate flask and dissolved in DCM (2 mL) under dry conditions. The latter solution was added to the PCL-containing solution and stirred overnight at room temperature. Next, deionized water was added to the reaction mixture and stirred for an additional 3 hours at room temperature. Purification involved washing with 1M HCl (3X), 1M  $\text{Na}_2\text{CO}_3$  (3X) and concentrated brine (1X), followed by drying with  $\text{MgSO}_4$  and reduced pressure solvent removal.

Yield: 0.35 g, 83%  $^1\text{H}$  NMR:  $\delta$ , 4.24 (t, 2H,  $J = 4.7$  Hz), 4.04-4.10 (m, 18H), 3.70 (t, 2H,  $J = 5.1$  Hz), 3.63-3.66 (m, 2H), 3.54-3.56 (m, 2H), 3.40 (br. s, 2H) 3.39 (s, 3H), 2.51 (t, 2H,  $J = 6.1$  Hz), 2.29-2.37 (m, 16H), 1.60-1.69 (m, 32H), 1.43 (s, 9H), 1.34-1.42 (m, 16H). SEC:  $M_w = 3160$  g/mol, PDI = 1.33. IR: 1047, 1105, 1171, 1246, 1366, 1420, 1472, 1569, 1728, 2947, 2866, 3393, 3439  $\text{cm}^{-1}$ .

Polymer **3.8b** was prepared using the same procedure as described for polymer **3.8a**, expect that PCL homopolymer of 3500 g/mol (**3.7b**) (0.40 g, 0.114 mmol, 1.0 equiv.) was used.



Yield: 0.38 g, 88%  $^1\text{H}$  NMR:  $\delta$ , 4.13 (td, 2H,  $J = 7.8, 4.7$  Hz), 4.06 (t, 62H,  $J = 6.8$  Hz), 3.39 (q, 2H,  $J = 6.1$  Hz), 2.51 (t, 2H,  $J = 6.1$  Hz), 2.3 (t, 62H,  $J = 7.4$  Hz), 1.62-1.68 (m, 124H), 1.43 (s, 9H), 1.34-1.42 (m, 62H), 1.25 (t, 3H,  $J = 7$  Hz). SEC:  $M_w = 9202$  g/mol, PDI = 1.22. IR: 1047, 1105, 1171, 1246, 1366, 1420, 1472, 1569, 1728, 2947, 2866, 3393, 3439  $\text{cm}^{-1}$ .

Polymer **3.11** was prepared using the same procedure as described for polymer **3.8a**, expect that PDLA homopolymer of 2800 g/mol (**3.10**) (0.40 g, 0.143 mmol, 1.0 equiv.) was used.

Yield: 0.31 g, 81%  $^1\text{H}$  NMR:  $\delta$ , 5.12-5.25 (m, 39H), 4.23-4.32 (m, 2H), 3.57 (m, 2H), 3.42 (br. s, 2H), 3.36 (s, 3H), 2.59 (m, 2H), 1.54-1.59 (m, 117H), 1.43 (s, 9H). SEC:  $M_w = 5098$  g/mol, PDI = 1.19. IR: 1134, 1267, 1512, 1757, 2949, 2997, 3517, 3435  $\text{cm}^{-1}$ .

#### 4.2.2 Synthesis of Polymer 3.9a

Polymer **3.8a** (0.34 g, 0.373 mmol, 1.0 equiv.) was dissolved in 1.25 mL DCM: 1.25 mL trifluoroacetic acid (TFA) (1:1) and the reaction mixture was stirred for 2 hours. DCM and TFA were removed by pressurized air. The product was redissolved in DCM and dried *in vacuo*.

Yield: 0.34 g, > 99%  $^1\text{H}$  NMR:  $\delta$ , 4.24 (t, 2H,  $J = 4.7$  Hz), 4.16 (t, 2H,  $J = 6.4$  Hz), 4.06 (t, 16H,  $J = 6.6$  Hz), 3.7 (t, 2H,  $J = 4.7$  Hz), 3.64-3.66 (m, 2H), 3.55-3.58 (m, 2H), 3.39 (s, 3H), 3.33 (br. s, 2H), 2.8 (t, 2H,  $J = 5.9$  Hz), 2.29-2.34 (m, 16H), 1.60-1.69 (m, 32H), 1.34-1.42 (m, 16H). SEC:  $M_w = 2450$  g/mol, PDI = 1.45. IR: 1047, 1105, 1171, 1246, 1366, 1420, 1472, 1569, 1728, 2947, 2866, 3445  $\text{cm}^{-1}$ .

Polymer **3.9b** was prepared using the same procedure as described for polymer **3.9a**, expect that polymer **3.8b** (0.40 g, 0.114 mmol, 1.0 equiv.) was used.

Yield: 0.40 g, > 99%  $^1\text{H}$  NMR:  $\delta$ , 4.17 (t, 2H,  $J = 6.5$  Hz), 4.10-4.15 (m, 2H), 4.06 (t, 62H,  $J = 6.5$  Hz), 3.33 (t, 2H,  $J = 5.9$  Hz), 2.83 (t, 2H,  $J = 5.3$  Hz), 2.31 (t, 62H,  $J = 7.6$  Hz), 1.62-1.68 (m, 124H), 1.36-1.41 (m, 62H), 1.25 (t, 3H,  $J = 7.6$  Hz). SEC:  $M_w =$

9030 g/mol, PDI = 1.22. IR: 1047, 1105, 1171, 1246, 1366, 1420, 1472, 1569, 1728, 2947, 2866, 3445  $\text{cm}^{-1}$ .

#### 4.2.3 Synthesis of Polymer 3.12

Polymer **3.11** and 2 mL of DCM were charged in a round-bottom flask equipped with stir bar under dry conditions. TFA was added (0.70 g, 6.11 mmol, 100 equiv.) and stirred at 0°C for 2 hours. Next, DCM and TFA were removed under low pressure (~20 mbar), re-dissolved in DCM and passed over a  $\text{K}_2\text{CO}_3$  plug to remove residual TFA.

Yield: 0.65 g, 91%  $^1\text{H}$  NMR:  $\delta$ , 5.13-5.23 (m, 39H), 4.23-4.32 (m, 2H), 3.57 (tt, 2H,  $J = 2.35, 3.52\text{Hz}$ ), 3.36 (s, 3H), 3.29 (br. s, 2H), 2.83 (br. s, 2H), 1.54-1.58 (m, 117H). SEC:  $M_w = 4740$  g/mol, PDI = 1.31. IR: 1134, 1267, 1512, 1757, 2949, 2997, 3508  $\text{cm}^{-1}$ .

#### 4.2.4 Synthesis of Graft Copolymer 3.14

In a round-bottom flask equipped with stir bar, **3.9a** (0.95 g, 1.06 mmol, 1.2 equiv.) was dissolved in 20mL of dry toluene at 60°C. A solution of PNPC-activated IIR (**3.13**)<sup>147</sup> (2.19g, 0.882mmol of 4-nitrophenylcarbonate units, 1.0 equiv.) in 25mL of dry toluene was added dropwise to the reaction mixture. DMAP (0.43g, 3.52mmol, 4.0 equiv.) dissolved in 4mL dry toluene was also added to the reaction mixture, which was then stirred overnight at 60°C. The solvent was removed *in vacuo* and the graft copolymer was redissolved in DCM, washed with deionized water (3X), dried with  $\text{MgSO}_4$ , concentrated and precipitated from DCM into acetone to afford copolymer **3.14**.

Yield: 2.45 g, 85%  $^1\text{H}$  NMR:  $\delta$ , 5.20 (br. s, 1H), 5.10 (s, 1H), 5.05 (s, 1H), 4.87 (s, 1H), 4.24 (t, 2H,  $J = 5.3$  Hz), 4.06 (t, 16H,  $J = 6.5$  Hz), 3.7 (t, 2H,  $J = 4.7$  Hz), 3.6-3.65 (m, 2H), 3.54-3.56 (m, 2H), 3.45 (q, 2H,  $J = 5.9$  Hz), 3.38 (s, 3H), 2.53 (t, 2H,  $J = 6.2$  Hz), 2.3 (t, 16H,  $J = 7.6$  Hz), 1.62-1.68 (m, 32H), 1.41 (s, 88H), 1.37-1.39 (m, 16H), 1.11 (s, 264H). PCL content from  $^1\text{H}$  NMR = 15 wt%. DSC:  $T_g = -67^\circ\text{C}$ . IR: 1165, 1230, 1366, 1390, 1470, 1736, 2955, 3445  $\text{cm}^{-1}$ .

Graft copolymer **3.15** was prepared using the same procedure as described for polymer **3.14**, expect that polymer **3.9b** (1.02 g, 0.292 mmol, 0.8 equiv. relative to 4-nitrophenylcarbonate units) was used.

Yield: 1.17 g, 70% with a conversion of 50% (based on proton integrations corresponding to a and a' (Figure 3.5).  $^1\text{H NMR}$ :  $\delta$ , 8.27 (d, 1.5H,  $J = 9.1$  Hz), 7.38 (d, 1.5H,  $J = 9.1$  Hz), 5.27 (s, 0.50H), 5.20 (br. s, 0.50H), 5.12 (s, 0.50H), 5.10 (s, 0.50H), 5.05 (s, 0.50H), 4.87 (s, 0.50H), 4.13 (q, 2H,  $J = 7.2$  Hz), 4.07 (t, 62H,  $J = 6.5$  Hz), 3.45 (q, 2H  $J = 5.9$  Hz), 2.53 (t, 2H,  $J = 5.9$  Hz), 2.31 (t, 62H,  $J = 7.3$  Hz), 1.62-1.68 (m, 124H), 1.41 (s, 88H), 1.36-1.40 (m, 62H), 1.25 (t, 3H,  $J = 7.3$  Hz), 1.11 (s, 264H). PCL content from  $^1\text{H NMR} = 32$  wt%. DSC:  $T_g = -65^\circ\text{C}$ ,  $T_m = 44^\circ\text{C}$ . IR: 1165, 1230, 1366, 1390, 1470, 1736, 2955, 3445  $\text{cm}^{-1}$ .

Graft copolymer **3.16** was prepared using the same procedure as described for polymer **3.14**, expect that polymer **3.9b** (0.34 g, 0.2098 mmol, 1.2 equiv. relative to 4-nitrophenylcarbonate units) was used.

Yield: 0.18 g, 75%  $^1\text{H NMR}$ :  $\delta$ , 5.19 (br. s, 1H), 5.1 (s, 1H), 5.05 (br. s, 1H), 4.87 (br. s, 1H), 4.13 (q, 2H,  $J = 7.2$  Hz), 4.07 (t, 62H,  $J = 6.5$  Hz), 3.46 (q, 2H,  $J = 5.9$  Hz), 2.53 (t, 2H,  $J = 5.9$  Hz), 2.31 (t, 62H,  $J = 7.3$  Hz), 1.62-1.68 (m, 124H), 1.41 (s, 88H), 1.36-1.40 (m, 62H), 1.25 (t, 3H,  $J = 7.3$  Hz), 1.11 (s, 264H). PCL content from  $^1\text{H NMR} = 44$  wt%. DSC:  $T_g = -62^\circ\text{C}$ ,  $T_m = 50^\circ\text{C}$ . IR: 1165, 1230, 1366, 1390, 1470, 1736, 2955, 3445  $\text{cm}^{-1}$ .

Graft copolymer **3.17** was prepared using the same procedure as described for polymer **3.14**, expect that polymer **3.12** (0.65 g, 0.231 mmol, 1.2 equiv. relative to 4-nitrophenylcarbonate units) was used.

Yield: 0.51 g, 86%  $^1\text{H NMR}$ :  $\delta$ , 5.14-5.25 (m, 39H), 5.11 (br. s, 1H), 5.04 (br. s, 1H), 4.86 (s, 1H), 4.23-4.32 (m, 2H), 3.57-3.59 (m, 2H), 3.45-3.50 (m, 2H), 3.36 (s, 3H), 2.61 (t, 2H,  $J = 2\text{Hz}$ ), 1.54-1.59 (m, 117H), 1.41 (s, 88H), 1.11 (s, 264H). PDLA content from  $^1\text{H NMR} = 46$  wt%. DSC:  $T_{g,1} = -63^\circ\text{C}$ ;  $T_{g,2} = 23^\circ\text{C}$ . SEC:  $M_w = 485$  kDa,  $\text{PDI} = 3.81$ . IR: 1094, 1132, 1188, 1365, 1388, 1468, 1757, 2896, 2952  $\text{cm}^{-1}$ .

## 4.3 Physical Characterization

### 4.3.1 Atomic Force Microscopy

Silicon wafers were cut into small pieces ( $\sim 1\text{cm}^2$ ) and treated with “Piranha” solution, a mixture of 3:1  $\text{H}_2\text{SO}_4:\text{H}_2\text{O}_2$  for approximately 1 hour to generate a clean, hydrophilic oxide surface. The surface was then cleaned with deionized water, acetone and subsequently dried overnight in a desiccator. Polymer thin films were prepared by spin-casting 100  $\mu\text{L}$  of a 3 wt% solution of the material in toluene on 1  $\text{cm}^2$  of silicon wafer at 6000 rpm for 30 seconds. The surfaces were kept under vacuum for at least 24 hours prior to image analysis. Surfaces were visualized by an atomic force microscope (XE-100 microscope from psia). Images were obtained by scanning surfaces in tapping mode with rectangular-shaped silicon cantilevers with a spring constant of 48 N/m. Images were then refined using XEI Image Processing software for SPM data by applying surface smoothing and glitch removal.

### 4.3.2 Water Contact Angle

The water contact angle of the polymer film surface in air was measured by using a sessile drop method on a KRÜSS DSA100 Drop Shape Analysis System (Hamburg, Germany). Timing started after dosing a water droplet onto the testing surface, allowing for an incubation period of 30 seconds for consistency. After 30 seconds, angles were recorded via tangent analysis.

### 4.3.3 Scanning Electron Microscopy

SEM micrographs were obtained using a Hitachi 3400-N Variable Pressure Scanning Electron Microscope. Images were taken at 100X and 1000X magnification utilizing variable pressure mode to avoid sample preparation via gold sputtering techniques (possible damage to rubber films).

### 4.3.4 Mechanical Testing of Graft Copolymers

A 40 mm x 5 mm x 0.3 mm (length x width x thickness) strip of polymer was cut from a polymer film (prepared via compression-molding with Carver Model 385-OC heated manual press) and its mechanical properties were measured on an INSTRON universal

testing machine 3300 series, at 25 mm/min and 25°C, in accordance with ASTM D882 – 12. For each copolymer, at least 6 samples were tested in separate analyses, and the data reported is the calculated means.

### 4.3.5 Degradation Study

#### 4.3.5.1 Preparation

Graft copolymers and control materials were compression-moulded using a Carver Model 385-OC (Carver Inc., Wabash) heated manual press into films approximately 0.35 mm in thickness. Disks were punched out of the films with a diameter of 5mm, producing a mass of approximately 5 mg per disk.

#### 4.3.5.2 Procedure

The degradation was performed over a 4-month time period. 3 discs were measured at each time point to obtain an average of 3 measurements. Samples were immersed in 1 mL of 5M NaOH at 37°C in sealed vials and on completion of each time point, each sample was rinsed with deionized water and placed in a vacuum oven at 37°C for 24 h. Lastly, dried samples were weighed to determine % mass loss (as per Equation 9), analyzed by size exclusion chromatography (SEC) and by scanning electron microscopy (SEM, 1 month intervals).

$$\% \text{ Mass Loss} = \left( \frac{m_{ia} - m_{fa}}{m_{ia}} \right) \times 100 \quad 9)$$

**Equation 9 – Where  $m_{ia}$  = average mass of initial 3 discs for a given time point and  $m_{fa}$  = average mass of final 3 discs for a given time point.**

The mass loss percentage was determined by calculating the average change in mass and dividing this value by the initial average mass and multiplying by 100 for each sample at each time point.

## 4.4 Biological Characterization

### 4.4.1 Cell Growth on Polymer Films

C2C12 mouse myoblast cells were maintained at 37°C and 5% CO<sub>2</sub> in Dulbecco's Modified Eagle Medium (DMEM, Invitrogen) supplemented with 10% fetal bovine serum (Invitrogen) and supplemented with 1% Glutamax (100×) solution and 1% Penstrep (100×). Microscope glass cover slips (circular, 10 mm diameter) were coated using a 30 mg/mL solution of the copolymers **2**, **3**, **4** and **5** in toluene by drop-casting (3 coats of 60 μL). The surfaces were placed in the wells of a 24-well (1 mL working volume, Nunclon® Multidishes) plate and sterilized by submersion in 70% ethanol for approximately 30 minutes, aspirated, then left to dry under UV light for approximately 1 hour. Next, the samples were conditioned overnight in Hank's balanced salt solution (HBSS). The sterilized samples were seeded with 2000 cells/surface and incubated for 3 hours to promote cell adhesion. Upon adhesion, 0.5 mL of cell culture media was added to each well. The 24-well plate was incubated for 48 hours; samples were first washed with pre-warmed 1X phosphate-buffered saline (PBS, pH 7.2) (Invitrogen) and subsequently fixed with 4% paraformaldehyde in 1X PBS. Samples were washed three times with 1X PBS and then treated with 0.5mL of acetone at -20°C for 5 minutes to permeabilize the membrane. Next, they were washed another 3 times with 1X PBS, stained with Alexa Fluor 568 phalloidin (20X dilution with 1X PBS, Invitrogen) for 15 minutes; 4'-6-diamidino-2-phenylindole dyhydrochloride (DAPI, 300nM, 500X dilution with 1X PBS, Invitrogen) was added directly to the surfaces for an additional 5 minutes. The samples were washed a final 3 times with 1X PBS, placed face up onto glass microscope slides, sealed with ProLong® Gold Antifade Reagent (Invitrogen) and contained with coverslips (type 1). Confocal images were obtained using a confocal laser scanning microscope (LSM 510 Duo Vario, Carl Zeiss) using a 20x objective and excitation wavelengths of 405 (DAPI) and 578 nm (Alexa Fluor 568 phalloidin). Cells were counted using cellc12, MATLAB-based program. Statistical analyses (ANOVA followed by Tukey's honestly significant difference (HSD) post hoc method when statistically significant) were performed using Prism software.

#### 4.4.2 MTT Toxicity Assay

C2C12 mouse myoblast cells were first resuspended by use of Gibco® Trypsin/ethylenediaminetetraacetic acid (EDTA) (solution of 0.025% trypsin and 0.01% EDTA in phosphate buffered saline); a cell count was performed with a haemocytometer. Based on this count, cells were seeded in a Nunclon® 96-well U bottom transparent polystyrol plate to obtain 10 000 cells/well in a volume of 100µL Dulbecco's Modified Eagle Medium (Invitrogen) supplemented with 10% fetal bovine serum (Invitrogen), 1% Glutamax (100×) solution and 1% Penstrep (100×) to columns labelled C<sub>1</sub>-C<sub>8</sub>, SDS, 1-4 and VC (vehicle control). 100µL of DMEM was introduced to the column labeled JM (just media). The 96-well plate was then placed in a 5% CO<sub>2</sub> incubator at 37°C for 24 hours. Testing samples were melt-pressed (0.015") to obtain uniformity (and to provide more surface area for potentially toxic leachates) and cut into squares of 1cm x 1cm. Samples were then sterilized in 70% ethanol for approximately 30 minutes and subsequently dried for 2 hours under UV light. Afterwards, they were placed in Petri dishes; 2 mL of DMEM was added and the resulting Petri dishes were placed in a CO<sub>2</sub> incubator at 37°C for 24 hours. After 24 hours, anything that was water soluble would be leached out of the testing samples; DMEM that samples were subjected to was then acquired via syringe and passed through a filter (to prevent particles >200 nm). Next, growth media from the Nunclon® 96-well plate was aspirated. 1200 µL of the filtered DMEM testing sample was obtained; 100µL was placed in each C<sub>8</sub> well (as depicted in Table 4.1) to obtain a 100% leachate testing column. 600 µL of fresh DMEM was then added to the remaining 600 µL of filtered DMEM testing sample to create a 50% leachate; 100 µL was then added to each of the wells labeled C<sub>7</sub>. This process was repeated until C<sub>1</sub> was reached with a 0.78% leachate dilution was attained. As a positive control to confirm cell death, sodium lauryl sulfate (SDS) was added to the columns labeled SDS1, SDS2, SDS3 and SDS4 with SDS concentrations in DMEM of 0.2 mg/mL, 0.15 mg/mL, 0.10 mg/mL and 0.05mg/mL, respectively. Lastly, the columns labeled VC and media (M) had fresh DMEM introduced. The Nunclon® 96-well plate was then returned to a 5% CO<sub>2</sub> incubator at 37°C for 24 hours. MTT (3-(4,5-Dimethylthiazol-2-yl)-2,5-Diphenyltetrazolium Bromide) reagent was prepared at 5mg/mL in deionized water; 1 mL of this solution was added to 10 mL of DMEM. Media was aspirated from the 96-

well plate and replaced with 110  $\mu$ L of the prepared MTT solution. The 96-well plate was returned to the incubator for an additional 4 hours. Lastly, the MTT solution was aspirated and replaced with 50  $\mu$ L of spectroscopy grade dimethyl sulfoxide (DMSO) to solubilize reacted product crystals. The plate was subjected to M1000-Pro (plate reader) using Tecan i-control software at a wavelength of 540 nm. Samples were shook linearly for 1 s with amplitude of 2 mm and a frequency of 654 rpm prior to 25 flashes.

**Table 4.1 – Modified protocol adapted from ISO 10993 Technical Committee. (2007). International Organization for Standardization (ISO)**

SDS3	b	b	b	b	b	b	b	b	b	b	SDS1
SDS3	M	C <sub>1</sub>	C <sub>2</sub>	C <sub>3</sub>	C <sub>4</sub>	C <sub>5</sub>	C <sub>6</sub>	C <sub>7</sub>	C <sub>8</sub>	VC	SDS1
SDS3	M	C <sub>1</sub>	C <sub>2</sub>	C <sub>3</sub>	C <sub>4</sub>	C <sub>5</sub>	C <sub>6</sub>	C <sub>7</sub>	C <sub>8</sub>	VC	SDS1
SDS3	M	C <sub>1</sub>	C <sub>2</sub>	C <sub>3</sub>	C <sub>4</sub>	C <sub>5</sub>	C <sub>6</sub>	C <sub>7</sub>	C <sub>8</sub>	VC	SDS1
SDS4	M	C <sub>1</sub>	C <sub>2</sub>	C <sub>3</sub>	C <sub>4</sub>	C <sub>5</sub>	C <sub>6</sub>	C <sub>7</sub>	C <sub>8</sub>	VC	SDS2
SDS4	M	C <sub>1</sub>	C <sub>2</sub>	C <sub>3</sub>	C <sub>4</sub>	C <sub>5</sub>	C <sub>6</sub>	C <sub>7</sub>	C <sub>8</sub>	VC	SDS2
SDS4	M	C <sub>1</sub>	C <sub>2</sub>	C <sub>3</sub>	C <sub>4</sub>	C <sub>5</sub>	C <sub>6</sub>	C <sub>7</sub>	C <sub>8</sub>	VC	SDS2
SDS4	b	b	b	b	b	b	b	b	b	b	SDS2



## Chapter 5

---

### 5 Conclusions and Future Work

IIR is currently used for a variety of applications ranging from foodstuffs (chewing gum), bladders of sporting goods and most notably, as the innerliner for automotive tires.

However, in recent years there has been significant interest in expanding its application in biomedical areas. Because of IIRs high elasticity and low strength, it has the inherent ability to mimic various soft tissues in the body. However, in order to use it in such applications as vascular prosthetics or orthopaedic implants, its properties have to be tuned in order to ensure the maintenance of its structural integrity. Therefore this thesis focused on synthesizing IIR-aliphatic polyester graft copolymers in order to tune IIR's chemical, physical and biological properties.

First, copolymer synthesis involving a “grafting-from” approach was investigated. Performing the ROP of PCL from hydroxyl moieties on the IIR backbone proved to be problematic and irreproducible. Therefore, the “grafting-to” method involving functionalization of both the IIR backbone as well as PCL and PDLLA homopolymers resulted in near 100% functionalization of IP units under mild conditions. Upon successful synthesis of copolymers, they were chemically ( $^1\text{H}$  NMR, SEC, DSC and FTIR), physically (AFM, WCA, strain-controlled fatigue testing and accelerated degradability) and biologically (cell growth on polymer films and cytotoxicity testing) characterized.

By studying the aforementioned characterization data, some important property changes were imparted by grafting PCL or PDLLA to the IIR backbone. First, changes in thermal properties upon copolymer preparation suggested that physical properties may be altered. In fact, by increasing PCL/PDLLA wt%, it was found to induce phase separation, which was confirmed via AFM analysis. By increasing the percentage of PCL from 32 wt% (copolymer **3.15**) to 44 wt% (copolymer **3.16**), properties were significantly altered, as uniaxial tensile testing results showed a dramatic increase in copolymer strength. In addition, IIR-PDLLA graft copolymer **3.17** (30 wt% PDLLA) also exhibited a comparative (IIR) increase in UTS. The grafting of these aliphatic polyesters appeared to

provide physical crosslinks, thereby increasing their strength while still maintaining compliance and structural integrity. These properties are especially important for applications involving implantable biomaterials. In addition, grafting of polyesters may supply ‘green strength,’ which is a measure of mechanical performance prior to vulcanization, which is associated with harsh chemical conditions.

Copolymers consisting of lower PCL contents (copolymers **3.14** and **3.15**) were interesting in terms of increased degradability that resulted from decreased levels of crystallinity. Long-term implantable devices that do not degrade at all elicit inflammation due to incompatibilities with the biological host. Perhaps such limitations could be remedied for extended-period applications through prolonged degradation and subsequent excretion of PCL from the body. In addition, imparting degradability to oxidatively, hydrolytically and enzymatically stable IIR may provide an avenue toward synthesis of environmentally friendly applications.

Overall, this thesis provides an important contribution, establishing the groundwork for understanding the properties of IIR-PCL/PDLLA graft copolymers. Thorough analysis of chemical structure and its relation to property modification has led to the discovery of materials with potential for usage outside the breadth of typical IIR-based applications. Future *in vivo* and rheological studies will be used to elucidate their biocompatibility and mechanical properties, respectively. These aspects require critical analysis before copolymers can be successfully employed in biomedical applications.

## References

- (1) Langer, R. S.; Peppas, N. A. *Biomaterials* **1981**, *2*, 201.
- (2) Peppas, N. A.; Langer, R. *Science* **1994**, *263*, 1715.
- (3) Langer, R. *Nature* **1998**, *392*, 5.
- (4) Langer, R. *Chemical Engineering Science* **1995**, *50*, 4109.
- (5) Langer, R.; Tirrell, D. A. *Nature* **2004**, *428*, 487.
- (6) Langer, R.; Cima, L. G.; Tamada, J. A.; Wintermantel, E. *Biomaterials* **1990**, *11*, 738.
- (7) Legge, N. R.; Holden, G.; Schroeder, H. E.; Editors *Thermoplastic Elastomers. A Comprehensive Review*; Hanser Publ., 1987.
- (8) Sionkowska, A. *Progress in Polymer Science* **2011**, *36*, 1254.
- (9) Nair, L. S.; Laurencin, C. T. *Progress in Polymer Science* **2007**, *32*, 762.
- (10) Altman, G. H.; Diaz, F.; Jakuba, C.; Calabro, T.; Horan, R. L.; Chen, J.; Lu, H.; Richmond, J.; Kaplan, D. L. *Biomaterials* **2003**, *24*, 401.
- (11) Huynh, T.; Abraham, G.; Murray, J.; Brockbank, K.; Hagen, P. O.; Sullivan, S. *Nature Biotechnology* **1999**, *17*, 1083.
- (12) Narotam, P. K.; José, S.; Nathoo, N.; Taylon, C.; Vora, Y. *Spine*. **2004**, *29*, 2861.
- (13) Bloomfield, S. E.; Miyata, T.; Dunn, M. W.; Bueser, N.; Stenzel, K. H.; Rubin, A. L. *Archives of Ophthalmology* **1978**, *96*, 885.
- (14) Rubin, A. L.; Stenzel, K. H.; Miyata, T.; White, M. J.; Dunn, M. *Journal of Clinical Pharmacology* **1973**, *13*, 309.
- (15) Pleyer, U.; Elkins, B.; Ruckert, D.; Lutz, S.; Grammer, J.; Chou, J.; Schmidt, K. H.; Mondino, B. J. *Current Eye Research* **1994**, *13*, 177.
- (16) Ponticiello, M. S.; Schinagl, R. M.; Kadiyala, S.; Barry, F. P. *Journal of Biomedical Materials Research* **2000**, *52*, 246.
- (17) Shantha, K. L.; Rao, K. P. *Journal of Bioactive and Compatible Polymers* **1993**, *8*, 142.
- (18) Jeyanthi, R.; Panduranga Rao, K. *Biomaterials* **1990**, *11*, 238.
- (19) Marty, J. J.; Oppenheim, R. C.; Speiser, P. *Pharmaceutica Acta Helveticae* **1978**, *53*, 17.
- (20) Müller, R. H.; Mäder, K.; Gohla, S. *European Journal of Pharmaceutics and Biopharmaceutics* **2000**, *50*, 161.
- (21) Bell, E.; Sher, S.; Hull, B.; Merrill, C.; Rosen, S.; Chamson, A.; Asselineau, D.; Dubertret, L.; Coulomb, B.; Lapiere, C.; Nusgens, B.; Neveux, Y. *Journal of Investigative Dermatology* **1983**, *81*, 2S.
- (22) Boyce, S. T.; Goretsky, M. J.; Greenhalgh, D. G.; Kagan, R. J.; Rieman, M. T.; Warden, G. D. *Annals of Surgery* **1995**, *222*, 743.
- (23) Lee, C. H.; Singla, A.; Lee, Y. *International Journal of Pharmaceutics* **2001**, *221*, 1.
- (24) Weinberg, C. B.; Bell, E. *Science* **1986**, *231*, 397.
- (25) Freyman, T. M.; Yannas, I. V.; Gibson, L. J. *Progress in Materials Science* **2001**, *46*, 273.
- (26) O'Brien, F. J.; Harley, B. A.; Yannas, I. V.; Gibson, L. J. *Biomaterials* **2005**, *26*, 433.

- (27) Seol, Y. J.; Lee, J. Y.; Park, Y. J.; Lee, Y. M.; Ku, Y.; Rhyu, I. C.; Lee, S. J.; Han, S. B.; Chung, C. P. *Biotechnology Letters* **2004**, *26*, 1037.
- (28) Takahashi, Y.; Yamamoto, M.; Tabata, Y. *Biomaterials* **2005**, *26*, 4856.
- (29) Terbojevich, M.; Cosani, A.; Conio, G.; Marsano, E.; Bianchi, E. *Carbohydrate Research* **1991**, *209*, 251.
- (30) Borchard, G. *Advanced Drug Delivery Reviews* **2001**, *52*, 145.
- (31) Di Martino, A.; Sittinger, M.; Risbud, M. V. *Biomaterials* **2005**, *26*, 5983.
- (32) Kim, T. H.; Jiang, H. L.; Jere, D.; Park, I. K.; Cho, M. H.; Nah, J. W.; Choi, Y. J.; Akaike, T.; Cho, C. S. *Progress in Polymer Science (Oxford)* **2007**, *32*, 726.
- (33) Kim, I. Y.; Seo, S. J.; Moon, H. S.; Yoo, M. K.; Park, I. Y.; Kim, B. C.; Cho, C. S. *Biotechnology Advances* **2008**, *26*, 1.
- (34) Krajewska, B. *Enzyme and Microbial Technology* **2004**, *35*, 126.
- (35) Puppi, D.; Chiellini, F.; Piras, A. M.; Chiellini, E. *Progress in Polymer Science* **2010**, *35*, 403.
- (36) Campoccia, D.; Doherty, P.; Radice, M.; Brun, P.; Abatangelo, G.; Williams, D. F. *Biomaterials* **1998**, *19*, 2101.
- (37) Ramamurthi, A.; Vesely, I. *Journal of Biomedical Materials Research* **2002**, *60*, 196.
- (38) Li, D.-H.; Liu, L.-M.; Tian, K.-L.; Liu, J.-C.; Fan, X.-Q. *Carbohydrate Polymers* **2007**, *67*, 40.
- (39) Azab, A. K.; Orkin, B.; Doviner, V.; Nissan, A.; Klein, M.; Srebnik, M.; Rubinstein, A. *Journal of Controlled Release* **2006**, *111*, 281.
- (40) Lauto, A.; Ohebshalom, M.; Esposito, M.; Mingin, J.; Li, P. S.; Felsen, D.; Goldstein, M.; Poppas, D. P. *Biomaterials* **2001**, *22*, 1869.
- (41) Shi, C.; Zhu, Y.; Ran, X.; Wang, M.; Su, Y.; Cheng, T. *Journal of Surgery Research* **2006**, *133*, 185.
- (42) Khor, E.; Lim, L. Y. *Biomaterials* **2003**, *24*, 2339.
- (43) Mao, H. Q.; Roy, K.; Troung-Le, V. L.; Janes, K. A.; Lin, K. Y.; Wang, Y.; August, J. T.; Leong, K. W. *Journal of Controlled Release* **2001**, *70*, 399.
- (44) Martinac, A.; Filipovic-Grcic, J.; Voinovich, D.; Perissutti, B.; Franceschinis, E. *International Journal of Pharmacology* **2005**, *291*, 69.
- (45) Vin, F.; Teot, L.; Meaume, S. *Journal of Wound Care* **2002**, *11*, 335.
- (46) Purna, S. K.; Babu, M. *Burns* **2000**, *26*, 54.
- (47) Thornton, J. F.; Rohrich, R. J. *Plastic and Reconstructive Surgery* **2005**, *116*, 677.
- (48) Gruessner, U.; Clemens, M.; Pahlplatz, P. V.; Sperling, P.; Witte, J.; Rosen, H. R. *American Journal of Surgery* **2001**, *182*, 502.
- (49) Olsen, D.; Yang, C.; Bodo, M.; Chang, R.; Leigh, S.; Baez, J.; Carmichael, D.; Perala, M.; Hamalainen, E.-R.; Jarvinen, M.; Polarek, J. *Advanced Drug Delivery Reviews* **2003**, *55*, 1547.
- (50) Weigel, P. H.; Hascall, V. C.; Tammi, M. *Journal of Biological Chemistry* **1997**, *272*, 13997.
- (51) Brekke, J. H.; Thacker, K.; CRC Press LLC: 2006, p 219.
- (52) Prestwich, G. D.; Marecak, D. M.; Marecek, J. F.; Vercruyse, K. P.; Ziebell, M. R. *Journal of Controlled Release* **1998**, *53*, 93.

- (53) Campoccia, D.; Doherty, P.; Radice, M.; Brun, P.; Abatangelo, G.; Williams, D. F. *Biomaterials* **1998**, *19*, 2101.
- (54) Cui, W.; Zhu, X.; Yang, Y.; Li, X.; Jin, Y. *Materials Science and Engineering C* **2009**, *29*, 1869.
- (55) Ji, C.; Annabi, N.; Hosseinkhani, M.; Sivaloganathan, S.; Dehghani, F. *Acta Biomaterialia* **2012**, *8*, 570.
- (56) Hong, Y.; Ye, S.-H.; Pelinescu, A. L.; Wagner, W. R. *Biomacromolecules* **2012**, *13*, 3686.
- (57) Vert, M. *Biomacromolecules* **2005**, *6*, 538.
- (58) Drobny, J. G. *Handbook of thermoplastic elastomers*; PDL(Plastics Design Library)/William Andrew Pub: Norwich, NY, 2007.
- (59) Holden, G.; John Wiley & Sons, Inc.: 2007; Vol. 24, p 695.
- (60) Schollenberger, C. S.; Scott, H.; Moore, G. R. *Rubber World* **1958**, *137*, 549.
- (61) Storey, R. F.; Wiggins, J. S.; Puckett, A. D. *Journal of Polymer Science, Part A: Polymer Chemistry* **1994**, *32*, 2345.
- (62) Zhang, J.-Y.; Doll, B. A.; Beckman, E. J.; Hollinger, J. O. *Tissue Engineering and Regenerative Medicine* **2003**, *9*, 1143.
- (63) Guelcher, S. A. *Tissue Engineering, Part B* **2008**, *14*, 3.
- (64) Gogolewski, S.; Gorna, K. *Journal of Biomedical Materials Research, Part A* **2006**, *80A*, 94.
- (65) Laschke, M. W.; Strohe, A.; Menger, M. D.; Alini, M.; Eglin, D. *Acta Biomaterialia* **2010**, *6*, 2020.
- (66) Kavlock, K. D.; Pechar, T. W.; Hollinger, J. O.; Guelcher, S. A.; Goldstein, A. S. *Acta Biomaterialia* **2007**, *3*, 475.
- (67) Laschke, M. W.; Strohe, A.; Scheuer, C.; Eglin, D.; Verrier, S.; Alini, M.; Pohlemann, T.; Menger, M. D. *Acta Biomaterialia* **2009**, *5*, 1991.
- (68) Heller, J. *Biomaterials* **1980**, *1*, 51.
- (69) Heller, J. *Advanced Polymer Science* **1993**, *107*, 41.
- (70) Heller, J.; Barr, J.; Ng, S. Y.; Abdellaoui, K. S.; Gurny, R. *Advanced Drug Delivery Reviews* **2002**, *54*, 1015.
- (71) Heller, J.; Barr, J. *Biomacromolecules* **2004**, *5*, 1625.
- (72) Schwach-Abdellaoui, K.; Vivien-Castioni, N.; Gurny, R. *European Journal of Pharmacology Biopharmacology* **2000**, *50*, 83.
- (73) Okada, M. *Progress in Polymer Science* **2002**, *27*, 87.
- (74) Vert, M.; Christel, P.; Chabot, F.; Leray, J.; CRC: 1984, p 119.
- (75) Webb, A. R.; Yang, J.; Ameer, G. A. *Expert Opinion on Biological Theory* **2004**, *4*, 801.
- (76) Hayashi, T. *Progress in Polymer Science* **1994**, *19*, 663.
- (77) Pistner, H.; Bendix, D. R.; Muhling, J.; Reuther, J. F. *Biomaterials* **1993**, *14*, 291.
- (78) Ali, S. A. M.; Doherty, P. J.; Williams, D. F. *Journal of Biomedical Materials Research* **1993**, *27*, 1409.
- (79) Engelberg, I.; Kohn, J. *Biomaterials* **1991**, *12*, 292.
- (80) Storey, R. F.; Sherman, J. W. *Macromolecules* **2002**, *35*, 1504.

- (81) Rathi, S. R.; Coughlin, E. B.; Hsu, S. L.; Golub, C. S.; Ling, G. H.; Tzivanis, M. J. *Polymer* **2012**, *53*, 3008.
- (82) Woodruff, M. A.; Hutmacher, D. W. *Progress in Polymer Science* **2010**, *35*, 1217.
- (83) Shao, J.; Sun, J. R.; Bian, X. C.; Cui, Y.; Li, G.; Chen, X. S. *Journal of Physical Chemistry B* **2012**, *116*, 9983.
- (84) Woodruff, M. A.; Hutmacher, D. W. *Progress in Polymer Science (Oxford)* **2010**, *35*, 1217.
- (85) Maurus, P. B.; Kaeding, C. C. *Operative Techniques in Sports Medicine* **2004**, *12*, 158.
- (86) Fischer, E. W.; Sterzel, H. J.; Wegner, G. *Kolloid-Zeitschrift & Zeitschrift für Polymere* **1973**, *251*, 980.
- (87) Chu, C. C. *J. Appl. Polym. Sci.* **1981**, *26*, 1727.
- (88) Fukushima, K.; Luis Feijoo, J.; Yang, M.-C. *European Polymer Journal* **2013**, *49*, 706.
- (89) Pitt, C. G.; Gratzl, M. M.; Kimmel, G. L.; Surles, J.; Schindler, A. *Biomaterials* **1981**, *2*, 215.
- (90) Christopher, X. F. L.; Monica, M. S.; Swee-Hin, T.; Dietmar, W. H. *Biomedical Materials* **2008**, *3*, 034108.
- (91) Lee, K. H.; Kim, H. Y.; Khil, M. S.; Ra, Y. M.; Lee, D. R. *Polymer* **2003**, *44*, 1287.
- (92) Luciani, A.; Coccoli, V.; Orsi, S.; Ambrosio, L.; Netti, P. A. *Biomaterials* **2008**, *29*, 4800.
- (93) Thomas, V.; Jose, M. V.; Chowdhury, S.; Sullivan, J. F.; Dean, D. R.; Vohra, Y. K. *Journal of Biomedical Science, Polymer Edition* **2006**, *17*, 969.
- (94) Huang, Q.; Goh, J. C. H.; Hutmacher, D. W.; Lee, E. H. *Tissue Eng.* **2002**, *8*, 469.
- (95) Li, W. J.; Danielson, K. G.; Alexander, P. G.; Tuan, R. S. *Journal of Biomedical Materials Research - Part A* **2003**, *67*, 1105.
- (96) Kazımođlu, C.; Bölükbaşı, S.; Kanatlı, U.; Şenköylü, A.; Altun, N. Ş.; Babaç, C.; Yavuz, H.; Pişkin, C. *International Journal of Artificial Organs* **2003**, *26*, 804.
- (97) Ajili, S. H.; Ebrahimi, N. G.; Soleimani, M. *Acta Biomaterialia* **2009**, *5*, 1519.
- (98) Jeong, S. I.; Kim, B. S.; Kang, S. W.; Kwon, J. H.; Lee, Y. M.; Kim, S. H.; Kim, Y. H. *Biomaterials* **2004**, *25*, 5939.
- (99) Ananta, M.; Aulin, C. E.; Hilborn, J.; Aibibu, D.; Houis, S.; Brown, R. A.; Mudera, V. *Tissue Engineering - Part A* **2009**, *15*, 1667.
- (100) Den Dunnen, W. F. A.; Van Der Lei, B.; Schakenraad, J. M.; Stokroos, I.; Blaauw, E.; Bartels, H.; Pennings M, A. J.; Robinson, P. H. *Microsurgery* **1997**, *17*, 348.
- (101) Hakkarainen, M. *Advanced Polymer Science* **2002**, *157*, 113.
- (102) Ray, S. S.; Okamoto, M. *Macromolecular Materials and Engineering* **2003**, *288*, 936.
- (103) Newman, D.; Laredo, E.; Bello, A.; Grillo, A.; Feijoo, J. L.; Muller, A. J. *Macromolecules* **2009**, *42*, 5219.
- (104) Hakkarainen, M.; Albertsson, A. C.; Karlsson, S. *Polymer Degradation and Stability* **1996**, *52*, 283.



- (105) Reed, A. M.; Gilding, D. K. *Polymer* **1981**, 22, 494.
- (106) Høglund, A.; Hakkarainen, M.; Albertsson, A. C. *Journal of Macromolecular Science Part a-Pure and Applied Chemistry* **2007**, 44, 1041.
- (107) Puskas, J. E.; Chen, Y. H. *Biomacromolecules* **2004**, 5, 1141.
- (108) Puskas, J. E.; Chen, Y. H.; Dahman, Y.; Padavan, D. *Journal of Polymer Science Part A-Polymer Chemistry* **2004**, 42, 3091.
- (109) Morton, M.; Editor *Rubber Technology. 3rd Ed*; Van Nostrand Reinhold, 1987.
- (110) Kroschwitz, J. I. *Encyclopedia of Polymer Science and Engineering* 1985, Vol. 8; Wiley, 1987.
- (111) Kennedy, J. P. *Rubber Chemistry and Technology* **1996**, 69, G63.
- (112) Kennedy, J. P. *Cationic Polymerization of Olefins: A Critical Inventory*; Wiley-Interscience, 1975.
- (113) Young, R. J. *Introduction to Polymers*; Methuen, Inc., 1981.
- (114) Rehner Jr, J.; Holowchak, J. *Industrial and Engineering Chemistry* **1944**, 16, 98.
- (115) Matyjaszewski, K.; Sigwalt, P. *Polymer International* **1994**, 35, 1.
- (116) Odian, G. *Principles of Polymerization, 4th Edition*; Wiley, 2004.
- (117) Cadieux, P.; Watterson, J. D.; Denstedt, J.; Harbottle, R. R.; Puskas, J.; Howard, J.; Gan, B. S.; Reid, G. *Colloids and Surfaces B: Biointerfaces* **2003**, 28, 95.
- (118) Pinchuk, L.; Wilson, G. J.; Barry, J. J.; Schoephoerster, R. T.; Parel, J.-M.; Kennedy, J. P. *Biomaterials* **2008**, 29, 448.
- (119) Puskas, J. E.; Dos Santos, L. M.; Orlowski, E. *Rubber Chemistry and Technology* **2010**, 83, 235.
- (120) Van Amerongen, G. J. *Journal of Applied Physics* **1946**, 17, 972.
- (121) Roland, C. M.; Ngai, K. L.; Plazek, D. J. *Computational and Theoretical Polymer Science* **1997**, 7, 133.
- (122) Puskas, J. E.; Gergely, A. L.; Kaszas, G. *Journal of Polymer Science Part a-Polymer Chemistry* **2013**, 51, 29.
- (123) Paulo, C.; Puskas, J. E. *Macromolecules* **2001**, 34, 734.
- (124) Crawford, R. A.; Morrissey, R. T.; B. F. Goodrich Co.: 1953.
- (125) Morrissey, R. T. *Journal of Industrial Engineering Chemistry* **1955**, 47, 1562.
- (126) Morrissey, R. T.; Weiss, H. J.; B. F. Goodrich Co.: 1958.
- (127) Baldwin, F. P.; Thomas, R. M.; Esso Research and Engineering Co.: 1960.
- (128) Baldwin, F. P.; Thomas, R. M.; Esso Research and Engineering Co.: 1960.
- (129) Walker, J.; Jones, R. H.; Feniak, G. *Rubber Age (NY)* **1976**, 108, 45.
- (130) Edwards, D. C. *Elastomerics* **1990**, 122, 19.
- (131) Kuntz, I.; Zapp, R. I.; Pancirov, R. J. *Rubber Chemistry and Technology* **1984**, 57, 813.
- (132) McLean, J. K.; Guillen-Castellanos, S. A.; Parent, J. S.; Whitney, R. A.; Resendes, R. *European Polymer Journal* **2007**, 43, 4619.
- (133) Xiao, S.; Parent, J. S.; Whitney, R. A.; Knight, L. K. *Journal of Polymer Science, Part A: Polymer Chemistry* **2010**, 48, 4691.
- (134) Malmberg, S. M.; Parent, J. S.; Pratt, D. A.; Whitney, R. A. *Macromolecules* **2010**, 43, 8456.

- (135) Whitney, R. A.; Penciu, A.; Parent, J. S.; Resendes, R.; Hopkins, W. *Macromolecules* **2005**, *38*, 4625.
- (136) Parent, J. S.; White, G. D. F.; Thom, D. J.; Whitney, R. A.; Hopkins, W. *Journal of Polymer Science, Part A: Polymer Chemistry* **2003**, *41*, 1915.
- (137) Guillén-Castellanos, S. A.; Parent, J. S.; Whitney, R. A. *Macromolecules* **2006**, *39*, 2514.
- (138) Puskas, J. E.; Antony, P.; El Fray, M.; Altstädt, V. *European Polymer Journal* **2003**, *39*, 2041.
- (139) Kennedy, J. P.; Richard, G. C. *Macromolecules* **1993**, *26*, 567.
- (140) Keszler, B.; Fenyvesi, G. Y.; Kennedy, J. P. *Journal of Polymer Science, Part A: Polymer Chemistry* **2000**, *38*, 706.
- (141) Feldthusen, J.; Iván, B.; Müller, A. H. E. *Macromolecules* **1998**, *31*, 578.
- (142) Ojha, U.; Kulkarni, P.; Cozzens, D.; Faust, R. *Journal of Polymer Science Part A-Polymer Chemistry* **2010**, *48*, 3767.
- (143) Gong, C.; Fréchet, J. M. J. *Journal of Polymer Science, Part A: Polymer Chemistry* **2000**, *38*, 2970.
- (144) Groenewolt, M.; Brezesinski, T.; Schlaad, H.; Antonietti, M.; Groh, P. W.; Iván, B. *Advanced Materials* **2005**, *17*, 1158.
- (145) Zhang, Y.; Zhang, Y.; Chen, X. Z.; Zhang, Y. *Reactive and Functional Polymers* **2001**, *47*, 93.
- (146) Zhang, Y.; Chen, X.; Zhang, Y.; Zhang, Y. *Macromolecular Materials and Engineering* **2001**, *286*, 443.
- (147) Bonduelle, C. V.; Gillies, E. R. *Macromolecules* **2010**, *43*, 9230.
- (148) Bonduelle, C. V.; Karamdoust, S.; Gillies, E. R. *Macromolecules* **2011**, *44*, 6405.
- (149) Suksawad, P.; Yamamoto, Y.; Kawahara, S. *European Polymer Journal* **2011**, *47*, 330.
- (150) Pukkate, N.; Yamamoto, Y.; Kawahara, S. *Colloid and Polymer Science* **2008**, *286*, 411.
- (151) Bhakuni, R. S.; Mowdood, S. K.; Waddell, W. H.; Rai, I. S.; Knight, D. L.; Wiley: 1989; Vol. 16, p 834.
- (152) Dunn, J. R. *Elastomerics* **1991**, *123*, 15.
- (153) Trexler, H. E.; Lee, M. C. H. *Journal of Applied Polymer Science* **1986**, *32*, 3899.
- (154) Wong, W. K. *Rubber World* **2009**, *240*, 20.
- (155) Pinchuk, L.; Wilson, G. J.; Barry, J. J.; Schoephoerster, R. T.; Parel, J. M.; Kennedy, J. P. *Biomaterials* **2008**, *29*, 448.
- (156) Puskas, J. E.; Chen, Y. *Biomacromolecules* **2004**, *5*, 1141.
- (157) Acosta, A. C.; Espana, E. M.; Yamamoto, H.; Davis, S.; Pinchuk, L.; Weber, B. A.; Orozco, M.; Dubovy, S.; Fantes, F.; Parel, J. M. *Archives of Ophthalmology* **2006**, *124*, 1742.
- (158) Gallocher, S. L.; Aguirre, A. F.; Kasyanov, V.; Pinchuk, L.; Schoephoerster, R. T. *Journal of Biomedical Materials Research - Part B Applied Biomaterials* **2006**, *79*, 325.
- (159) Kennedy, J. P.; Askew, M. J.; Richard, G. C. *Journal of biomaterials science. Polymer edition* **1993**, *4*, 445.



- (160) Kennedy, J. P. *Macromolecular Symposia* **2001**, 175, 127.
- (161) Kennedy, J. P.; Midha, S.; Gadkari, A. *Journal of Macromolecular Science-Chemistry* **1991**, A28, 209.
- (162) Isayeva, I. S.; Kasibhatla, B. T.; Rosenthal, K. S.; Kennedy, J. P. *Biomaterials* **2003**, 24, 3483.
- (163) Andrade, J. D.; Hlady, V.; Jeon, S. I. *Advances in Chemistry Series* **1996**, 248, 57.
- (164) Puskas, J. E.; Kwon, Y.; Antony, P.; Bhowmick, A. K. *Journal of Polymer Science Part a-Polymer Chemistry* **2005**, 43, 1811.
- (165) Aguilar, M.; Yamamoto, H.; Espana, E.; Acosta, A. C.; Orozco, M.; Aly, M.; Arrieta, E.; Hernandez, E.; Martin, J.; Dubovy, S.; Smiddy, W.; Pinchuk, L.; Parel, J.-M. *Proceedings of SPIE - The International Society for Optical Engineering* **2006**, 6138, 61381S/1.
- (166) Perez-Santonja, J. J.; Alio, J. L.; Jimenez-Alfaro, I.; Zato, M. A. *Journal of Cataract and Refractive Surgery* **2000**, 26, 1288.
- (167) Gallocher, S. L.; Aguirre, A. F.; Kasyanov, V.; Pinchuk, L.; Schoephoerster, R. T. *Journal of Biomedical Materials Research Part B-Applied Biomaterials* **2006**, 79B, 325.
- (168) Yin, W.; Gallocher, S.; Pinchuk, L.; Schoephoerster, R. T.; Jesty, J.; Bluestein, D. *Artificial Organs* **2005**, 29, 826.
- (169) Levy, Y.; Mandler, D.; Weinberger, J.; Domb, A. J. *Journal of Biomedical Materials Research - Part B Applied Biomaterials* **2009**, 91, 441.
- (170) Ormiston, J. A.; Webster, M. W.; Ruygrok, P. N.; Stewart, J. T.; Currie, E.; Panther, M. J. *American Journal of Cardiology* **2002**, 90, 76H.
- (171) Otsuka, Y.; Chronos, N. A.; Apkarian, R. P.; Robinson, K. A. *The Journal of invasive cardiology* **2007**, 19, 71.
- (172) Duraiswamy, N.; Choksi, T. D.; Pinchuk, L.; Schoephoerster, R. T. *Journal of Biomaterials Applications* **2009**, 23, 367.
- (173) Janssen, D.; De Palma, R.; Verlaak, S.; Heremans, P.; Dehaen, W. *Thin Solid Films* **2006**, 515, 1433.
- (174) Frommer, J. *Angewandte Chemie-International Edition* **1992**, 104, 1325.
- (175) Magonov, S. N.; Whangbo, M. H.; Editors *Surface Analysis with STM and AFM: Experimental and Theoretical Aspects of Image Analysis*; VCH, 1995.
- (176) Magonov, S. N.; Elings, V.; Whangbo, M. H. *Surface Science* **1997**, 375, L385.
- (177) Van, N. S. J. T.; Van, d. W. K. O.; De, G. B. G.; Van, H. N. F.; Greve, J. *Ultramicroscopy* **1997**, 69, 117.
- (178) Magonov, S. N.; Cleveland, J.; Elings, V.; Denley, D.; Whangbo, M. H. *Surface Science* **1997**, 389, 201.
- (179) Haward, R.; Young, R. J.; Editors *The Physics of Glassy Polymers, Second Edition*; Chapman & Hall, 1997.
- (180) Bassett, D. C. *Principles of Polymer Morphology*; Cambridge Univ. Press, 1981.
- (181) Schultz, J. *Polymer Materials Science*; Prentice-Hall, 1973.
- (182) Bartczak, Z.; Galeski, A. *Macromolecular Symposia* **2010**, 294, 67.
- (183) Boyer, R. F. *Rubber Chemistry Technology* **1963**, 36, 1303.

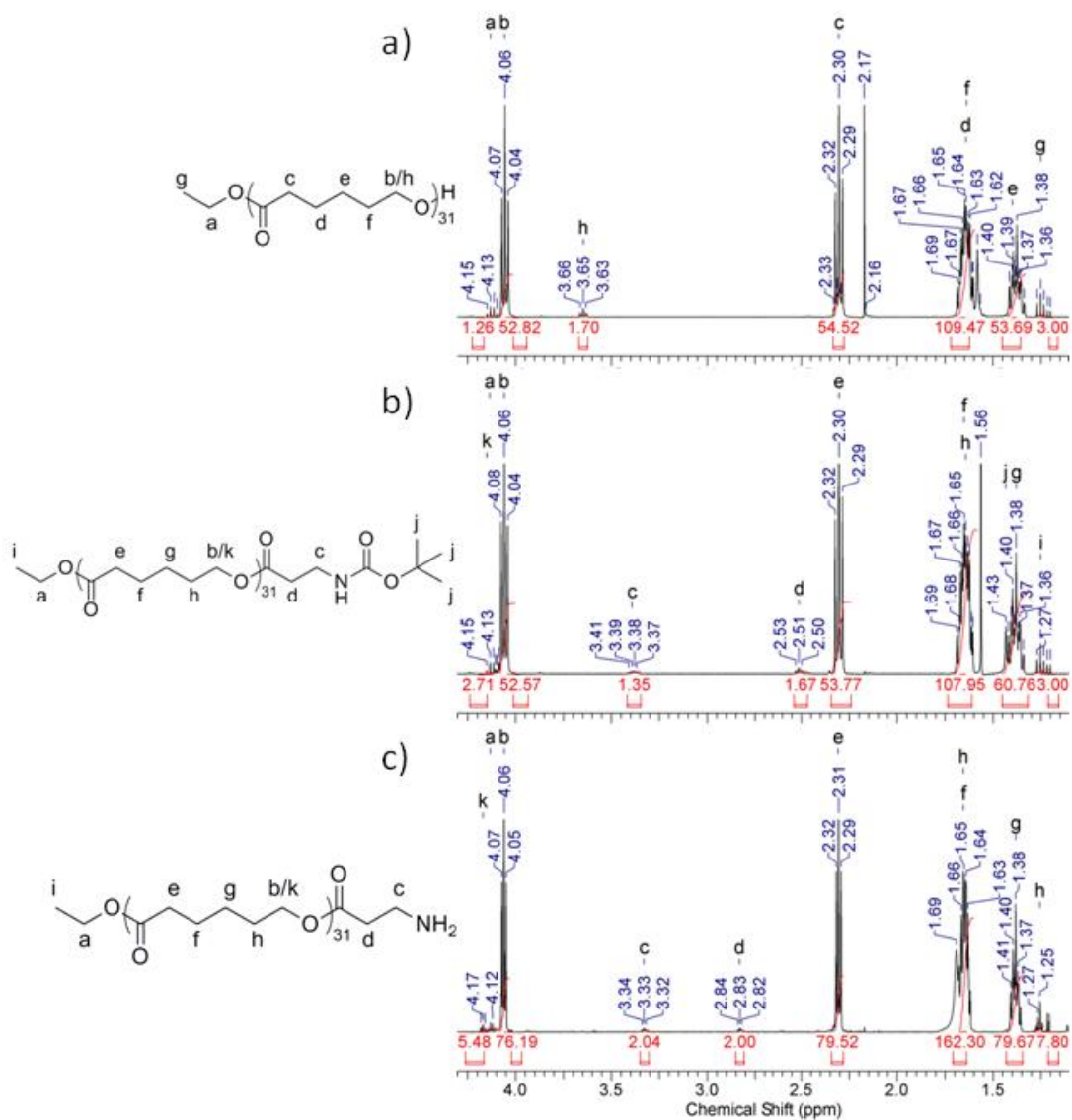
- (184) Legge, N. R.; Holden, G.; Schroeder, H. E. *Thermoplastic elastomers: a comprehensive review*; Hanser Publishers, 1987.
- (185) Semon, W. L.; B. F. Goodrich Co. . 1933.
- (186) Perego, G.; Cesari, M.; Vitali, R. *Journal of Applied Polymer Science* **1984**, *29*, 1157.
- (187) Birley, A. W. *British Polymer Journal* **1989**, *21*, 181.
- (188) Callister, W. D., Jr. *Fundamentals of Materials Science and Engineering: An Interactive E-Text, 2nd Edition*; Wiley, 2004.
- (189) Ashby, M. F.; Ferreira, P. J.; Schodek, D. L. In *Nanomaterials, Nanotechnologies and Design*; Butterworth-Heinemann: Boston, 2009, p 87.
- (190) Albert, D.; Hoffmann, A. *Medical Device and Diagnostic Industry* **2008**, *30*.
- (191) Pizzoferrato, A.; Ciapetti, G.; Stea, S.; Cenni, E.; Arciola, C. R.; Granchi, D.; Savarino, L. *Clinical Materials* **1994**, *15*, 173.
- (192) Ratner, B. D.; Hoffman, A. S.; Schoen, F. J.; Lemons, J. E.; Editors *Biomaterials Science, An Introduction to Materials in Medicine, 2nd Edition*; Elsevier, 2004.
- (193) Chen, H.; Yuan, L.; Song, W.; Wu, Z.; Li, D. *Progress in Polymer Science* **2008**, *33*, 1059.
- (194) Ryoo, S.-R.; Kim, Y.-K.; Kim, M.-H.; Min, D.-H. *ACS Nano* **2010**, *4*, 6587.
- (195) Shin, Y. M.; Kim, K.-S.; Lim, Y. M.; Nho, Y. C.; Shin, H. *Biomacromolecules* **2008**, *9*, 1772.
- (196) Huang, J.; Grater, S. V.; Corbellini, F.; Rinck, S.; Bock, E.; Kemkemer, R.; Kessler, H.; Ding, J.; Spatz, J. P. *Nanoscience and Nanotechnology Letters* **2009**, *9*, 1111.
- (197) Discher, D. E.; Janmey, P.; Wang, Y.-I. *Science* **2005**, *310*, 1139.
- (198) Brunetti, V.; Maiorano, G.; Rizzello, L.; Sorce, B.; Sabella, S.; Cingolani, R.; Pompa, P. P. *Proceedings of the National Academy of Sciences of the U. S. A.* **2010**, *107*, 6264.
- (199) Cheng, Z.; Teoh, S.-H. *Biomaterials* **2004**, *25*, 1991.
- (200) Dugan, J. M.; Gough, J. E.; Eichhorn, S. J. *Biomacromolecules* **2010**, *11*, 2498.
- (201) Huang, N. F.; Patel, S.; Thakar, R. G.; Wu, J.; Hsiao, B. S.; Chu, B.; Lee, R. J.; Li, S. *Nanoscience and Nanotechnology Letters* **2006**, *6*, 537.
- (202) Lampin, M.; Warocquier-Clérout, R.; Legris, C.; Degrange, M.; Sigot-Luizard, M. F. *Journal of Biomedical Materials Research* **1997**, *36*, 99.
- (203) Brash, J. L.; Horbett, T. A. *ACS Symposium Series* **1995**, *602*, 1.
- (204) de Vos, W. M.; de Keizer, A.; Kleijn, J. M.; Cohen Stuart, M. A. *Langmuir* **2009**, *25*, 4490.
- (205) Norde, W.; Gage, D. *Langmuir* **2004**, *20*, 4162.
- (206) Aulich, D.; Hoy, O.; Luzinov, I.; Brücher, M.; Hergenröder, R.; Bittrich, E.; Eichhorn, K. J.; Uhlmann, P.; Stamm, M.; Esser, N.; Hinrichs, K. *Langmuir* **2010**, *26*, 12926.
- (207) Uhlmann, P.; Houbenov, N.; Brenner, N.; Grundke, K.; Burkert, S.; Stamm, M. *Langmuir* **2007**, *23*, 57.

- (208) Jeon, S. I.; Lee, J. H.; Andrade, J. D.; De Gennes, P. G. *Journal of Colloid And Interface Science* **1991**, *142*, 149.
- (209) Taunton, H. J.; Toprakcioglu, C.; Fetters, L. J.; Klein, J.; 1 ed. 1989; Vol. 30, p 368.
- (210) Unsworth, L. D.; Sheardown, H.; Brash, J. L. *Biomaterials* **2005**, *26*, 5927.
- (211) Harder, P.; Grunze, M.; Dahint, R.; Whitesides, G. M.; Laibinis, P. E. *Journal of Physical Chemistry B* **1998**, *102*, 426.
- (212) Yamashita, S.; Kodama, K.; Ikeda, Y.; Kohjiya, S. *Journal of Polymer Science Part A: Polymer Chemistry* **1993**, *31*, 2437.
- (213) Bonduelle, C. V.; Lau, W. M.; Gillies, E. R. *ACS Applied Materials & Interfaces* **2011**, *3*, 1740.
- (214) Karamdoust, S.; Bonduelle, C. V.; Amos, R. C.; Turowec, B. A.; Guo, S.; Ferrari, L.; Gillies, E. R. *Journal of Polymer Science Part A: Polymer Chemistry* **2013**, n/a.
- (215) Vert, M.; Li, S. M.; Spenlehauer, G.; Guerin, P. *Journal of Materials Science: Materials in Medicine* **1992**, *3*, 432.
- (216) Wei, X.; Bagdi, K.; Ren, L.; Shah, P.; Seethamraju, K.; Faust, R. *Polymer* **2013**, *54*, 1647.
- (217) Li, B.; Martin, A. L.; Gillies, E. R. *Chemical Communications* **2007**, 5217.
- (218) Chakrapani, V. Y.; Gnanamani, A.; Giridev, V. R.; Madhusoothanan, M.; Sekaran, G. *Journal of Applied Polymer Science* **2012**, *125*, 3221.
- (219) Fan, Y. J.; Chen, G. P.; Tanaka, J.; Tateishi, T. *Biomacromolecules* **2005**, *6*, 3051.
- (220) Harrane, A.; Belaouedj, M. E. A.; Belbachir, M. *Reactive and Functional Polymers* **2011**, *71*, 126.
- (221) Zhang, P.; Huang, H.; Yan, D.; He, T. *Langmuir* **2012**, *28*, 6419.
- (222) Vasilev, C.; Reiter, G.; Pispas, S.; Hadjichristidis, N. *Polymer* **2006**, *47*, 330.
- (223) Nojima, S.; Nakano, H.; Takahashi, Y.; Ashida, T. *Polymer* **1994**, *35*, 3479.
- (224) Hsu, J.-Y.; Hsieh, I. F.; Nandan, B.; Chiu, F.-C.; Chen, J.-H.; Jeng, U. S.; Chen, H.-L. *Macromolecules* **2007**, *40*, 5014.
- (225) Nandan, B.; Hsu, J.-Y.; Chen, H.-L. *Polymer Reviews* **2006**, *46*, 143.
- (226) Gheno, S. M.; Passador, F. R.; Pessan, L. A. *Journal of Applied Polymer Science* **2010**, *117*, 3211.
- (227) Kumar, S.; Rath, T.; Mahaling, R. N.; Das, C. K.; Srivastava, R. B.; Yadaw, S. B. *Polymer Composites* **2009**, *30*, 655.
- (228) Tsou, A. H.; Duvdevani, I.; Datta, S. *Journal of Applied Polymer Science* **2006**, *102*, 4447.
- (229) Corrales, T.; Larraza, I.; Catalina, F.; Portoles, T.; Ramirez-Santillan, C.; Matesanz, M.; Abrusci, C. *Biomacromolecules* **2012**, *13*, 4247.
- (230) Huang, Y.; Zhang, S.; Niu, B.; Wang, D.; Wang, Z.; Feng, S.; Xu, H.; Kong, D.; Qiao, M. *Colloids and Surfaces B: Biointerfaces* **2013**, *101*, 361.
- (231) Li, Y.; Zhang, B.; Ruan, C.; Wang, P.; Sun, J.; Pan, J.; Wang, Y. *Journal of Biomedical Materials Research - Part A* **2012**, *100 A*, 3496.

- (232) Martínez, L.; Nevshupa, R.; Álvarez, L.; Huttel, Y.; Méndez, J.; Román, E.; Mozas, E.; Valdés, J. R.; Jimenez, M. A.; Gachon, Y.; Heau, C.; Faverjon, F. *Tribology International* **2009**, *42*, 584.
- (233) Bonduelle, C. V.; McEachran, M. J.; Karamdoust, S.; Gillies, E. R. *Journal of Coatings Technology Research* **2013**, *1*.
- (234) Jiang, T.; He, F.; Zhuo, R.-X. *Polymer Degradation and Stability* **2013**, *98*, 325.
- (235) Chen, Q.; Liang, S.; Thouas, G. A. *Progress in Polymer Science* **2013**, *38*, 584.
- (236) Balasubramanian, V.; Grusin, N. K.; Bucher, R. W.; Turitto, V. T.; Slack, S. M. *Journal of Biomedical Materials Research* **1999**, *44*, 253.
- (237) Cozzens, D.; Luk, A.; Ojha, U.; Ruths, M.; Faust, R. *Langmuir* **2011**, *27*, 14160.
- (238) Harte, I.; Birkinshaw, C.; Jones, E.; Kennedy, J.; Debarra, E. *Journal of Applied Polymer Science* **2013**, *127*, 1997.
- (239) Castilla-Cortázar, I.; Más-Estellés, J.; Meseguer-Dueñas, J. M.; Escobar Ivirico, J. L.; Marí, B.; Vidaurre, A. *Polymer Degradation and Stability* **2012**, *97*, 1241.
- (240) Ji, C.; Annabi, N.; Hosseinkhani, M.; Sivaloganathan, S.; Dehghani, F. *Acta Biomaterialia* **2012**, *8*, 570.
- (241) Pok, S.; Myers, J. D.; Madihally, S. V.; Jacot, J. G. *Acta Biomaterialia* **2013**, *9*, 5630.
- (242) Roy, R. V.; Das, M.; Banerjee, R.; Bhowmick, A. K. *Bioresource Technology* **2006**, *97*, 2485.
- (243) Ikeda, Y.; Kodama, K.; Kajiwara, K.; Kohjiya, S. *Journal of Polymer Science Part B-Polymer Physics* **1995**, *33*, 387.
- (244) Xu, Y.; Petrovic, Z.; Das, S.; Wilkes, G. L. *Polymer* **2008**, *49*, 4248.
- (245) Kaszas, G. 1993; Vol. 68, p 325.
- (246) Safranski, D. L.; Smith, K. E.; Gall, K. *Polymer Reviews* **2013**, *53*, 76.
- (247) Kennedy, J. P. *Macromolecular Symposia* **2001**, *175*, 127.
- (248) Van, D. J. D.; Gnatowski, M.; Burczyk, A. *Journal of Applied Polymer Science* **2008**, *109*, 1535.
- (249) Htay, A. S.; Teoh, S. H.; Hutmacher, D. W. *Journal of Biomaterial Science, Polymer Edition* **2004**, *15*, 683.
- (250) Cam, D.; Hyon, S.-H.; Ikada, Y. *Biomaterials* **1995**, *16*, 833.
- (251) Li, S. M.; Chen, X. H.; Gross, R. A.; McCarthy, S. P. *Journal of Materials Science: Materials in Medicine* **2000**, *11*, 227.
- (252) Ojha, U.; Kulkarni, P.; Singh, J.; Faust, R. *Journal of Polymer Science Part A-Polymer Chemistry* **2009**, *47*, 3490.
- (253) Chen, C. M.; Yang, S. *Polymer International* **2012**, *61*, 1041.
- (254) Stafford, C. M.; Harrison, C.; Beers, K. L.; Karim, A.; Amis, E. J.; Vanlandingham, M. R.; Kim, H. C.; Volksen, W.; Miller, R. D.; Simonyi, E. E. *Nature Materials* **2004**, *3*, 545.
- (255) Kelch, S.; Choi, N. Y.; Wang, Z.; Lendlein, A. *Advanced Engineering Materials* **2008**, *10*, 494.
- (256) Lendlein, A.; Schmidt, A. M.; Langer, R. *Proceedings of the National Academy of Sciences* **2001**, *98*, 842.

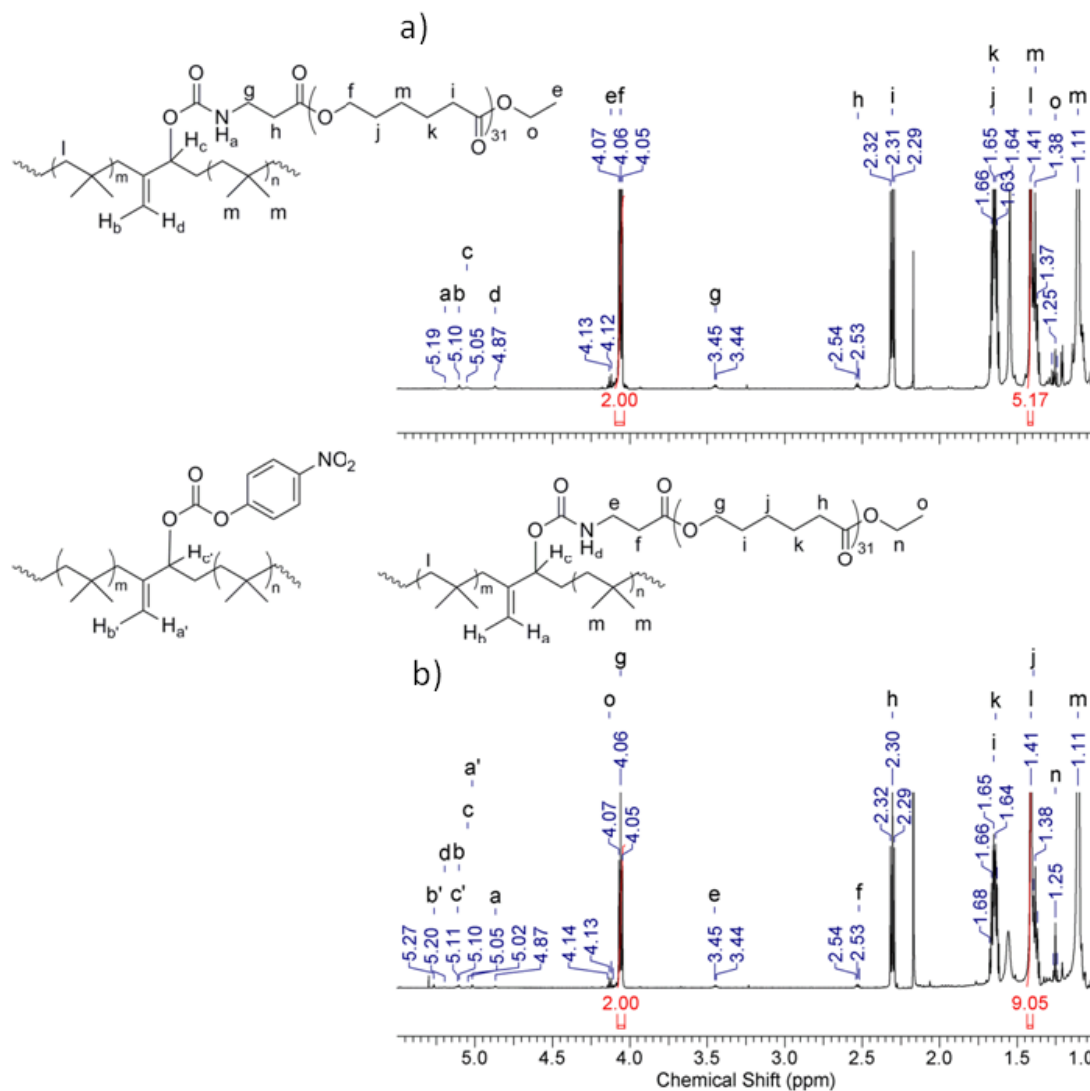
- (257) Yakacki, C. M.; Lyons, M. B.; Rech, B.; Gall, K.; Shandas, R. *Biomedical Materials (Bristol, U. K.)* **2008**, *3*, 015010/1.
- (258) Liu, C.; Mather, P. T. *Journal of Applied Medical Polymers* **2002**, *6*, 47.
- (259) Kelch, S.; Choi, N.-y.; Wang, Z.; Lendlein, A. *Advanced Engineering Materials* **2008**, *10*, 494.
- (260) Lendlein, A.; Schmidt, A. M.; Schroeter, M.; Langer, R. *Journal of Polymer Science, Part A: Polymer Chemistry* **2005**, *43*, 1369.
- (261) Smith, K. E.; Trusty, P.; Wan, B.; Gall, K. *Acta Biomaterialia* **2011**, *7*, 558.
- (262) Miao, H.; Hao, J.; Liu, Y.; Liu, Y.; Deng, X. *Polymer International* **2008**, *57*, 316.
- (263) Burkersroda, F. v.; Schedl, L.; Göpferich, A. *Biomaterials* **2002**, *23*, 4221.
- (264) Gopferich, A. *Biomaterials* **1996**, *17*, 103.
- (265) Pitt, C. G.; Chasalow, F. I.; Hibionada, Y. M.; Klimas, D. M.; Schindler, A. *Journal of Applied Polymer Science* **1981**, *26*, 3779.
- (266) Tanaka, S.; Ogura, A.; Kaneko, T.; Murata, Y.; Akashi, M. *Biomacromolecules* **2004**, *5*, 2447.
- (267) Cole, M. A.; Voelcker, N. H.; Thissen, H.; Griesser, H. J. *Biomaterials* **2009**, *30*, 1827.
- (268) Chinn, J. A.; Sauter, J. A.; Phillips Jr, R. E.; Kao, W. J.; Anderson, J. M.; Hanson, S. R.; Ashton, T. R. *Journal of Biomedical Materials Research* **1997**, *39*, 130.

## Appendices

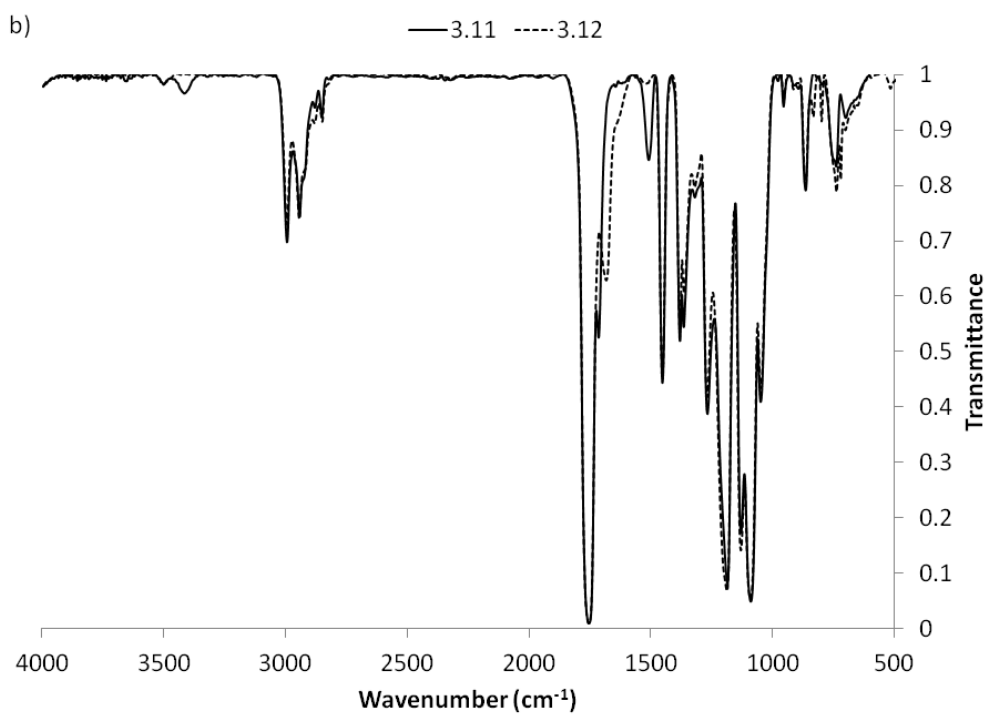
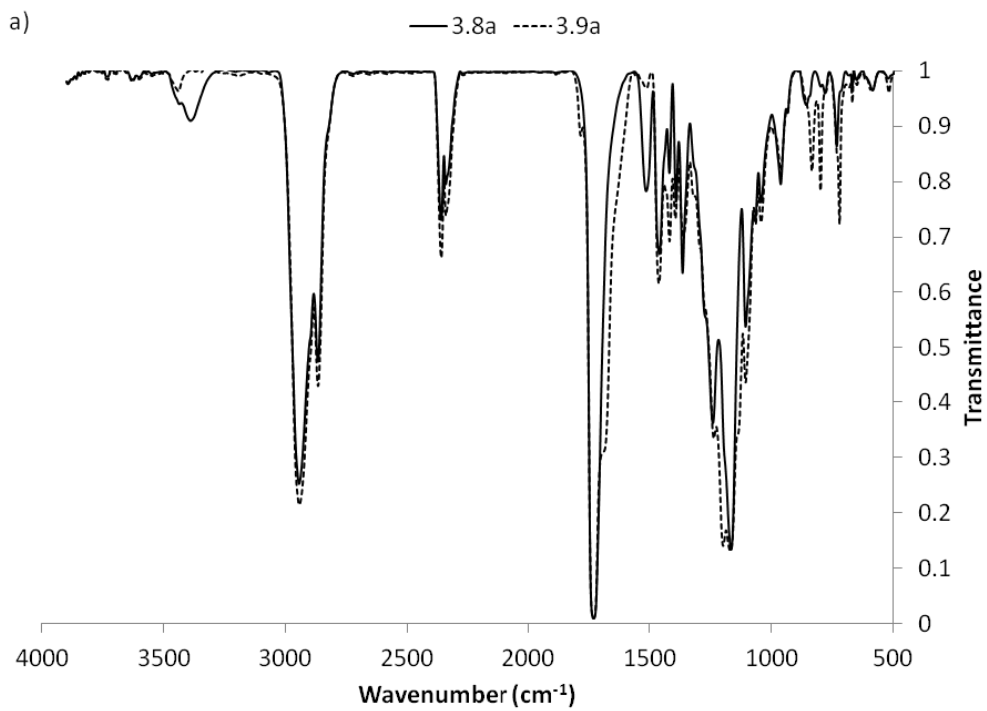


Appendix A –  $^1\text{H}$  NMR depicting functionalization of 3.7b: a) initial homopolymer; b) reacted with *t*-BOC-protected  $\beta$ -alanine (3.8b); c) and deprotected with TFA (3.9b).



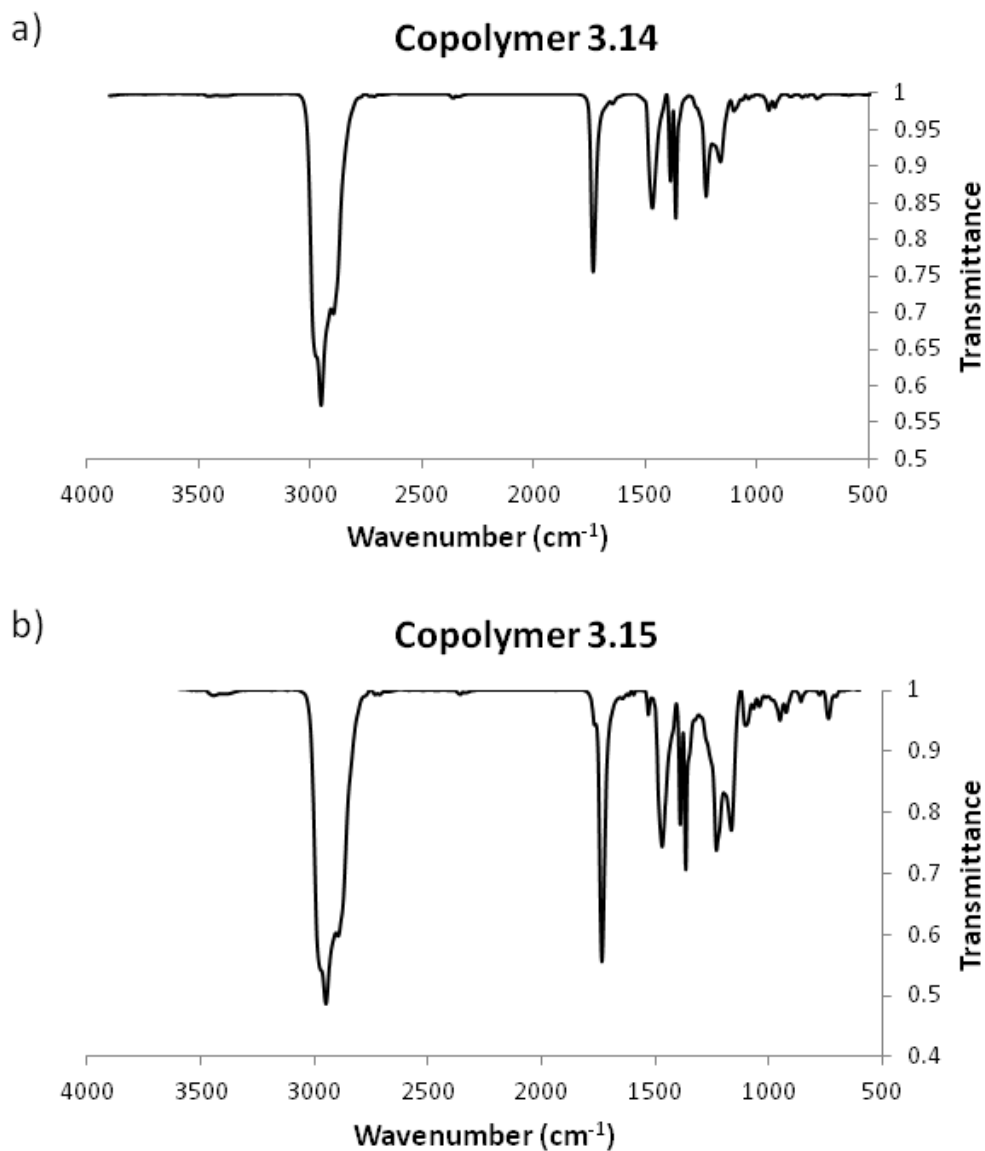


Appendix B –  $^1\text{H}$  NMR showing PCL content of: a) copolymer 3.16 (44 wt% PCL) and b) copolymer 3.15 (32wt% PCL).

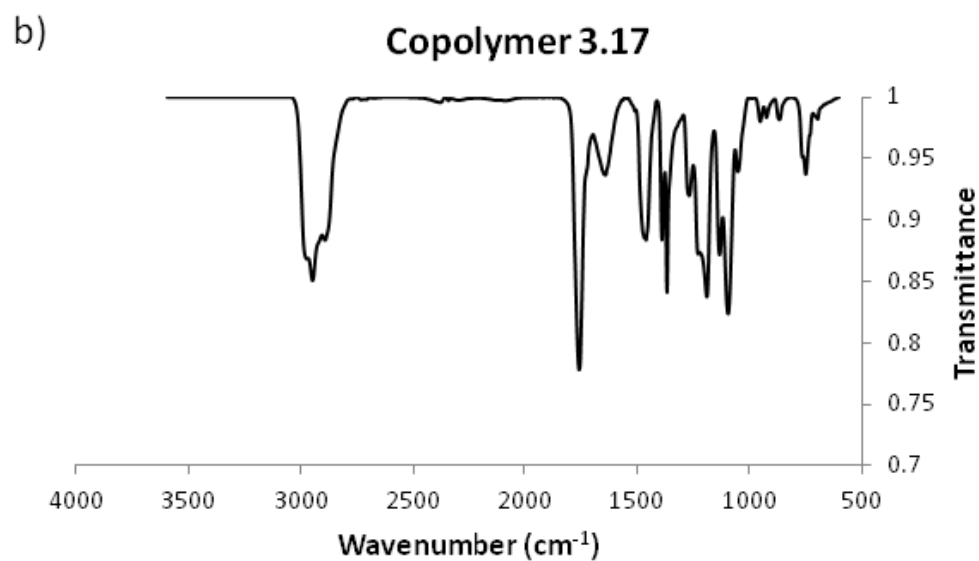
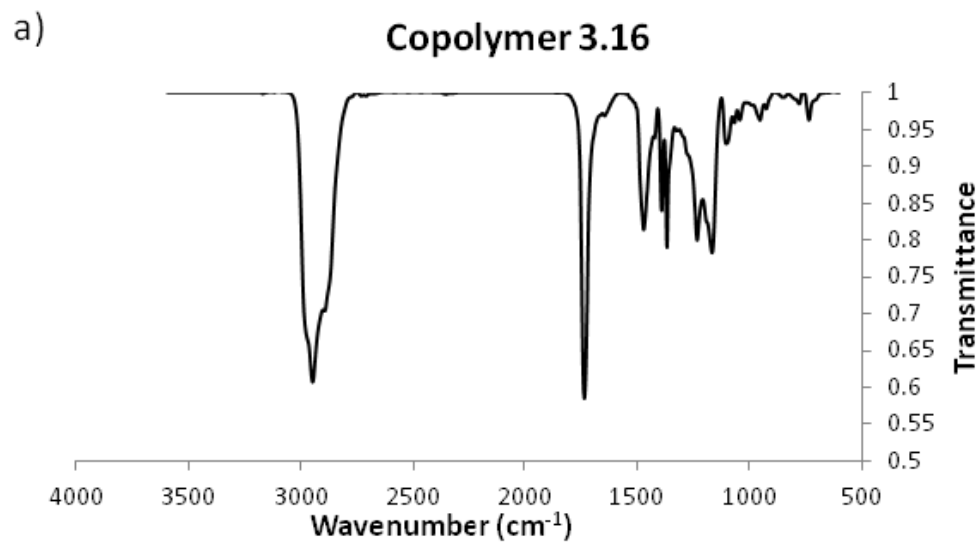


Appendix C – FTIR of: a) 3.8a and 3.9a; b) 3.11 and 3.12.

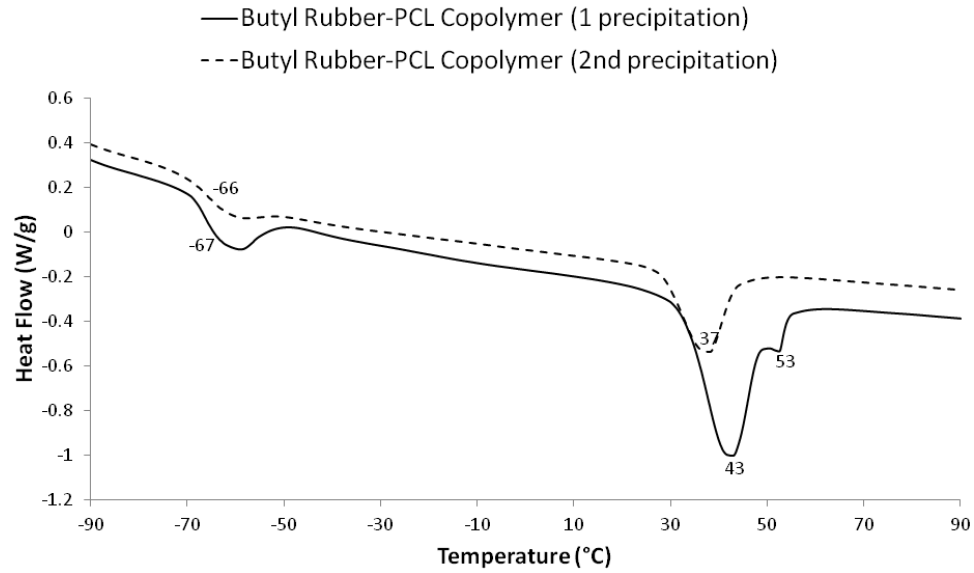




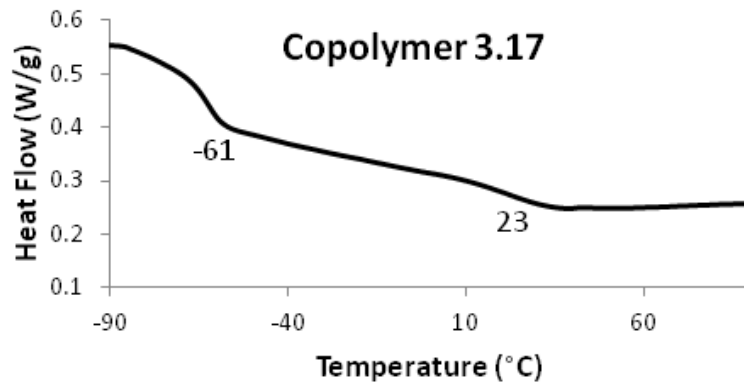
**Appendix D – FTIR of: a) copolymer 3.14; b) copolymer 3.15.**



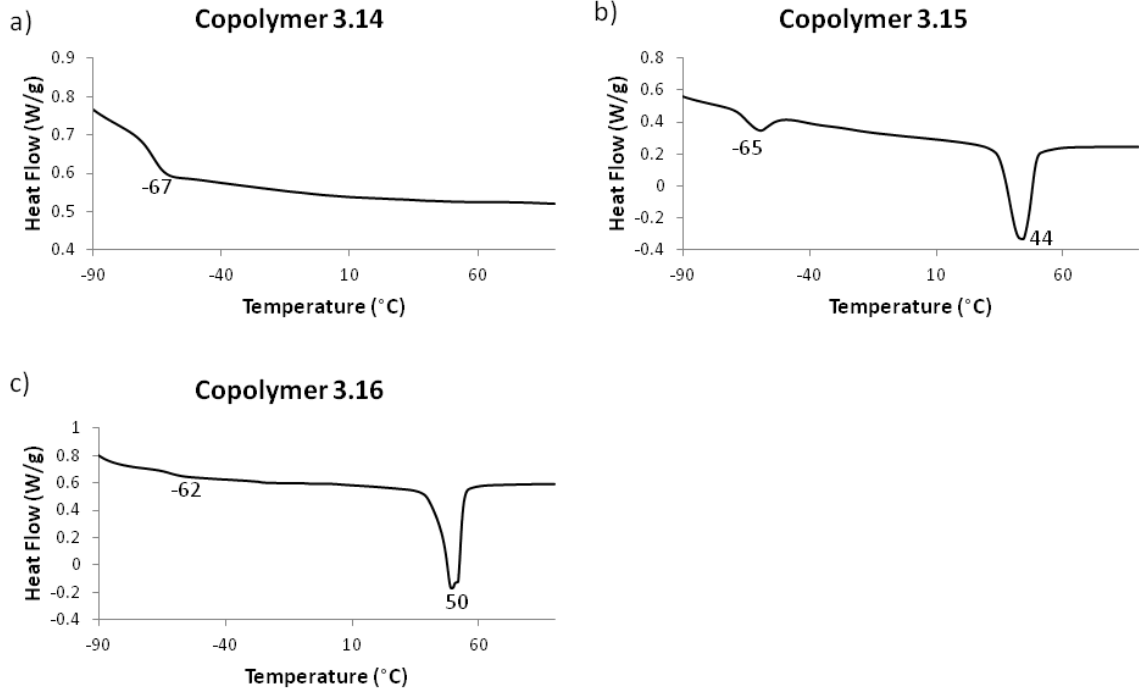
Appendix E – FTIR of: a) copolymer 3.16; b) copolymer 3.17.



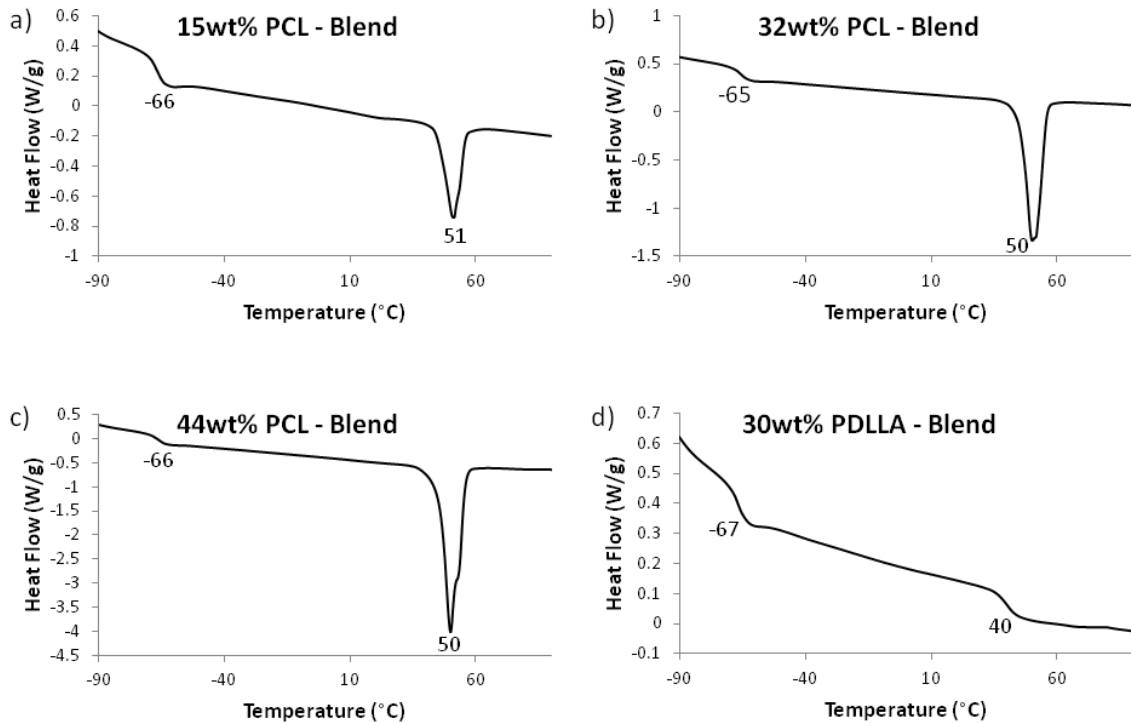
**Appendix F – DSC traces of: IIR-PCL copolymer after 1<sup>st</sup> precipitation; IIR-PCL copolymer after a 2<sup>nd</sup> precipitation into acetone, ridding of free homopolymer as evidenced by disappearance of the second T<sub>m</sub> at 53°C.**



**Appendix G – DSC trace depicting the two T<sub>g</sub>s of copolymer 3.17.**



**Appendix H – DSC traces depicting  $T_g$  and  $T_m$  of IIR-PCL graft copolymers: a) copolymer 3.14; b) copolymer 3.15; c) copolymer 3.16.**



**Appendix I – DSC traces depicting  $T_g$  and  $T_m$  of IIR-PCL/PLA blends.**

	Copolymer 2		Copolymer 3		Copolymer 4		Rubber Control	
	Average Initial Mass	% Mass Loss	Average Initial Mass	% Mass Loss	Average Initial Mass	% Mass Loss	Average Initial Mass	% Mass Loss
	Average Mass Change		Average Mass Change		Average Mass Change		Average Mass Change	
2 weeks	5.84 0.04	0.74	5.71 0.04	0.70	4.78 0.02	0.42	5.54 0.05	0.96
4 weeks	5.78 0.07	1.15	5.37 0.03	0.62	5.41 0.04	0.80	5.59 0.03	0.48
6 weeks	4.97 0.09	1.81	5.94 0.03	0.45	5.08 0.00	0.07	5.27 0.05	0.88
8 weeks	5.00 0.07	1.40	6.17 0.06	0.97	4.93 0.05	1.01	5.27 0.02	0.44
10 weeks	5.32 0.04	0.75	6.17 0.04	0.59	5.35 0.03	0.62	4.93 0.02	0.34
12 weeks	5.20 0.05	0.90	5.35 0.01	0.25	5.50 0.01	0.24	6.12 0.01	0.22
14 weeks	5.90 0.01	0.11	5.10 0.02	0.39	5.19 0.05	0.90	5.83 0.05	0.92
16 weeks	6.04 0.01	0.17	5.65 0.01	0.24	4.92 0.01	0.20	5.58 0.00	0.06

**Appendix J – Raw data coinciding with Figure 3.21 for the degradation study of IIR-PCL copolymers and IIR control.**

	Copolymer 3.17		Rubber Control	
	Average Initial Mass	% Mass Loss	Average Initial Mass	% Mass Loss
	Average Mass Change		Average Mass Change	
2 weeks	4.63 0.02	0.50	5.54 0.05	0.96
4 weeks	5.87 0.01	0.23	5.59 0.03	0.48
6 weeks	4.90 0.04	0.88	5.27 0.05	0.88
8 weeks	4.37 0.02	0.46	5.27 0.02	0.44

**Appendix K – Raw data coinciding with Figure 3.22 for the degradation study of IIR-PDLLA copolymer and IIR control.**

# Curriculum Vitae

## EDUCATION

- The University of Western Ontario, London, Ontario  
**Master of Engineering Science, Biomedical Engineering Graduate Program** **June 2013**  
 Dissertation: "Butyl Rubber and Polyester Graft Copolymers for Biomedical Applications"  
 Supervisor: Dr. Elizabeth Gillies
- The University of Western Ontario, London, Ontario  
**Bachelor of Engineering Science, Department of Chemical and Biochemical Engineering** **April 2011**  
 Specialization: Biochemical and Environmental Engineering  
 Graduated with Distinction  
 Honours Thesis: "Utilizing Mesoporous Ordered Silicates as Catalysts for Biodiesel Production"

## EMPLOYMENT EXPERIENCE

- The University of Western Ontario | London
- Teaching Assistant – to Dr. Shazhad Barghi in "Introduction to Plant Design and Safety"** **Jan – Apr 2013**  
 Provided student assistance for research assistance and plant development for group-dependent processes  
 Evaluated student performance based on a standardized rubric  
 Met with students upon request to optimize plant design
- Teaching Assistant – to Dr. Elizabeth Gillies in "Industrial Organic Chemistry"** **Sept 2012**  
 Explained methodologies to students pertaining to successful completion of hands-on experiments  
 Evaluated student in-lab performance as well as comprehension of background theory based on completion of formal reports  
 Available to meet with students upon request and marked course midterms
- Teaching Assistant – to Dr. Shazhad Barghi in "Introductory Engineering Design and Innovation Studio"** **Sept 2011**  
 Provided student assistance on the iterative development for several design-based projects  
 Evaluated student performance based on a standardized rubric  
 Met with students upon request and graded all written work
- Research Assistant – to Dr. Elizabeth Gillies | Department of Chemistry** **May – Aug 2011**  
 Developed synthetic laboratory skills necessary for working in a polymer research facility  
 Worked on butyl rubber project investigating graft copolymerization to enhance material properties  
 Optimized toxicity cell assays and imaging for biocompatibility testing
- NSERC Undergraduate Student Researcher – to Dr. Sohrab Rohani | Chemical Engineering** **Ap/10 – Ma/11**  
 Developed and optimized biodiesel production with a heterogeneous-based catalyst  
 Worked as a team member and enhanced laboratory, communication and research skills  
 Obtained particle characterization skills using various instruments

## AWARDS

- Ontario Graduate Scholarship, *The University of Western Ontario* **September 2012**  
 Natural Science and Engineering Research Council of Canada, Undergraduate Student Research Award **May 2010**  
 Dean's Honour List, Faculty of Engineering Science **April 2008**  
 All Canadian/Ontario University Athletics Academic Achievement Award **2007 – 2012**  
 Queen Elizabeth II Aiming for the Top Scholarship **2007 – 2011**  
 The Governor General's Academic Medal (highest overall average) **June 2006**

## PUBLICATIONS AND PAPERS

- Turowec, B.;** Gillies, E.; Functionalized Polyisobutylene-Based Materials for Biomedical Applications.  
96<sup>th</sup> Canadian Chemistry and Exhibition, Québec City, Québec.  
Presented in oral format. May 2013
- Karamdoust, S.; Bonduelle, C.V.; Amos, R.C.; **Turowec, B.A.;** Guo, S.; Ferrari, L.; Gillies, E.;  
Journal of Polymer Science: Part A, **2013**. *Synthesis and properties of butyl rubber – poly(ethylene oxide) graft copolymers with high PEO content.* May 2013
- Turowec, B.;** Gillies, E.R.; Polyisobutylene-based Rubber and Polyester Graft Copolymers for Biomedical Applications.  
The University of Western Ontario, Biomedical Engineering Seminar Presentation.  
Presented in oral format. April 2013
- Kazemian, H.; **Turowec, B.;** Siddiquee, M. N.; Rohani, S.; Fuel, **2013**, 103, 719.  
*Biodiesel Production using cesium modified mesoporous ordered silica as heterogeneous base catalyst.* January 2013
- Turowec, B.;** Gillies, E.R.; The Expansion of Polyisobutylene into Biomedical Applications.  
The University of Western Ontario, Biomedical Engineering Seminar Presentation.  
Presented in oral format. April 2012
- Turowec, B.;** Gillies, E.R.; Developing Polyisobutylene for Biomedical Applications.  
The University of Western Ontario, The London Health Research Day. Presented in poster format. March 2012
- Turowec, B.;** Siddiquee, M.N.; Kazemian, H.; and Rohani, S.; Zeolitic Mesoporous Ordered Silica as Heterogeneous Solid Catalysts for Biodiesel Production.  
The University of Western Ontario, Particle Technology Research Centre Conference, London, ON. Presented in poster format. Received 3rd prize. August 2010

## MEMBERSHIPS

- The University of Western Ontario | London
- Programs Operation Committee** 2011 – 2013  
Department of Biomedical Engineering
- Leader's Circle** 2011 – 2012  
Mustang Varsity Athletics

## VOLUNTEER ACTIVITIES

- The University of Western Ontario Student Orientation Guide 2011  
The Western Fair 2010 & 2011  
Chemistry/Calculus Tutor 2009 – 2011

## CO-CURRICULAR ACTIVITIES

- Kawartha Lakes Lacrosse, Senior 'A' Team, Ontario** 2010 – Present
- Women's Varsity Lacrosse, The University of Western Ontario** 2007 – 2011
- Won Ontario University Athletic Championship (2009, 2011)
  - Captain of Lacrosse Team
- Women's Ontario Ball Hockey Team** 2004 – 2011
- Won National Championship (2009)
- Women's Varsity Hockey Team, The University of Western Ontario** 2006 – 2007
- Lady Blue Knights Lacrosse, U19 A Team, Ontario**
- Won Provincial Finals 2005 – 2006